# Discovery and Characterization of Antibodies that Bind Nanoparticles

by

Supriya Ravichandran

Submitted in Partial Fulfillment

of the

Requirements for the Degree

Doctor of Philosophy

Supervised by

Professor Lisa A. DeLouise

Department of Biomedical Engineering

Arts, Sciences and Engineering

Edmund A. Hajim School of Engineering and Applied Sciences

University of Rochester

Rochester, New York

2015

# Dedication

*This thesis is dedicated to my parents Rajalakshmi Ravichandran and G. Ravichandran, and my aunt, Bharati Sadasivam, whose love and trust have helped me believe in myself and make this effort what it is today.*

# Biographical Sketch

Supriya Ravichandran was born in Mumbai, India on October 20th, 1986. She attended SASTRA University, Thanjavur, India, from 2004 to 2008, where she graduated with a Bachelor of Technology degree in Biotechnology. She then enrolled in the University of Rochester in the Biomedical Engineering Department and received a Master of Science degree in 2010. She pursued her Ph.D. in Biomedical Engineering at the University of Rochester and has been working under the guidance of Prof. Lisa A. DeLouise in the fields of nanotechnology, nanomaterial interaction with skin and phage display.

# Acknowledgements

I would like to thank my advisor Lisa A. DeLouise for her constant support and encouragement throughout my years at Rochester. She has made me a better researcher by always reminding me to seek answers fearlessly and develop resilience. I will always remember this and will be grateful for her belief in me. Prof. Mark A. Sullivan has been another invaluable mentor during my years as a Ph.D. student. I will always be grateful to him for his exceptional patience with me in my initial years, for our stimulating discussions, and for all that he taught me in molecular biology, stimulating my interest in the subject. I learnt many techniques under his guidance, which gave me the right approach for my experiments and will help me to become the scientist I aspire to be. I would like to thank my committee members Prof. Benjamin Miller, Prof. Alison Elder and Prof. James McGrath for their invaluable advice and suggestions. I am particularly indebted to Prof. Benjamin Miller for his guidance and advice during group meeting sessions which helped me overcome some challenges. Next, I would like to thank Karen Bentley for helping me perform the TEM experiments and for the TEM images she acquired for me. I would also like to thank Paivi Jordan and Linda Callahan for their help with confocal imaging and LCM imaging. Wojciech Wojciechowski in the flow

cytometry core had a number of interesting suggestions on making the image stream experiments a success. He helped me a lot with data analysis and made it possible to obtain data for this thesis. Bob Gelein in the Elder lab helped by performing AAS analysis and guiding me with data interpretation. JoAnne VanBurskirk and Andrea Kennell have been good and kind friends to me.

I am grateful to the administrators of the Biomedical Engineering and Dermatology Departments, particularly Donna Porcelli, Melody Newman and Jayne Kresinske, for their immense help in getting all the paperwork done on time.

This work would not have been possible without the friendship and support help of my past and current lab members. I would like to first thank my mentor Dr. Luke Mortensen for his support, friendship and guidance which made my time in the lab more enjoyable I am truly grateful to Dr. Ut-Binh Giang for standing by me during some challenging months. I would like to thank my current lab members Samreen Jatana, Brian Palmer and Dana Phelan for all their help and support to my research. Samreen, in particular, has been a close friend and companion both inside and outside the lab, helpful and with a great sense of humor. Brian and Dana have given me great inputs and advice during our group meetings. I am also grateful to all past and current members of the Miller lab, since many ideas stemmed from interesting discussions during our group meetings and otherwise and helped to shape my research.

I would like to thank my parents, Rajalakshmi Ravichandran and G. Ravichandran, and my aunt and uncle, Bharati Sadasivam and Scott Sherman, for all their support during the course of my graduate work. I would like to thank my grandparents,

Jaya Sadasivam and M.S. Sadasivam, for their faith in me and for constantly motivating me to do my best during these years. My sibling Abhinandan, has also been very supportive of my thesis work.

Finally, I would like to acknowledge my funders, the Centers for Disease Control and Prevention (1R21OH009970), which supported my work.

# Abstract

Nanoparticle (NP) safety concerns stem from their unique physiochemical properties such as high surface area to volume ratio and small size, and reactivity otherwise not present in the bulk form. These NP properties contribute to the potential toxicity and altered tissue function when in contact with biological systems. Since skin is one of the major routes of NP entry into the system upon contact with NP-enabled products, researchers have focused on determining if NPs can penetrate the stratum corneum, which is the outermost skin barrier layer. Semiconductor quantum dots (QDs) and metal oxide NPs (titanium dioxide ($TiO_2$)) have been widely used to study NP-skin interactions due to their commercial importance. However, studies show varying results on NP skin penetration depending upon the NP size and surface chemistry, skin model used and the NP detection techniques employed. Conventional techniques employed to detect NPs in tissues such as transmission electron microscopy coupled with energy dispersive x-ray spectroscopy offer superior nanoscale resolution, however pose limitations due to the high cost of sample processing and limited sample analysis throughput. Confocal and fluorescence microscopy are also common techniques used to detect fluorescent NPs, however their detection ability is often obscured by tissue autofluorescence and are limited to detecting fluorescent NPs. Therefore, a simple economical technique which can provide information on both the presence of NPs and their form in biological systems and the environment is required.

We have developed NP binding antibodies to commercially important NPs including QDs and $TiO_2$ NPs using phage display technology. Phage display is used to identify protein or peptide binders to a wide variety of targets. Typically, nucleotide sequences encoding the protein/peptide library are fused to a gene encoding a phage coat protein thus allowing them to be

displayed on the phage exterior. An affinity based selection technique (biopanning) is used to identify binders from the library. In this work, we have developed antibodies to NPs from a phage library containing ~$2x10^9$ unique single-chain variable fragment (scFv) antibodies each displayed monovalently on the gene III coat protein of a M13 filamentous phage. The scFv antibodies are engineered with a FLAG tag to allow for secondary detection using standard immunohistochemistry methods.

This thesis discusses the discovery of novel antibodies binding QDs and $TiO_2$ NPs and their functionality by demonstrating their binding both *in vitro* and in an *ex vivo* human skin model. The antibodies isolated against GSH-QDs and $TiO_2$ NPs by panning in solution, can recognize the respective NPs in skin and did not show any non-specific binding to skin samples without NPs. Non-fluorescent $TiO_2$ NPs were detected using simple microscopic techniques with the scFv antibody isolated against them. The antibodies do not exhibit non-specific binding to dissimilar NPs such as gold NPs or carbon nanotubes as demonstrated through custom-designed *in vitro* assays. Additionally, the antibodies have been characterized for their binding and cross-reactivity properties to several other NPs, and some challenges associated with the isolation of the antibodies from a large library and alternative method for selection of antibodies have been discussed. It was found that enrichment on NPs in solution does not render off-target clones or false positives when compared to enrichment on immobilized target, conventionally used in phage display. This is the first time antibodies to dispersed NPs in solution have been isolated.

The novel antibodies isolated when used in conjunction with other existing techniques for NP detection will comprise a powerful tool kit, and enable researchers to use them to detect NPs both in the environment and in a biological milieu.

# Contributors and Funding Sources

This work was supported by a dissertation committee consisting of Prof. Lisa A. DeLouise (advisor, Dermatology), Prof. Benjamin L. Miller (Dermatology), Prof. James L. McGrath (Biomedical Engineering) and Prof. Alison Elder (Environmental Medicine). All experiments were performed by the author. The different phage libraries, transductions done and expression constructs used in the thesis were constructed by Prof. Mark A. Sullivan (URMC). Phages were prepared and all phage titer experiments were performed in the Sullivan Lab. TEM and SEM imaging was performed by Karen L. Bentley (URMC Electron Microscopy Core). Confocal microscopy imaging was performed by Paivi Jordan (URMC Confocal Core). Quartz coverslips used in the electron microscopy experiments were prepared by Brian McIntyre. Image Stream experiments were performed in collaboration with and help from Wojciech Wojciechowski (URMC Flow Core). The work was supported by the Centers for Disease Control and Prevention (1R21OH009970) and NEIHS (P30ES01247).

Portions of this thesis have been adapted from,

*Ravichandran, S., Sullivan, M. A., DeLouise, L. A. Development and Characterization of Antibody Reagents for Detecting Nanoparticles in Biological Systems., Submitted, June 2015.*

# Table of Contents

# List of Tables

# List of Figures

# List of Abbreviations

| | |
|---|---|
| **AAS** | Atomic Absorption Spectroscopy |
| **AP** | Alkaline Phosphatase |
| **CDR** | Complementarity Determining Region |
| **CNT** | Carbon Nanotubes |
| **DHLA** | Dihydroxy Lipoic Acid |
| **EDS** | Energy Dispersive x-ray Spectroscopy |
| **GSH** | Glutathione |
| **HRP** | Horse Radish Peroxidase |
| **ICP-MS** | Inductively Coupled Mass Spectroscopy |
| **IHC** | Immunohistochemistry |
| **LC** | Langerhans Cells |
| **LCM** | Laser Capture Microdissection |
| **mAbs** | Monoclonal Antibodies |
| **MRI** | Magnetic Resonance Imaging |
| **MW** | Molecular Weight |
| **NP** | Nanoparticle |
| **ODA** | Octadecyl Amine |

| | |
|---|---|
| **PEG** | Polyethlyene Glycol |
| **PEI** | Polyethlyene Imine |
| **QD** | Quantum Dot |
| **ROI** | Region of Interest |
| **ROS** | Reactive Oxygen Species |
| **SC** | Stratum Corneum |
| **scFv** | Single Chain Variable Fragment |
| **SEM** | Scanning Electron Microscopy |
| **SG** | Stratum Granulosum |
| **TEM** | Transmission Electron Microscopy |
| **TOF-SIMS** | Time of Flight Secondary Ion Mass Spectrometry |
| **TOPO** | Trioctylphosphine Oxide |
| **UVA** | Ultraviolet Radiation A |
| **UVB** | Ultraviolet Radiation B |
| **UVR** | Ultraviolet Radiation |

# Chapter 1

## *Introduction*

*Nanoparticles, Detection of Nanoparticles and Phage Display*

# 1.1 The Promise of Nanotechnology

The world is rapidly progressing towards the nanoscale of things. The global total market value for nanoparticles (NPs) in biotechnology is estimated to reach $53.5B US dollars in 2017[1]. This continuous drift towards the use of nanomaterials and NPs could potentially increase levels of NP exposure to humans. NPs are defined as particles having a size less than 100 nm in one dimension, and nanotechnology is defined as the manipulation of materials at the atomic and molecular level to create materials with unique size-dependent physiochemical properties, otherwise not present in the bulk form. These properties are attributed to the quantum confinement effect and their high surface area to volume ratio, which has led to a multitude of applications NPs can offer ranging from healthcare and life sciences to electronics, and consumer goods including textiles and food products[3]. In medicine, nanotechnology has been applied to drug delivery (fullerenes, polymer NPs), gene therapy (silica NPs), diagnostics (gold (Au) NPs), biomedical imaging (quantum dots (QDs)) including MRI contrast enhancement (iron oxide NPs)[4]. Nanomaterials can be used for passive tumor targeting as they demonstrate enhanced permeability and retention effects[5,6], and active targeting using tethered tissue homing ligands[5,7]. Carbon nanotubes have been used extensively in sports equipment[8] and nano-sized titanium dioxide ($TiO_2$) and zinc oxide (ZnO) are formulated into ~70% of all sunscreens[9] in the market available for daily consumer use (33 million people in the United States including children use a sunscreen product daily[10]), and contain 5-10% by weight NPs[11]. $TiO_2$ and ZnO NPs offer broad protection against ultraviolet (UV)-A (320-400 nm) and UVB (290-320 nm) radiation by absorbing the light energy and

scattering and reflecting incident radiation[12]. Nano-$TiO_2$ is an important industrial material and has always been used as the white pigment in a variety of consumer goods such as paint, paper, ceramics and plastics, among others[13]. In food industry, some nanomaterials have been used for beneficial effects on foods leading to an increased shelf-life, enhanced flavor release and increased absorption of nutrients. Additionally, traditional methods of food manufacturing processes such as grinding and spray-drying can produce nanoscale variants of natural materials that would otherwise not be found in such a size range[14]. Other applications pertaining to consumer products include nano-engineered membranes for water purification systems medical implants and use of nano-zirconium oxide in medical implants[15]. Therefore, given the expansive advantageous properties of nanomaterials and the endless possibilities for their exploitation to the benefit of humans, our contact with these nanomaterials via the skin, respiratory system and digestive tract is inevitable and only increasing by the day.

## 1.2 Quantum Dots

QDs are fluorescent semiconductor NPs which exhibit size-dependent quantum confinement properties. They are widely used in biomedical imaging, biosensing and photovoltaic applications due to their advantageous properties such as broad excitability, narrow emission bandwidth, easily modifiable surface properties and high quantum yield. Fluorescent QDs and near-infrared QDs that can overcome tissue autofluorescence have been used for *in vivo* tumor and sentinel lymph node tracking. QDs are estimated to have a commercial value of $1.1 billion in 2016[16]. Core-shell type composite QDs are widely

used in experimental and practical applications due to their novel properties. Coating the nanocrystalline core with inorganic shell materials has been shown to improve the photoluminescence quantum yields by passivating surface recombination sites. For example, various core-shell QD structures have been reported such as CdS on CdSe, ZnS on CdS, ZnS on CdSe and ZnSe on CdSe[17]. ZnS overcoated CdSe particles have higher efficiencies, greater photostability and greater quantum yields, making them more useful for optoelectronic device structures, and electroluminescent and photovoltaic devices[18]. QDs used widely in biolabeling applications are synthesized in an organic phase and have good monodispersity and photoluminescence[17]. However, their surface chemistry dictates their biocompatibility. QDs are often capped with hydrophobic ligands such as trioctylphosphine oxide (TOPO) and octadecylamine (ODA) thus making it a challenge to use them in aqueous biocompatible environments. Ligand exchange methods allow for the substitution of an organic ligand with a hydrophilic ligand. The key to choosing the right ligand is to maintain colloidal stability (no aggregation) in a biological milieu, low or lack of cytotoxicity and a high quantum yield[19]. The ligand exchange method also allows for stabilization of the core and minimizing any toxic effects, which come into question due to QDs often being composed of a heavy metal core (eg. Cd). Many such ligands have been successfully used and reported such as thiol-polyethylene glycol (PEG)[20], dihydrolipoic acid (DHLA)[21] and glutathione (GSH)[17]. GSH is an antioxidant and imparts a negative charge to the QDs, previously has been reported to exhibit superior optical properties and stability[19], and will be the choice of ligand used for all QD studies described in this thesis.

Due to above mentioned widespread applications of QDs, which is on the steady rise, their potential exposure to researchers and consumers has been of primary interest resulting in a spike of studies investigating QD interaction with skin[22-26]. In this thesis QDs were used as a model NP as they have a size comparable to commercially important $TiO_2$ and ZnO NPs. Moreover, QDs generate reactive oxygen species (ROS)[27], and carboxylated QDs (such as GSH-QDs) have a similar negative oxide surface chemistry to $TiO_2$ and ZnO NPs[28].

## 1.3 Titanium dioxide Nanoparticles

The global production of $TiO_2$ for all uses is in the millions of tons per year[29]. $TiO_2$ as a bulk material is primarily used because of its brightness, high refractive index and resistance to discoloration. Nearly 70% of all $TiO_2$ produced is used as a bulk material as a pigment in glazes, enamels, plastics, paper, foods, pharmaceuticals, and toothpastes[30]. Applications of nano-$TiO_2$ include cosmetic formulations, antimicrobial applications and catalysts for air and water purification[29]. Therefore, many sources of pigment and nanoscale $TiO_2$ can result in human exposure and subsequent entry into the environment (air, water, soil). Pigment and nanoscale $TiO_2$ are synthesized with a crystalline structure (anatase, rutile, brookite), each of which have their own unique properties. The most common $TiO_2$ NP synthesis procedure utilizes the hydrolysis of Ti salts in an acidic solution[31]. In order to increase photostability and prevent aggregation, $TiO_2$ NPs are commonly coated with aluminium, silicon or polymers[32,33]. $TiO_2$ nanomaterials in foods and consumer products are discharged into the environment as feces/urine, washed off of

surfaces or disposed to sewage that enters wastewater treatment plants. Although sewage treatment plants are efficient in removing larger $TiO_2$ from sewage waste water, particles measuring 4-30 nm in size were still found in the treated effluent[34,35]. Extensive fate, transport and toxicity studies have used a readily available $TiO_2$ NP (Evonik Degussa, P25) because the primary crystals are <50 nm in size, uncoated and is present in commercial products. P25 is advertised as "titanium without pigment properties" and is primarily used as a photocatalyst and heat stabilizer for silicone rubber[29]. P25 exists as an aggregate in the dry powder state and readily aggregates to several hundred nanometers in water[36]. Although not a direct representative of the food-grade $TiO_2$ (E171), in this thesis all the studies with $TiO_2$ NPs have been reported based on the use of P25 in experiments.

# 1.4 Nanotoxicology

Nanotoxicology can be defined as the "science of engineered nanodevices and nanostructures that deals with their effects in the living organisms"[37]. Numerous experimental studies have focused on the enhanced toxicological potential of engineered NPs in contrast to the larger sized particles of the same material[38,39]. There is also evidence that the nano-sized fraction of particles associated with air pollution is a major contributor to the adverse effects attributed to air pollution[40,41]. The benefiting high surface area to volume ratio in NPs can elicit a greater biological reactivity per unit mass in an organism compared to the bulk form of the same materials due to the increasing ratio of surface to total atoms with decreasing particle size. This increased biological

reactivity can elicit positive and desirable responses (antioxidant activity, drug delivery) or be negative and undesirable (toxicity, oxidative stress, cellular dysfunction)[40,41]. Nanomaterials and NPs may elicit toxic effects in biological systems via various mechanisms. Primarily, the production of ROS leading to oxidative stress is a mechanism, which can lead to DNA damage, unregulated cell signaling, cytotoxicity, apoptosis and even tumor initiation[42-44]. Other potential side effects due to long-term presence of NPs in cells include leaching of toxic ions[45], exposure of cryptic epitopes[46] and genotoxicity[47]. The toxicity effects of metal oxide NPs such as $TiO_2$ and ZnO and semiconductor NPs such as QDs has been well reported[43,48-50]. Yin et al., studied the photocytotoxicity of different sizes of $TiO_2$ NPs in both forms (anatase and rutile) *in vitro* using human keratinocytes, and found that upon UVA irradiation all the $TiO_2$ NPs induced photocytotoxicity and cell membrane damage mediated by production of ROS[51]. Wu et al., observed pathological lesions of varying degrees on mice skin after 8 weeks of nano-$TiO_2$ application accompanied by wrinkles, excessive keratinization and atrophy of dermis implying skin aging[13]. The skin from these mice also showed oxidative stress due to exposure to $TiO_2$ suggested by increased lipid peroxidation products and reduced collagen contents. It was also found in these mice that the liver had focal necrosis sections due to localization of Degussa P25 $TiO_2$ NPs (21 nm), which may lead to its functional impairment. Upon application of 0.4 mg/cm$^2$ $TiO_2$ NP on hairless rat skin, Adachi et al., observed focal parakeratosis in the SC and epidermal spongiosis with dermal inflammatory infiltration using light microscopy, absent in control groups[52]. This recent study concluded that the histopathological changes including eczema-like lesions

suggested the irritation action caused by $TiO_2$ NP and possible ROS production leading to contact dermatitis and spongiosis respectively. Titania has also been linked to Crohn's disease, asthma and has been classified as a possible carcinogen[53-55].

QDs have also been shown to induce toxicity based on their composition, size and surface chemistry. Mahto et al., have shown that QDs (CdSe/ZnS core/shell) dispersed in aqueous cell media induced ROS formation and released calcium leading to toxicity[56]. Hoshino et al., showed QD induced reversible DNA damage in vitro using WTK1 cells at a 2 µM concentration[57]. Shiohara et al., showed coated CdSe/ZnS QDs to be cytotoxic to HeLa cells and primary human hepatocytes at a 100 µg/mL concentration[58]. Cadmium and selenium, the widely used constituent metals in QDs are known to cause acute and chronic toxicities to vertebrates and are a human health and an environmental concern[49,59]. Some gaps and discrepancies exist in literature studies focusing on the metabolic processes, and the systemic localization and excretion mechanisms of QDs *in vivo*. Given their metalloid core, uniqueness of their physiochemical properties, their oxidative and photochemical lability and the prevalence of QD-based products in the market accelerates the need to understand their localization in tissue and bridge the gaps in the current understanding of QD impact on human health and the environment.

# 1.5 Nanoparticle Entry into the Body

NPs may breach epithelial barriers and reach various target organs in the body. Three main routes of NP entry into the body include the respiratory tract, the gastrointestinal tract and skin. Both the anatomical features of the target organ, and NP surface and

physiochemical properties play a role in determining the ultimate fate of NPs. Surface properties of NPs include chemical composition, surface functionalization, shape, surface crystallinity, heterogeneity and hydrophobicity or hydrophilicity[37,43], whereas NP physiochemical properties include size, surface charge, surface coating, dissolution characteristics, aggregation state and core/shell composition, both of which play a role in determining the NP dose reaching a specific organ[60,61]. However, the surface charge is cell-type specific (type I alveolar epithelial cells have no or few anionic sites, type II cells have anionic sites[62]), and correspondingly QDs whose surface chemistry has been modified using carboxyl moieties show enhanced retention by lung tissue and greater interaction with type I alveolar epithelial cells[60]. In the gut, a highly specialized cell lineage knows as microfold cells (M cells) uptake particles less than 1 μm and transport them across the lymphoid follicles grouped as patches (Peyer's Patches). These M cells represent a unique site in the gastrointestinal tract for NP binding and uptake[60]. In order to understand NP interaction with skin, which is the goal of this thesis, it is important to first consider the skin barrier formation and its architecture.

### 1.5.1 Skin Structure and Barrier Function

Of all the routes of entry of NPs into the body, skin is a major route with a surface area of 1-2 $m^2$ in human adults[63]. Among the multitude of functions provided by the skin, it serves a very important function by acting as a two-way barrier between the body and the external environment. It behaves as an inside-out barrier to prevent water loss from the body and an outside-in barrier to protect the body from harmful environmental insults. The epidermis and the dermis are the two main layers in skin varying vastly in their

morphology and function. While the dermis is highly vascular and is composed of the extracellular matrix elements, adipose cells, mast cells and sweat glands, the epidermis is avascular and composed of primarily keratinocytes interspersed with melanocytes, Langerhans cells (LCs) and Merkel cells. Particle beam analysis and cytochemical studies[64,65] have shown the presence of an extracellular calcium ($Ca^{2+}$) gradient in mammalian skin *in vivo,* with low $Ca^{2+}$ in the basal proliferating layers and progressively higher $Ca^{2+}$ content as the epidermis stratifies and differentiates. This gradient is a driving force for the transitioning of a keratinocyte into a corneocyte (terminally differentiated keratinocyte) with an intermediate granular form (Figure 1.1). The epidermis comprises the physical, the chemical/biochemical (antimicrobial, innate immunity) and the adaptive immunological barrier functions of skin. The physical barrier consists of the stratum corneum (SC), the nucleated epidermis, and the cell-cell junctions. The SC presents a long, torturous, interdigitated paracellular pathway[66]. The chemical/biochemical barrier is composed of lipids (ceramides, free fatty acids and cholesterol), antimicrobial peptides, hydrolytic enzymes and macrophages. Lipids prevent water loss from the body (inside-out barrier) and form the outside-in barrier by preventing permeation of hydrophilic substances (>500 MW)[67]. Penetration of hydrophilic substances occurs via a transcellular polar pathway[68], and the polar channels present within the lipid lamellae can also support the paracellular transport of hydrophilic substances[60]. The adaptive immunological barrier is composed of humoral and cellular constituents of the immune system[69]. LCs are antigen-presenting cells, which sequester foreign substances invading the skin (microbes, particles as large as 0.5-3.0 μm[70]) and

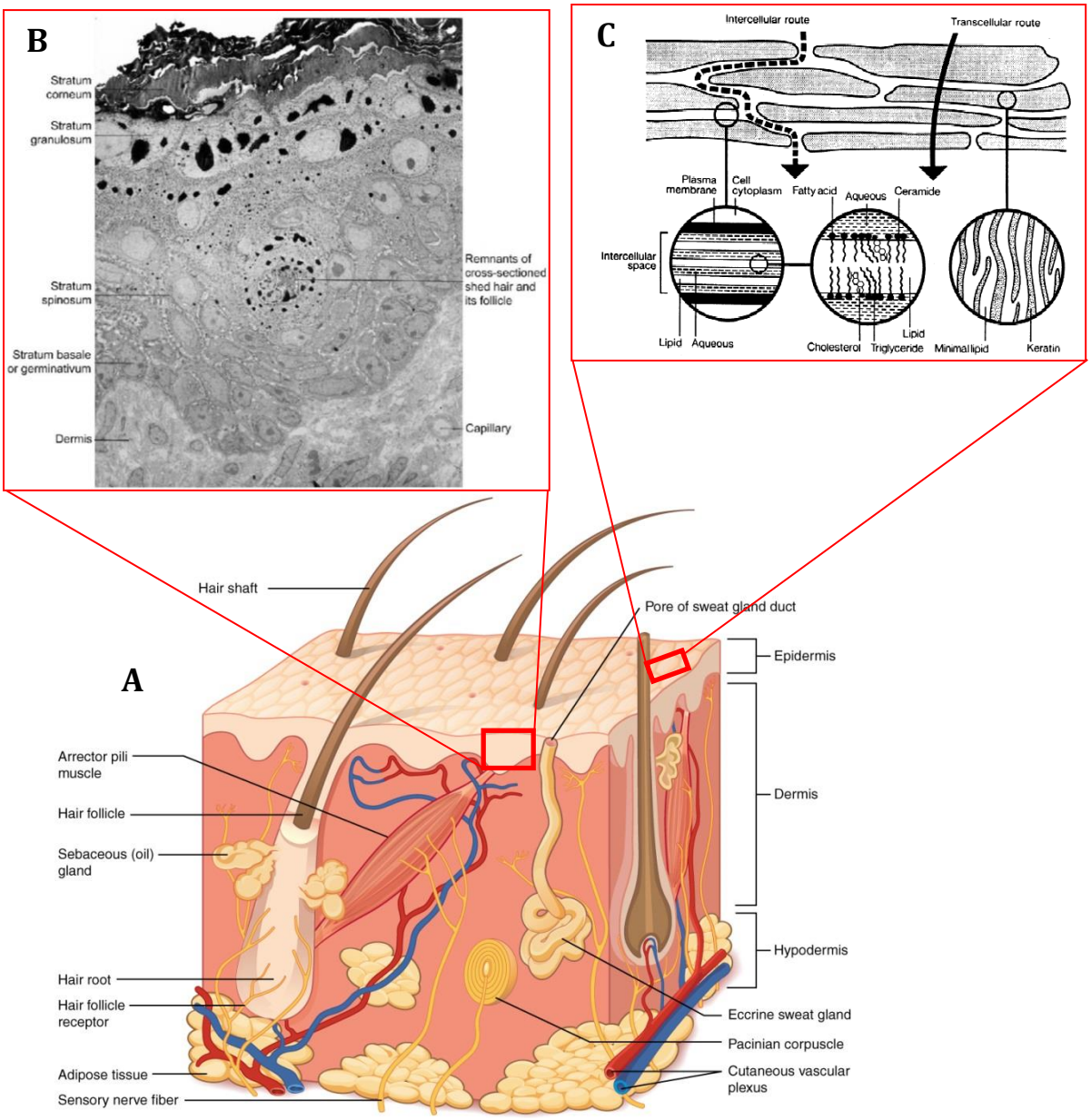


**Figure 1.1 Skin Anatomy**

A) Structure of skin showing various layers (adapted from https://voer.edu.vn/m/layers-of-the-skin). B) Micrograph showing different epidermal layers and part of the dermis (adapted from micrograph by Michigan medical school). C) Scheme showing SC structure and various modes of drug and particle transport namely intercellular (via the lipid matrix between corneocytes) and transcellular routes (across corneocytes and intercellular lipid matrix)[2].

present it to T cells in local lymph nodes. Hair follicles are a major feature in the skin forming about 0.5-2% of the skin surface area[71] and play an important role in skin permeation of various substances. It has been well documented that their invaginated structure is a site for accumulation and storage of substances including NPs[72-74]. The base of the hair follicle is located in the dermis and is connected to the blood and lymph systems through which NPs can potentially be shuttled into systemic circulation[75,76].

### 1.5.2 Nanoparticle Interaction with Skin

Aging, chemical, and physical stressors can cause a skin barrier disruption resulting in the skin becoming susceptible to environmental insults. Immersing the SC in water causes the intercellular lipid complex to be disrupted resulting in the SC being more permeable to polar molecules and tropically applied drugs[77]. Skin extraction using solvents such as acetone can leech lipids and proteins causing a barrier disruption[78]. In addition, although the SC is resistant to injury, the cellular component of the skin predominantly the basal keratinocytes are not. Injuries to the skin via exposure to UVA, UVB, and other radiation can cause a barrier defect with abnormal transepidermal water loss and triggers an inflammatory response with production of cytokines and prostaglandins[79,80]. Tape stripping, which is an accepted method of inducing barrier disruption, has also been used to study skin penetration of various compounds including NPs[72,81-84]. This involves repeated pressing and removal of tape from skin to physically remove the upper layers of the SC and corneocytes. Understanding the fate and transport of NPs that contact skin has been an area of active research in the fields of toxicology and for therapeutic applications. Various types of nanomaterials have been extensively

studied in terms of their skin penetration potential including metals[70,85], metal oxides[86,87], carbon-based NPs[88], silica[89] and semiconductor nanomaterials[23,25,26]. A very expansive literature collection fails, however, to draw a general conclusion regarding the penetration profiles of NPs through skin. This can be attributed to the wide variety of NP types used, *ex vivo* models, animal models, skin barrier status being intact or disrupted, and the limitations and sensitivity of the analytical and detection techniques employed. This thesis will be limited in scope to discussing studies pertaining to skin interaction with NPs namely $TiO_2$, ZnO, QDs, iron NPs, beryllium NPs and Au NPs.

Tan et al., conducted one of the first studies in the field where nanosized $TiO_2$-containing sunscreen was applied onto excised human skin for 2-6 weeks, following which inductively coupled mass spectroscopy (ICP-MS) was used to detect $TiO_2$ successfully in the lower epidermis. Upon excluding one extreme value from cadaver samples, the authors found a significant increase in the level of $TiO_2$ NPs in the dermis of skin[87]. Another study showed presence of nanosized $TiO_2$ in the dermis of rabbit skin when applied as a castor oil suspension whereas an aqueous solution did not[90]. $TiO_2$ water/oil (w/o) emulsions applied to *ex vivo* human skin found that the emulsion remained on the SC[91] while $TiO_2$/ZnO formulations (80-200 nm) applied *in vitro* on porcine skin for 24 h showed no penetration[28]. However, 20 nm $TiO_2$ NPs in a w/o emulsion applied for 5 h *in vitro* on human skin showed no penetration into the viable epidermal layers whereas $TiO_2$ oil/water (o/w) emulsions applied to *in vitro* human cultures for 24 h showed penetration evidence. This was further supported by a study where $TiO_2$ NPs in an o/w suspension and aqueous solution were applied and the SC was

tape stripped and the $TiO_2$ content on the tape was determined. It was found that more $TiO_2$ were found in the upper layers when applied as an o/w suspension than the aqueous suspension. This penetration was also enhanced by 10-fold when applied on hairy skin suggesting that hair follicles could be a route of NP penetration[86,92]. Menzel et al., on the contrary, suggested that hair follicles might not be important for penetration but were able to detect four different formulations of $TiO_2$ in the SC and stratum granulosum (SG) using ion beam analysis[93]. Upon compromising the skin barrier, NPs have been found to penetrate the skin[94], and specifically, $TiO_2$ has been found to penetrate the disorganized SC of psoriatic skin than normal skin but did not reach the viable epidermis. However, Monteiro Riviere et al., found that topical application of $TiO_2$-containing sunscreens to UVB-compromised pig skin resulted in no evidence of systemic absorption and $TiO_2$ to be localized in the upper layers of the SC in both normal and UVB treated skin, and slightly more penetration in the case of barrier defected skin[10].

While *ex vivo* topical application studies of $TiO_2$ on skin shows limited penetration through skin (confined to the upper layers of SC), it is important to consider the effects of repeated application in addition to UV-mediated barrier disrupted skin to mimic the event of chronic exposure of NPs to humans. This was achieved via repeated dermal exposure of nano-$TiO_2$ to a porcine model, which presented very different results[13]. It is well known that the structure and morphology of porcine skin is very similar to that of humans[28,95]. In this study, dermal exposures of 5% (amount of $TiO_2$ NPs in formulation)$TiO_2$ NP (4 and 60 nm) for 30 days showed that the particles can penetrate the SC, reach deeper epidermal layers even up to the basal cell layer, and that

the penetration was size dependent (smaller NP reach deeper layers). The same group also performed tissue distribution studies with BALB/c hairless mice where after 60 days of repeated exposure to nano-$TiO_2$ (Degussa P25, 21 nm, also used in this thesis) showed localization to various organs including liver, spleen, heart, lung and even the brain. Effects of repeated topical application of $TiO_2$ NP have been considered in other studies as well. Sadrieh et al., applied three different $TiO_2$-containing sunscreen formulations to minipigs for 22 days and found $TiO_2$ to be localized in the upper SC layers and follicular lumen using transmission electron microscopy (TEM) and energy dispersive X-ray spectroscopy (EDX). The group also found scattered particles in the dermis, which they rendered as contamination[86].

ZnO NPs are often studied in conjunction with $TiO_2$ NPs and have been found to penetrate the skin minimally even under the conditions where the skin barrier was disrupted using UV radiation (UVR)[10]. Other studies have shown almost no evidence of penetration of ZnO NP beyond the SC upon application to the forearms of human volunteers and the particles to be predominantly localized on the surface of the SC[96].

QDs have been used as a model NP by researchers in the context of NP skin penetration where their fluorescence can be used to track their location in the tissue. Modifying their surface chemistry with carboxyl moieties renders them to have a similar negatively charged surface chemistry to $TiO_2$ NPs, and have been the choice of particle for studying skin interaction of nanomaterials for many decades. Researchers have studied QD-skin interaction using a variety of QDs varying in size, shape, charge and surface chemistry on different animal models. Studies involving *ex vivo* porcine skin

using polyethlylene glycol (PEG)-coated neutrally charged QDs (40 nm hydrodynamic diameter[22]), *ex vivo* rat skin using negatively charged carboxylated QDs (round and ellipsoid of sizes 14 and 18 nm hydrodynamic diameter[84]), *ex vivo* human skin using negatively charged carboxylated QDs (round, 14 nm hydrodynamic diameter[26], *in vivo* SKH-1 hairless mouse skin with PEG-ylated nail-shaped QD (40 nm hydrodynamic diameter[94]) have supported the absence of QD penetration through intact skin. However, research in our lab[26] using depilatory agents to remove hair from an *ex vivo* human skin model or tape stripping the skin, and others[97] using low frequency sonophoresis in a porcine skin model, all inducing a barrier defect in the process have shown a substantial increase in QD penetration compared to intact skin. The effect of barrier impaired skin on NP penetration has also been studied by quantifying systemic levels of NPs *in vivo* in studies employing animal models.

Elemental analysis studies of PEG-ylated QDs (nail-shaped, CdSe/CdS core/shell, 37 nm) through dermabraded SKH-hairless mice skin showed that ~2% of the applied dose accumulated in the liver 48 h post-exposure[94]. This is higher than the systemic levels of negatively charged DHLA QDs (sphere-shaped, CdSe/ZnS core/shell, 14 nm) from studies conducted in our lab, which showed <0.001% of the applied dose to be localized in the lymph nodes of mice 24 h after UVB radiation exposure[25], which may suggest an effect of surface charge[5]. This is consistent with an *in vivo* human study which quantified systemic Zn levels in blood to be <0.001% of the applied dose following repeated application of ZnO NP-containing sunscreen to UVR-exposed skin[98]. Other NPs such as iron NPs and Au have also been implied in the context of skin

penetration. Baroli et al., found that 10 nm rigid iron NPs were able to passively penetrate full-thickness human skin through SC lipidic matrix and hair follicle orifices and reached the deepest layer of the SC and SG, and even found in small amounts in the viable epidermis[99]. They claimed that their results were in accordance with another work[100] studying penetration of rigid particles through skin (100-130 nm size) where rigid particles were only found in the superficial layers of the SC. The authors conclude that the extremely small dimensions of iron NPs might have been responsible for exceptionally deeper penetration in the viable epidermis. Tinkle et al., in this context however, reported that berryllium oxide particles of size ranging from 0.5-1 μm could penetrate the SC and reach the epidermal layers and occasionally the dermis only when a flexing-like motion was applied on the skin surface[70]. Au NPs have also been shown to be able to penetrate healthy intact skin in a particular size range. Au NPs of 15 nm hydrodynamic diameter were able to penetrate *ex vivo* rat skin[85], whereas particles of sizes 102 and 198 nm hydrodynamic diameter could not. Considering the above studies, despite the availability of significant amount of literature evidences warranting the ability of NPs to more efficiently penetrate barrier disrupted skin than intact healthy skin, some challenges need to be overcome in order to draw definitive conclusions from all the skin penetration studies of hard, insoluble metallic NPs.

## 1.6 Thesis Motivation

The development of more sensitive techniques and new assays that can be exploited to detect intact NPs in skin and organs have been indicated as a key challenge to advancing

the field of nanotoxicology and nanomedicine[5,10,101]. While all the penetration studies discussed above show ability of NPs to penetrate barrier disrupted skin, some contrasting reports exist. For example, Zhang et al.,[22] and Gopee et al.,[94] have conducted research suing PEG-ylated QDs on *ex vivo* rat skin and *in vivo* mouse skin and have shown that tape stripping, although a well-accepted technique for causing barrier disruption has no impact on QD skin penetration. Other techniques of inducing barrier disruption including abrasion and mechanical flexing have been used. Skin abrasion is often used in clinical settings for skin resurfacing and drug delivery[102,103] where the SC and the epidermis are almost removed completely to allow free access of penetrating substances to the dermal vasculature. Skin flexion is a method that simulates flexing movements (eg. repetitive wrist bending). It was found that QDs penetrated abraded skin but not flexed skin, as there were no differences when compared to a non-flexed control. Barring minute details in the method of barrier disruption, the detection techniques employed in each case is different resulting in different sensitivities of the NP study. In $TiO_2$ and ZnO NP skin penetration studies conducted by Monteiro-Riviere et al., it was found that TEM and tissue histology results suggest that NPs predominantly localize as aggregates on the skin surface when using intact skin and that UVR exposure slightly enhances penetration into the deeper SC layers. However, upon using a more sensitive technique albeit with a low spatial resolution namely time-of-flight secondary ion mass spectrometry (TOF-SIMS), higher levels of both elemental Ti and Zn was found in the epidermal layers[10], which emphasizes on the importance of considering the detection sensitivity of the analytical technique employed to detect NPs (detection limit may be too high to detect low levels of

NP absorption). A wide variety of NP detection techniques are employed including mass spectrometry, wide-field fluorescent microscopy, TEM confocal microscopy (occasionally with additional capabilities like raman spectroscopy or time delay gating) and various forms of multiphoton microscopy.

### 1.6.1 Limitations of Current Nanoparticle Detection Techniques

Mass spectrometry has been widely used, mainly for its good sensitivity, however, it is a destructive technique and can only be used on whole organs or skin that has already been separated into transverse layers (eg. using tape stripping[82]) at the time of completion of the experiment to obtain a depth penetration report of NPs. Although this technique has an advantage of quantification, it does not provide localization information of NPs in skin (hair follicles, skin cellular structures) or skin layer (SC, terminally differentiating epidermis, basal membrane or dermis)[101].

Conventional TEM is widely and frequently used to characterize NP structure[104,105] and to demonstrate intracellular localization of NP[106,107] due to its superior nanoscale resolution and elemental detection capability (with add-ins). However, some limitations of this technique include long times, cost of processing, and sampling error. The thickness of slices analyzed by TEM is typically around 70-100 nm which makes it difficult to achieve a large sampling area; ~1000 slices need to be analyzed to completely sample 1 $mm^2$ of skin[101]. Therefore, NPs present at low levels in tissue may be missed due to limited sample analysis throughput. Furthermore, NP can sometimes be indistinguishable from cellular structures of the same size range. For example, $TiO_2$ NPs which are electron dense can show similarity with glycogen granules or ribosomes

whereas electron lucent particles such as polystyrene may be confused with spherical cellular structures[108,109]. This poses a technical bias, which using conventional TEM alone cannot be overcome. Since quantification of TEM results are difficult, most of the data analyzed are reported as supporting data[23,97,110] and without further proof of particle identity. Baroli et al., have also concluded in their studies that TEM may not be the elective method to study penetration of metallic NPs. Although attempts were made to visualize the NPs (iron NPs) in this study at a magnification of up to 200,000X, the authors reported discriminating between the NPs and the skin structure to be a challenge. Electron dense structures present in the sample and not in the control led them to believe that the deposits could be iron NPs; however the authors concluded that corneodesmosomes and other natural components of intercorneal space similar in morphology could render the presence of iron NP deposits as questionable[99]. Further proof for presence of iron NPs in this study had to be obtained using a scanning electron microscope (SEM) equipped with an energy dispersive X-ray spectrometer (EDX).

Despite its wide use, data from TEM needs to be accompanied by methods that allow identification of every NP independent of size, shape and electron transmissibility[108]. A colloidal silver strategy has been developed to image NPs better using TEM[111]. In this, colloidal silver selectively deposits onto semiconductor/metal NPs to produce larger particles that can be more readily distinguished from other spurious dark features using the EDX technique. We have reported in previous work using this technique higher QD presence in the viable epidermis compared to histological analysis using fluorescence microscopy[23,101]. In studies focusing on NP interaction with

lung tissue, one problem is the inability to distinguish between cellular structures and NP. Energy filtered TEM (EFTEM) combines high resolution of TEM with electron energy loss spectroscopy which allows analysis and visualization of the spatial distribution of elemental composition of the particle[112]. NPs often contain elements such as Ti, Zn or Cd with no or low abundance in the living system. This differential atomic composition allows elemental mapping, and therefore of NP. This technique however, requires substantial technical expertise and a suitable microscope and hence is not widely established in life sciences. Furthermore, EFTEM is not efficient if the NP atomic composition is unknown or if the NP contains elements occurring in large amounts in biological systems.

Confocal microscopy and wide-field fluorescence microscopy are also widely used in order to detect NPs in tissues. For QD imaging, the brightness is adjusted by laser wavelength and output band pass filter. While these techniques allow for background noise reduction, tissue autofluorescence poses a significant challenge to image fluorescence NPs, such as QDs, and detect them conclusively from surrounding tissue features.

*In vivo* NP presence is quantified by elemental organ analysis, which is typically performed on digested organs and tissues using techniques such as atomic absorption spectroscopy (AAS) or ICP-MS. The tissue digestion process, however, obfuscates the ability to distinguish the transport of intact NPs from soluble ion transport[5]. For example, in the study by Gulson et al.,[98] it was unclear whether $^{68}$Zn used in the study (ZnO NP-containing sunscreen) was absorbed as ZnO NP or Zn ion in the case where

small increases of Zn were found in blood and urine of the human subjects in the study following UVR exposure. For some elements, the detection may also be masked by interference from trace metals or from endogenous elements such as carbon. For example, while Monteiro-Riviere et al., found in their flow-through studies in a porcine model that although TEM only detected ZnO on the surface of the SC in both intact and barrier disrupted skin[10], ICP-MS analysis of the perfusate found Zn in all samples as reported by Cross et al[113]. This is expected since Zn is the most abundant trace metal ion after iron and is ubiquitous in the body, especially in skin, and also is found in powdered gloves, glass and stainless steel[10,114]. The isotopic enrichment method described by Gulson et al.,[98] can be used to eliminate the uncertainty pertaining to background levels of trace elements; however, this method is prohibitively expensive and therefore impractical for routine NP studies.

Taken together, this suggests an urgent need for compositional analysis techniques and detection systems which can provide information on NP presence and form. The use of immunogold labeling has been described in the context of detecting and differentiating NPs from cellular organelles with the aid of TEM[108]. In this method, antigens are made visual by labeling them with a primary antibody, which in turn is visualized by a secondary antibody conjugated to colloidal Au NPs of a defined size. These Au NPs are visible under TEM due to their electron density and in contrast to light microscopy, allow determining the localization of antigens in the subcellular structures at the nanometer range. This concept can further be applied to nanostructures, where development of a probe such as an antibody or a protein that can bind the NP will allow

bio-recognition using a secondary reporter or an antibody. However, the availability of such recognition molecules for nanostructures is limited[115]. To this end, this thesis focuses on developing antibodies reagents (single-chain variable fragment (scFvs)) that bind intact whole NPs, which will further allow us to qualitatively detect NP presence and form at the same time using phage display technology. These antibodies function similar to those used in conventional immunohistochemistry (IHC) and can detect NPs in a biological milieu even when surrounded by a protein corona which in turn is dictated by the NP surface chemistry. Prior reports suggesting a development of an immune response in mice to carbon-based and $TiO_2$ NPs[116,117] and isolation of peptides capable of binding NPs[118-120] indicate that antibodies (scFvs) can indeed be isolated from a library of bio-recognition molecules such as antibodies. While little is known currently about the ability of the immune system to recognize NPs[121,122], NP immunogenicity is not a requirement for enrichment of scFv binders through in vitro phage display technology. This is the first time antibodies to NPs such as QDs and $TiO_2$ have been isolated and tested for their binding to NPs *in vitro* and in a biological milieu. This approach when used in conjunction with to the existing techniques to quantify the dosage of NPs, will serve as a powerful universal tool to detect and understand NP behavior and interaction in biological systems and the environment. The phage display technology used to isolate the scFvs has been discussed next.

# 1.7 Phage Display

## 1.7.1 Introduction

In this thesis, phage display will be used to isolate scFv antibodies against QDs and $TiO_2$ NPs. Phage display technology was first introduced by George Smith in 1985. Phages are viruses that infect bacterial cells and many of the widely used vectors in recombinant DNA research are phages that infect the host, bacterium *Escherichia coli* (E.coli). Phage display is the term used to describe the presentation of proteins, peptides or antibody libraries on the surface of a filamentous phage which leads to the selection of the displayed entity with high binding capability and specificity to almost any target[123]. A large number of such phage display libraries have been constructed and used[124-126]. The technology is widely used in the fields of cell biology, pharmacology, immunology and drug discovery. The key feature of recombinant DNA vectors including phages is their ability to accommodate foreign pieces of DNA which are natural (eg. human) or chemically synthesized. The foreign DNA replicates when the vector DNA does in the host. In a phage display vector, the foreign DNA is expressed as a protein and upon incorporating the genetic sequence encoding the foreign DNA as a fusion to the genetic sequence encoding one of the phage coat proteins, the expressed protein is displayed on the surface of the phage coat protein. All the phage particles released from the *E.coli* host will have the 'hybrid' coat protein thus displaying the protein (or antibody) of interest. A phage display library is a heterogeneous mix of such phage particles (clones) each carrying a unique foreign DNA and thus displaying a unique protein on its surface[126].

Phage particles can withstand harsh conditions such as low pH, low temperature without losing bacterial infectivity[123]. Therefore, low pH is used to dissociate a bound phage from its target. The strength of the technology lies in its ability to identify interactive regions of proteins and other molecules without preexisting notions about the nature of the interaction[123].

### 1.7.2 Phage Display Applications

Phage display of peptides and antibodies has been implicated in a variety of applications. Since more than 80% of cellular proteins work in conjunction or as complexes with other proteins, phage display has been used to study protein-protein interactions[127-129], and in identifying novel interacting partners of proteins[130]. Phage display has also been used in enzymology to study substrate specificity[131,132] to display mutant enzymes in order to study their mechanism of action[133], and identification of substrates to proteases[131]. Phage display has been used to select stably folded proteins despite containing protease substrate sites. Such selections can be used to link the protein sequence to its structure and help engineer proteins with improved folding and stability[134]. Peptide inhibitors to anthrax toxin have also been developed using phage display, which can further give information on the mechanism of cytotoxicity of the toxin[135]. Identification of epitopes of an antigen involved in antibody interaction has been mapped using phage display. Both libraries displaying peptides and gene fragments have been used[136,137], where gene fragment libraries are useful in identifying epitopes that adopt a structural conformation or are longer[138]. Mimotopes, which are peptides mimicking discontinuous epitope structures can be affinity selected using phage display[130]. Peptide phage display libraries

have also been used to select against targets like G-protein coupled receptors. Antibodies specific to the receptor ligand can be used as a target to select mimotopes from the library, which then can be used to study the binding mechanism and interaction of ligand with the receptor to develop powerful agonists or antagonists[139]. Phage display has also found applications in material science and photovoltaics. The Belcher group[140] has shown the selection of peptides through phage display that bind to semiconductor surfaces with high specificity depending on orientation and composition of the material. These peptides allow the controlled placement and assembly of structurally similar materials thus broadening the scope for 'bottom-up' fabrication of electronic devices. The same group has also shown the incorporation of single-walled carbon nanotubes (SWCNTs) into nanocomposites to create efficient photovoltaic devices using phage display. The SWCNT-$TiO_2$ nanocomposite generated using genetically modified filamentous phage M13 was used as a photoanode in solar cells, where even small fractions of nanotubes improve the power conversion efficiency by increasing the electron collection efficiency[141]. Phage display of antibody fragments has been successfully used to generate antibodies which have found use in multiple fields including proteomics, diagnostics approaches, immunotherapy and vaccine development; this has been discussed next.

### 1.7.3 Antibody Phage Display

The first uses of phage display focused on peptides[136,142], in which displayed peptides were fused to one of the phage coat proteins. Peptides recognizing numerous inorganic materials including metals[143], semiconductors[140,144] and NPs[118,119,137] have been

reported using commercially available peptide libraries (eg. New England BioLabs). The majority of this work has been dedicated to forming controlled NP-phage assembly structures for novel device fabrication as discussed in detail above. However, antibody phage display has arguably been one of the more successful uses of phage display[145]. This is because peptide libraries are limited in amino acid sequence which can pose a structural constraint on binding affinity. Moreover, antibody display libraries yield high affinity and specificity binders due to the increased size of interaction surface and rigidity of the scaffold as opposed to a floppy peptide.

The production of monoclonal antibodies (mAbs) for research and clinical use has been revolutionized by the use of phage display[146]. Traditionally this process involved immunizing animals with the desired antigen and the use of hybridoma technology to generate mAb clones. However, with the advent of phage display of antibody fragments, the time to isolate a defined antibody has been reduced to about couple of weeks[147]. Additionally, antibodies with affinities comparable to those obtained using hybridoma technology can be selected from large antibody libraries and their affinity can be further increased through a variety of mutagenesis strategies[148,149]. A large number of scFv and fragment antigen binding (Fab) repertoires have been generated using phage display[150]. While mAbs are composed of two 50 kDa heavy chains and two 25 kDa light chains linked by disulphide bonds to form a Y-shaped molecule, scFvs are composed of a heavy and a light chain connected by a linker (Figure 1.2A). This thesis will focus on the use of a scFv library to generate antibodies with specificity towards different NPs.

Expression of scFvs in *E.coli* ensures that sufficient quantities of scFvs are produ-

ced for screening and characterization with relative ease. Moreover, antibodies to toxic targets such as doxorubicin can be obtained, which is a difficult task with immunization/hybridoma techniques[151]. Antibody libraries can be constructed either from a natural repertoire (immunized, or non-immunized (naïve)) of a B-cell population or synthetically. Naïve human antibody libraries are constructed from mRNA from human donors (typically >100 donors) cell source (eg. peripheral blood lymphocytes and/or bone marrow), which is reverse transcribed into cDNA followed by polymerase chain-reaction (PCR) with specific primers in order to amplify the $V_H$ and $V_L$ segments from the cDNA template, and linked together with a synthetic linker sequence (usually ~15 amino acids (aa) in length). The assembled segments are cloned into a phagemid display vector, which is then transformed into *E.coli* cells to generate the antibody repertoire. Upon electroporation, libraries with $10^8$-$10^{11}$ unique antibodies can be constructed. While an antibody repertoire formed from immunized donors is limited to generating antibodies to the antigen of the original response, naïve libraries can be used against a wide variety of antigens. In contrast, synthetic libraries contain defined frameworks with variable residues introduced using synthetic oligonucleotides.

### 1.7.4 M13 Phage Biology

M13 (or Fd) used in this thesis project is a filamentous bacteriophage. It is cylindrical in shape and 6-7 nm in diameter and ~1 μm long[152]. It contains a single-stranded DNA, which encodes 11 genes[153], 5 of them being coat proteins. The major coat protein is gene VIII protein (gVIIIp), which is present at about 2700 copies per particle encapsulating the DNA. The distal end is capped by gVIIp and gIXp. At the proximal end

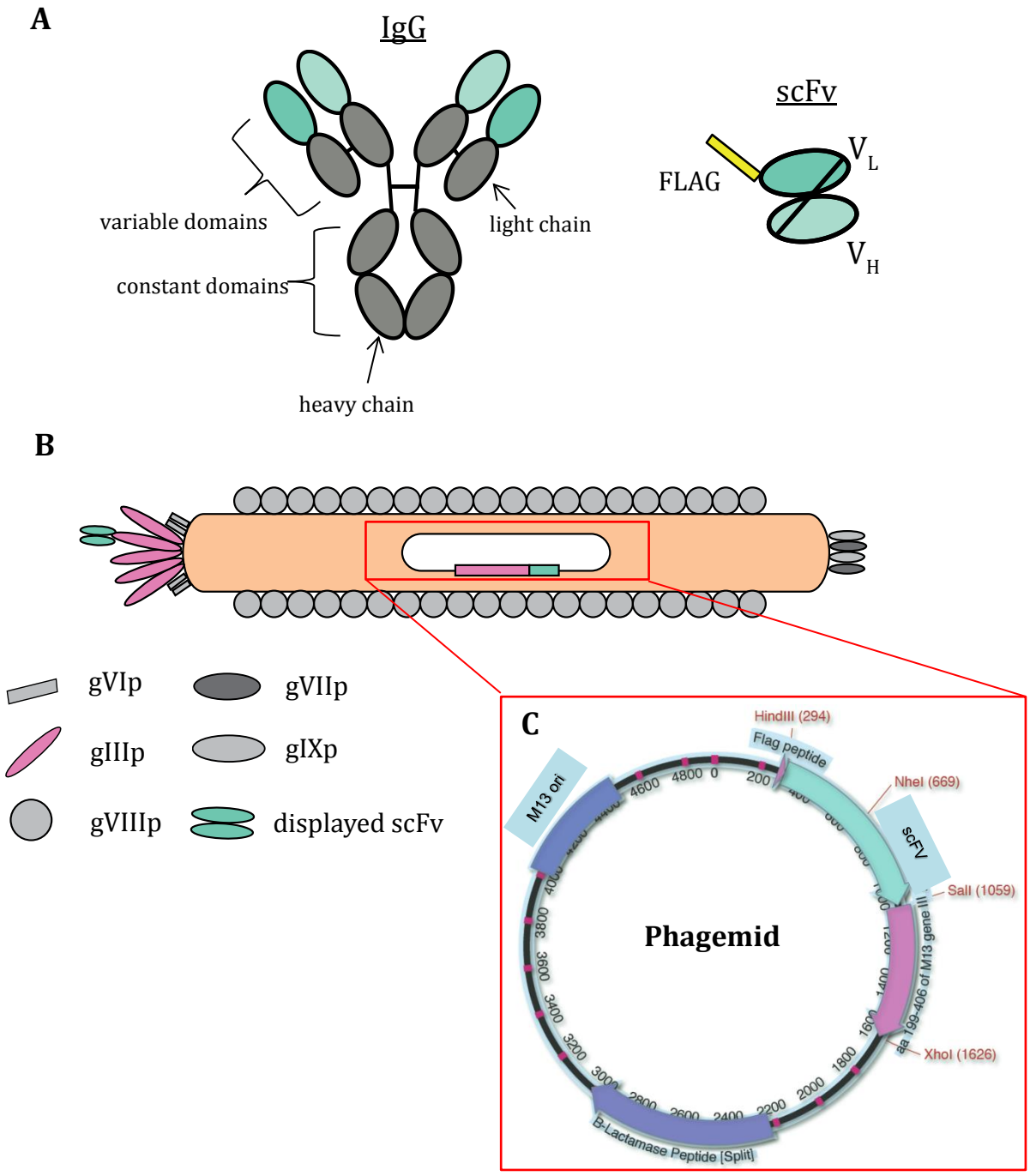


**Figure 1.2: Components of a Phage Display System**

A) A whole antibody (IgG) molecule and scFv molecule (heavy and light chain connected by a linker). B) M13 filamentous phage displaying scFv on the gene III coat protein. The phagemid containing the gene encoding the scFv fused to gene III has been highlighted in the blue box and C) detailed description of phagemid vector containing M13 origin of replication, antibiotic resistance and FLAG tag-containing scFv fused to gene III of M13.

3-5 copies each of gIIIp and gVIp exists (Figure 1.2B). The function of gIIIp is well studied; it is essential for phage infection and phage particle release following assembly in the host[154]. Phages infect male *E.coli* that bears the F.pilus through gIIIp. The gIIIp has a tripartite structure composed of three domains separated by glycine-rich regions (G1, G2): two exposed N-terminal domains (N1, N2) that binds F.pilus and enables phage entry into the bacterial cell and the buried C-terminal domain, which is an integral part of the capsid structure and is associated with phage morphogenesis[126,155]. No specific function apart from passive connectors of the three domains has been ascribed for regions G1 and G2. However, it has been observed that they do provide the flexibility necessary to enhance the infectivity of phage[156]. Filamentous phages do not lyse the host cell, but are able to replicate and be released from the cell membrane while the host cell continues to grow and divide in contrast to lytic bacteriophages such as T4. The circular DNA enters the host cell and is converted by host DNA synthesizing machinery into the double-stranded plasmid replicative form. By rolling circle amplification, this replicative form produces single-stranded DNA which is then packaged into phage particles or 'virions' and extruded from the cell[157].

### 1.7.5 Phagemid Vectors and Monovalent Display

Phagemids are plasmids that contain a phage replication origin in addition to the plasmid replication origin, the phage coat protein fused with the gene of interest (antibody or peptide) and an antibody resistance marker (Figure 1.2C). In most display applications, including the one described in this thesis, gIIIp is used for antibody or peptide expression. Although the protein has a low copy number and antibodies have also been fused to

gVIIIp, in direct comparisons between gIIIp and gVIIIp, gIIIp has been found to be far more efficient[158]. In this work, the site at the N-terminus of gIIIp is used to display the scFv antibody introduced as a fusion protein. The scFv itself is engineered with a peptide FLAG tag (DYKDDDDKL) to enable secondary detection with anti-FLAG antibodies. Phagemids cannot produce infective phage without the addition of helper phage such as VCSM13 that provides the proteins necessary for phage replication and assembly, including the wild-type gIIIp used for display. Thus two types of progeny virions are produced: particles carrying wild-type phage DNA and those carrying the phagemid DNA. During bacterial infection stage, virions infect *E.coli* cells and upon selecting for antibiotic resistance, only the phages carrying the phagemid DNA (with gene III-scFv fusion protein) are recovered. In order to achieve monovalent display, low levels of gIIIp-scFv fusion expression is ensured and the degree of display was quantitatively observed to be about 1% (*in vitro* anti-FLAG antibody panning assay), while 99% of the packaged phagemid-containing phages do not display the scFv fusion protein (antibody). The assembled phage particle displaying an antibody contains both the genotype (phagemid) and the phenotype (gIIIp-scFv fusion), which is the key feature of phage display.

# 1.8 Thesis Approach

This doctoral thesis describes three primary areas:

I. Selection of scFv antibodies that can bind to commercially important NPs such as QDs and $TiO_2$ using phage display technology.

II. Studying and understanding the binding and cross-reactive properties of the developed antibodies through various *in vitro* assays in order to determine their versatility in detecting different NPs with the same composition and similar NPs with different composition.

III. Validating the antibodies for their function in *ex vivo* tissue studies to prove their applicability and efficacy in detecting NPs in both the environment and in tissues.

## 1.9 Thesis Organization

The goal of this thesis is to develop antibodies (scFvs) against commercially important intact NPs such as QDs and $TiO_2$ NPs for the first time, test their binding and specificity *in vitro* to these NPs, and validate their functionality *ex vivo* in human skin tissue. These reagents can then be used to give information about NP form and presence, and following quantification using existing techniques can comprise a powerful tool kit that can be used to better understand NP interaction with biological systems. The first chapter of all the results and research findings in this thesis entitled *'Identification of Phage Clones that Bind QDs and $TiO_2$ NPs, and Verification of Binding in vitro'* deals with the methods used to identify for the first time phage binders to GSH-QDs and $TiO_2$ NPs using phage display, and assays used to prove binding of the phage clones to NPs have been discussed. The next chapter is entitled *'In vitro Verification of Binding of Isolated scFvs with Affinity to QDs and $TiO_2$ NPs'*. Results discuss the proof-of-concept studies with purified scFv antibodies using custom-designed *in vitro* assays where the binder clones are shown to bind the NPs with specificity. Attempts to use the purified scFvs in

detecting NPs in an *ex vivo* human skin model has been discussed in the next chapter *'Verification of Binding of scFvs to NPs in a Biological Milieu'*. Results proved that using an enzymatic colorimetric reporting method, both fluorescent and non-fluorescent NPs could be detected using standard IHC techniques by the scFvs isolated against the NPs. Upon using elemental detection and SEM, the colored areas under brightfield were shown to contain NPs thereby proving that these antibodies could be used to detect NPs in tissue. The next chapter entitled *'Characterization of Binders and Challenges Associated with Discovery of Binders to NPs'* deals with characterization of the clones in terms of their binding and cross-reactivity properties to other NPs (similar and dissimilar NPs). The challenges involved in identifying binders to GSH-QDs using target immobilization techniques as conventionally used in phage display were investigated. Attempts to find a better binder to GSH-QDs were also made using chain shuffling experiments. Lastly, some preliminary attempts to identify binders to carbon-based nanomaterials have been discussed in the chapter entitled *'Isolation of Binders to Carbon-Based Nanomaterials'*. While potential binders from the phage display library were not identified, this chapter nevertheless paves way to the use of phage display in finding antibodies to some of the widely used commercially important nanomaterials such as CNTs. A summary of the research findings has been included as the final chapter entitled *'Conclusions and Future Directions'* in this thesis along with potential future directions that can lead to the use of these novel antibodies as a tool kit to expand our understanding of NP-tissue interactions.

# References

[1] http://www.bccresearch.com/market-research/biotechnology/nanoparticles-biotechnology-drug-development-delivery-bio113a.html.

[2] Barry, B. W. Mode of Action of Penetration Enhancers in Human Skin. *journal of controlled release,* **1987**, 6(1), 85-97.

[3] Jena M, M. S., Jena S, Mishra SS. Nanotechnology- Future Prospect in Recent Medicine: A Review. *Int J Basic Clin Pharmacol,* **2013**, 2, 353-359.

[4] Nanotechnology in Medicine: Huge Potential, but What Are the Risks. http://www.medicalnewstoday.com/articles/244972. php.

[5] DeLouise, L. A. Applications of Nanotechnology in Dermatology. *J Invest Dermatol,* **2012**, 132(3 Pt 2), 964-975.

[6] Iyer, A. K., Khaled, G. *et al.* Exploiting the Enhanced Permeability and Retention Effect for Tumor Targeting. *Drug Discov Today,* **2006**, 11(17-18), 812-818.

[7] Reubi, J. C. Peptide Receptors as Molecular Targets for Cancer Diagnosis and Therapy. *Endocr Rev,* **2003**, 24(4), 389-427.

[8] Endo, M., Hayashi, T. *et al.* Applications of Carbon Nanotubes in the Twenty-First Century. *Philos Trans A Math Phys Eng Sci*, **2004**, 362(1823), 2223-2238.

[9] Faunce, T., Murray, K. *et al.* Sunscreen Safety: The Precautionary Principle, the Australian Therapeutic Goods Administration and Nanoparticles in Sunscreens. *NanoEthics,* **2008**, 2(3), 231-240.

[10] Monteiro-Riviere, N. A., Wiench, K. *et al.* Safety Evaluation of Sunscreen Formulations Containing Titanium Dioxide and Zinc Oxide Nanoparticles in Uvb Sunburned Skin: An in Vitro and in Vivo Study. *Toxicol Sci*, **2011**, 123(1), 264-280.

[11] Blue Lizard Sunscreens, Crown Laboratories, Inc., . Johnson City, TN.

[12] Lane, M. E. Nanoparticles and the Skin--Applications and Limitations. *J Microencapsul,* **2011**, 28(8), 709-716.

[13] Wu, J., Liu, W. *et al.* Toxicity and Penetration of $Tio_2$ Nanoparticles in Hairless Mice and Porcine Skin after Subchronic Dermal Exposure. *Toxicol Lett*, **2009**, 191(1), 1-8.

[14] Szakal, C., Roberts, S. M. *et al.* Measurement of Nanomaterials in Foods: Integrative Consideration of Challenges and Future Prospects. *ACS Nano*, **2014**, 8(4), 3128-3135.

[15] The Royal Society and the Royal Academy of Engineering. Nanoscience and Nanotechnologies: Opportunities and Uncertainties. Royal Society, 2004.

[16] Wellesley. Quantum Dots: Global Market Growth and Future Commercial Prospects. Report No. NAN027D, (April 2014).

[17] Qian, H., Dong, C. *et al.* Facile One-Pot Synthesis of Luminescent, Water-Soluble, and Biocompatible Glutathione-Coated Cdte Nanocrystals. *Small*, **2006**, 2(6), 747-751.

[18] Zhang, F., Yi, D. *et al.* Cadmium-Based Quantum Dots: Preparation, Surface Modification, and Applications. *J Nanosci Nanotechnol*, **2014**, 14(2), 1409-1424.

[19] Zheng, H., Mortensen, L. J. & DeLouise, L. A. Thiol Antioxidant-Functionalized Cdse/Zns Quantum Dots: Synthesis, Characterization, Cytotoxicity. *J Biomed Nanotechnol*, **2013**, 9(3), 382-392.

[20] Choi, H. S., Ipe, B. I. *et al.* Tissue- and Organ-Selective Biodistribution of Nir Fluorescent Quantum Dots. *Nano Lett*, **2009**, 9(6), 2354-2359.

[21] Clapp, A. R., Goldman, E. R. & Mattoussi, H. Capping of Cdse-Zns Quantum Dots with Dhla and Subsequent Conjugation with Proteins. *Nat Protoc*, **2006**, 1(3), 1258-1266.

[22] Monteiro-Riviere, N. A., Zhang, L. W. in *Nanomaterials: Risks and Benefits* (2009).

[23] Mortensen, L. J., Oberdorster, G. *et al.* In Vivo Skin Penetration of Quantum Dot Nanoparticles in the Murine Model: The Effect of Uvr. *Nano Lett*, **2008**, 8(9), 2779-2787.

[24] Mortensen, L. J., Ravichandran, S. & Delouise, L. A. The Impact of Uvb Exposure and Differentiation State of Primary Keratinocytes on Their Interaction with Quantum Dots. *Nanotoxicology,* **2012**,

[25] Mortensen, L. J., Jatana, S. *et al.* Quantification of Quantum Dot Murine Skin Penetration with Uvr Barrier Impairment. *Nanotoxicology,* **2013**, 7(8), 1386-1398.

[26] Ravichandran, S., Mortensen, L. J. & DeLouise, L. A. Quantification of Human Skin Barrier Function and Susceptibility to Quantum Dot Skin Penetration. *Nanotoxicology,* **2011**, 5, 675-686.

[27] Maysinger, D., Lovric, J. *et al.* Fate of Micelles and Quantum Dots in Cells. *European journal of pharmaceutics and biopharmaceutics : official journal of Arbeitsgemeinschaft fur Pharmazeutische Verfahrenstechnik e.V,* **2007**, 65(3), 270-281.

[28] Gamer, A. O., Leibold, E. & van Ravenzwaay, B. The in Vitro Absorption of Microfine Zinc Oxide and Titanium Dioxide through Porcine Skin. *Toxicol In Vitro,* **2006**, 20(3), 301-307.

[29] Weir, A., Westerhoff, P. *et al.* Titanium Dioxide Nanoparticles in Food and Personal Care Products. *Environ Sci Technol,* **2012**, 46(4), 2242-2250.

[30] Icis Titanium Dioxide Uses and Market. http://www.icis.com/ Articles/2007/11/07/9076546/titanium-dioxide-tio2-uses-andmarket-data.html (June 1st, 2011).

[31] Mahshid, S., Askari, M. & Ghamsari, M. S. Synthesis of Tio2 Nanoparticles by Hydrolysis and Peptization of Titanium Isopropoxide Solution. *Journal of Materials Processing Technology,* **2007**, 189(1–3), 296-300.

[32] Carlotti, M. E., Ugazio, E. *et al.* Role of Particle Coating in Controlling Skin Damage Photoinduced by Titania Nanoparticles. *Free Radic Res,* **2009**, 43(3), 312-322.

[33] Labille, J., Feng, J. *et al.* Aging of Tio(2) Nanocomposites Used in Sunscreen. Dispersion and Fate of the Degradation Products in Aqueous Environment. *Environ Pollut,* **2010**, 158(12), 3482-3489.

[34] Kiser, M. A., Westerhoff, P. *et al.* Titanium Nanomaterial Removal and Release from Wastewater Treatment Plants. *Environ Sci Technol,* **2009**, 43(17), 6757-6763.

[35] Westerhoff, P., Song, G. *et al.* Occurrence and Removal of Titanium at Full Scale Wastewater Treatment Plants: Implications for Tio2 Nanomaterials. *J Environ Monit,* **2011**, 13(5), 1195-1203.

[36] Zhang, Y., Chen, Y. *et al.* Stability of Commercial Metal Oxide Nanoparticles in Water. *Water Res,* **2008**, 42(8-9), 2204-2212.

[37] Oberdorster, G., Oberdorster, E. & Oberdorster, J. Nanotoxicology: An Emerging Discipline Evolving from Studies of Ultrafine Particles. *Environ Health Perspect,* **2005**, 113(7), 823-839.

[38] de Haar, C., Hassing, I. *et al.* Ultrafine but Not Fine Particulate Matter Causes Airway Inflammation and Allergic Airway Sensitization to Co-Administered Antigen in Mice. *Clin Exp Allergy,* **2006**, 36(11), 1469-1479.

[39] Renwick, L. C., Brown, D. *et al.* Increased Inflammation and Altered Macrophage Chemotactic Responses Caused by Two Ultrafine Particle Types. *Occup Environ Med*, **2004**, 61(5), 442-447.

[40] Peters, A., Wichmann, H. E. *et al.* Respiratory Effects Are Associated with the Number of Ultrafine Particles. *Am J Respir Crit Care Med,* **1997**, 155(4), 1376-1383.

[41] Schulz, H., Harder, V. *et al.* Cardiovascular Effects of Fine and Ultrafine Particles. *J Aerosol Med,* **2005**, 18(1), 1-22.

[42] Fu, P. P., Xia, Q. *et al.* Mechanisms of Nanotoxicity: Generation of Reactive Oxygen Species. *J Food Drug Anal,* **2014**, 22(1), 64-75.

[43] Nel, A., Xia, T. *et al.* Toxic Potential of Materials at the Nanolevel. *Science,* **2006**, 311(5761), 622-627.

[44] Zhu, X., Hondroulis, E. *et al.* Biosensing Approaches for Rapid Genotoxicity and Cytotoxicity Assays Upon Nanomaterial Exposure. *Small,* **2013**, 9(9-10), 1821-1830.

[45] Bottrill, M. & Green, M. Some Aspects of Quantum Dot Toxicity. *Chem Commun (Camb),* **2011**, 47(25), 7039-7050.

[46] Lynch, I., Dawson, K. A. & Linse, S. Detecting Cryptic Epitopes Created by Nanoparticles. *Sci STKE,* **2006**, 2006(327), pe14.

[47] AshaRani, P. V., Low Kah Mun, G. *et al.* Cytotoxicity and Genotoxicity of Silver Nanoparticles in Human Cells. *ACS Nano,* **2009**, 3(2), 279-290.

[48] Hardman, R. A Toxicologic Review of Quantum Dots: Toxicity Depends on Physicochemical and Environmental Factors. *Environmental Health Perspectives,* **2006**, 114(2), 165-172.

[49] Kondoh, M., Araragi, S. *et al.* Cadmium Induces Apoptosis Partly Via Caspase-9 Activation in Hl-60 Cells. *Toxicology,* **2002**, 170(1-2), 111-117.

[50] Saquib, Q., Al-Khedhairy, A. A. *et al.* Titanium Dioxide Nanoparticles Induced Cytotoxicity, Oxidative Stress and DNA Damage in Human Amnion Epithelial (Wish) Cells. *Toxicol In Vitro,* **2012**, 26(2), 351-361.

[51] Yin, J. J., Liu, J. *et al.* Phototoxicity of Nano Titanium Dioxides in Hacat Keratinocytes--Generation of Reactive Oxygen Species and Cell Damage. *Toxicol Appl Pharmacol,* **2012**, 263(1), 81-88.

[52] Adachi, K., Yamada, N. *et al.* Subchronic Exposure of Titanium Dioxide Nanoparticles to Hairless Rat Skin. *Exp Dermatol,* **2013**, 22(4), 278-283.

[53] Ccohs Titanium Dioxide Classified as Possibly Carcinogenic to Humans. http://www.ccohs.ca/headlines/text186.html (accessed May 2011 ).

[54] Hussain, S., Vanoirbeek, J. A. *et al.* Lung Exposure to Nanoparticles Modulates an Asthmatic Response in a Mouse Model. *Eur Respir J,* **2011**, 37(2), 299-309.

[55] Lomer, M. C., Thompson, R. P. & Powell, J. J. Fine and Ultrafine Particles of the Diet: Influence on the Mucosal Immune Response and Association with Crohn's Disease. *Proc Nutr Soc,* **2002**, 61(1), 123-130.

[56] Mahto, S. K., Yoon, T. H. & Rhee, S. W. A New Perspective on in Vitro Assessment Method for Evaluating Quantum Dot Toxicity by Using Microfluidics Technology. *Biomicrofluidics,* **2010**, 4(3),

[57] Hoshino, A., Fujioka, K. *et al.* Physicochemical Properties and Cellular Toxicity of Nanocrystal Quantum Dots Depend on Their Surface Modification. *Nano Letters,* **2004**, 4(11), 2163-2169.

[58] Shiohara, A., Hoshino, A. *et al.* On the Cyto-Toxicity Caused by Quantum Dots. *Microbiol Immunol,* **2004**, 48(9), 669-675.

[59] Fan, T. W., Teh, S. J. *et al.* Selenium Biotransformations into Proteinaceous Forms by Foodweb Organisms of Selenium-Laden Drainage Waters in California. *Aquat Toxicol,* **2002**, 57(1-2), 65-84.

[60] Elder, A., Vidyasagar, S. & DeLouise, L. Physicochemical Factors That Affect Metal and Metal Oxide Nanoparticle Passage across Epithelial Barriers. *Wiley Interdiscip Rev Nanomed Nanobiotechnol,* **2009**, 1(4), 434-450.

[61] Grenha, A., Seijo, B. & Remunan-Lopez, C. Microencapsulated Chitosan Nanoparticles for Lung Protein Delivery. *Eur J Pharm Sci,* **2005**, 25(4-5), 427-437.

[62] Simionescu, D. & Simionescu, M. Differentiated Distribution of the Cell Surface Charge on the Alveolar-Capillary Unit. Characteristic Paucity of Anionic Sites on the Air-Blood Barrier. *Microvasc Res,* **1983**, 25(1), 85-100.

[63] Tobin, D. J. Biochemistry of Human Skin--Our Brain on the Outside. *Chem Soc Rev,* **2006**, 35(1), 52-67.

[64] Hickie, R. A., Wei, J. W. *et al.* Cations and Calmodulin in Normal and Neoplastic Cell Growth Regulation. *Can J Biochem Cell Biol,* **1983**, 61(8), 934-941.

[65] Menon, G. K., Grayson, S. & Elias, P. M. Ionic Calcium Reservoirs in Mammalian Epidermis: Ultrastructural Localization by Ion-Capture Cytochemistry. *J Invest Dermatol,* **1985**, 84(6), 508-512.

[66] Pilgram, G. S., Engelsma-van Pelt, A. M. *et al.* Electron Diffraction Provides New Information on Human Stratum Corneum Lipid Organization Studied in Relation to Depth and Temperature. *J Invest Dermatol,* **1999**, 113(3), 403-409.

[67] Bos, J. D. & Meinardi, M. M. The 500 Dalton Rule for the Skin Penetration of Chemical Compounds and Drugs. *Exp Dermatol,* **2000**, 9(3), 165-169.

[68] Benson, H. A. Transdermal Drug Delivery: Penetration Enhancement Techniques. *Curr Drug Deliv*, **2005**, 2(1), 23-33.

[69] Proksch, E., Brandner, J. M. & Jensen, J. M. The Skin: An Indispensable Barrier. *Exp Dermatol*, **2008**, 17(12), 1063-1072.

[70] Tinkle, S. S., Antonini, J. M. *et al.* Skin as a Route of Exposure and Sensitization in Chronic Beryllium Disease. *Environmental Health Perspectives*, **2003**, 111(9), 1202-1208.

[71] Otberg, N., Richter, H. *et al.* Variations of Hair Follicle Size and Distribution in Different Body Sites. *J Invest Dermatol*, **2004**, 122(1), 14-19.

[72] Lademann, J. Penetration Studies of Topically Applied Substances: Optical Determination of the Amount of Stratum Corneum Removed by Tape Stripping. **2006**,

[73] Lademann, J., Richter, H. *et al.* Hair Follicles - a Long-Term Reservoir for Drug Delivery. *Skin Pharmacol Physiol*, **2006**, 19(4), 232-236.

[74] Lademann, J., Richter, H. *et al.* Penetration and Storage of Particles in Human Skin: Perspectives and Safety Aspects. *European journal of pharmaceutics and biopharmaceutics : official journal of Arbeitsgemeinschaft fur Pharmazeutische Verfahrenstechnik e.V*, **2011**, 77(3), 465-468.

[75] Meidan V. M., B. M. C., Michniak B. B. Transfollicular Drug Delivery—Is It a Reality? *Int J Pharm*, **2006**, 306(1-2), 1-14.

[76] Toll, R., Jacobi, U. *et al.* Penetration Profile of Microspheres in Follicular Targeting of Terminal Hair Follicles. *J Invest Dermatol*, **2004**, 123(1), 168-176.

[77] Warner, R. R., Boissy, Y. L. *et al.* Water Disrupts Stratum Corneum Lipid Lamellae: Damage Is Similar to Surfactants. *J Invest Dermatol*, **1999**, 113(6), 960-966.

[78] Fore-Pfliger, I. & CW, F. The Epidermal Skin Barrier: Implications. *Adv Skin Wound Care*, **2004**, 17(9), 480-488.

[79] Black, A. K., Fincham, N. *et al.* Time Course Changes in Levels of Arachidonic Acid and Prostaglandins D2, E2, F2 Alpha in Human Skin Following Ultraviolet B Irradiation. *Br J Clin Pharmacol*, **1980**, 10(5), 453-457.

[80] Kupper, T. S., Chua, A. O. *et al.* Interleukin 1 Gene Expression in Cultured Human Keratinocytes Is Augmented by Ultraviolet Irradiation. *J Clin Invest*, **1987**, 80(2), 430-436.

[81] Hattori, T., Umetsu, M. *et al.* A High-Affinity Gold-Binding Camel Antibody: Antibody Engineering for One-Pot Functionalization of Gold Nanoparticles as Biointerface Molecules. *Bioconjug Chem*, **2012**, 23(9), 1934-1944.

[82] Lademann, J., Jacobi, U. *et al.* The Tape Stripping Procedure--Evaluation of Some Critical Parameters. *European journal of pharmaceutics and biopharmaceutics : official journal of Arbeitsgemeinschaft fur Pharmazeutische Verfahrenstechnik e.V*, **2009**, 72(2), 317-323.

[83] Lindemann, U., Wilken, K. *et al.* Quantification of the Horny Layer Using Tape Stripping and Microscopic Techniques. *J Biomed Opt*, **2003**, 8(4), 601-607.

[84] Zhang, L. W. & Monteiro-Riviere, N. A. Assessment of Quantum Dot Penetration into Intact, Tape-Stripped, Abraded and Flexed Rat Skin. *Skin Pharmacol Appl*, **2008**, 21, 166-180.

[85] Sonavane, G., Tomoda, K. *et al.* In Vitro Permeation of Gold Nanoparticles through Rat Skin and Rat Intestine: Effect of Particle Size. *Colloids Surf B Biointerfaces*, **2008**, 65(1), 1-10.

[86] Sadrieh, N., Wokovich, A. M. *et al.* Lack of Significant Dermal Penetration of Titanium Dioxide from Sunscreen Formulations Containing Nano- and Submicron-Size Tio2 Particles. *Toxicol Sci*, **2010**, 115(1), 156-166.

[87] Tan, M. H., Commens, C. A. *et al.* A Pilot Study on the Percutaneous Absorption of Microfine Titanium Dioxide from Sunscreens. *Australas J Dermatol*, **1996**, 37(4), 185-187.

[88] Rouse, J. G., Yang, J. *et al.* Effects of Mechanical Flexion on the Penetration of Fullerene Amino Acid-Derivatized Peptide Nanoparticles through Skin. *Nano Lett*, **2007**, 7(1), 155-160.

[89] Rancan, F., Gao, Q. *et al.* Skin Penetration and Cellular Uptake of Amorphous Silica Nanoparticles with Variable Size, Surface Functionalization, and Colloidal Stability. *ACS Nano*, **2012**, 6(8), 6829-6842.

[90] Lansdown, A. B. & Taylor, A. Zinc and Titanium Oxides: Promising Uv-Absorbers but What Influence Do They Have on the Intact Skin? *Int J Cosmet Sci*, **1997**, 19(4), 167-172.

[91] Dussert, A. S., Gooris, E. & Hemmerle, J. Characterization of the Mineral Content of a Physical Sunscreen Emulsion and Its Distribution onto Human Stratum Corneum. *Int J Cosmet Sci,* **1997**, 19(3), 119-129.

[92] Bennat, C. & Muller-Goymann, C. C. Skin Penetration and Stabilization of Formulations Containing Microfine Titanium Dioxide as Physical Uv Filter. *Int J Cosmet Sci,* **2000**, 22(4), 271-283.

[93] Menzel, F., Reinert, T. *et al.* Investigations of Percutaneous Uptake of Ultrafine Tio2 Particles at the High Energy Ion Nanoprobe Lipsion. *Nuclear Instruments and Methods in Physics Research Section B: Beam Interactions with Materials and Atoms*, **2004**, 219–220(0), 82-86.

[94] Gopee, N. V., Roberts, D. W. *et al.* Quantitative Determination of Skin Penetration of Peg-Coated Cdse Quantum Dots in Dermabraded but Not Intact Skh-1 Hairless Mouse Skin. *Toxicol Sci,* **2009**, 111(1), 37-48.

[95] Diembeck, W., Beck, H. *et al.* Test Guidelines for in Vitro Assessment of Dermal Absorption and Percutaneous Penetration of Cosmetic Ingredients. European Cosmetic, Toiletry and Perfumery Association. *Food Chem Toxicol,* **1999**, 37(2-3), 191-205.

[96] Zvyagin, A. V., Zhao, X. *et al.* Imaging of Zinc Oxide Nanoparticle Penetration in Human Skin in Vitro and in Vivo. *J Biomed Opt,* **2008**, 13(6), 064031.

[97] Paliwal, S., Menon, G. K. & Mitragotri, S. Low-Frequency Sonophoresis: Ultrastructural Basis for Stratum Corneum Permeability Assessed Using Quantum Dots. *J Invest Dermatol*, **2006**, 126(5), 1095-1101.

[98] Gulson, B., McCall, M. *et al.* Small Amounts of Zinc from Zinc Oxide Particles in Sunscreens Applied Outdoors Are Absorbed through Human Skin. *Toxicol Sci*, **2010**, 118(1), 140-149.

[99] Baroli, B., Ennas, M. G. *et al.* Penetration of Metallic Nanoparticles in Human Full-Thickness Skin. *J Invest Dermatol*, **2007**, 127(7), 1701-1712.

[100] Honeywell-Nguyen, P. L., Gooris, G. S. & Bouwstra, J. A. Quantitative Assessment of the Transport of Elastic and Rigid Vesicle Components and a Model Drug from These Vesicle Formulations into Human Skin in Vivo. *J Invest Dermatol*, **2004**, 123(5), 902-910.

[101] Mortensen, L. J., Ravichandran, S. *et al.* Progress and Challenges in Quantifying Skin Permeability to Nanoparticles Using a Quantum Dot Model. *J Biomed Nanotechnol*, **2010**, 6(5), 596-604.

[102] Grimes, P. E. Microdermabrasion. *Dermatol Surg*, **2005**, 31(9 Pt 2), 1160-1165; discussion 1165.

[103] Orentreich, N. & Orentreich, D. S. Dermabrasion. *Dermatol Clin*, **1995**, 13(2), 313-327.

[104] Nemmar, A., Al-Maskari, S. *et al.* Cardiovascular and Lung Inflammatory Effects Induced by Systemically Administered Diesel Exhaust Particles in Rats. *Am J Physiol Lung Cell Mol Physiol*, **2007**, 292(3), L664-670.

[105] Penn, A., Murphy, G. *et al.* Combustion-Derived Ultrafine Particles Transport Organic Toxicants to Target Respiratory Cells. *Environ Health Perspect*, **2005**, 113(8), 956-963.

[106] Pulskamp, K., Diabate, S. & Krug, H. F. Carbon Nanotubes Show No Sign of Acute Toxicity but Induce Intracellular Reactive Oxygen Species in Dependence on Contaminants. *Toxicol Lett*, **2007**, 168(1), 58-74.

[107] Stearns, R. C., Paulauskis, J. D. & Godleski, J. J. Endocytosis of Ultrafine Particles by A549 Cells. *Am J Respir Cell Mol Biol*, **2001**, 24(2), 108-115.

[108] Muhlfeld, C., Rothen-Rutishauser, B. *et al.* Visualization and Quantitative Analysis of Nanoparticles in the Respiratory Tract by Transmission Electron Microscopy. *Part Fibre Toxicol*, **2007**, 4, 11.

[109] Panyam, J., Sahoo, S. K. *et al.* Fluorescence and Electron Microscopy Probes for Cellular and Tissue Uptake of Poly(D,L-Lactide-Co-Glycolide) Nanoparticles. *Int J Pharm*, **2003**, 262(1-2), 1-11.

[110] Zhang, L. W., Yu, W. W. *et al.* Biological Interactions of Quantum Dot Nanoparticles in Skin and in Human Epidermal Keratinocytes. *Toxicol Appl Pharmacol*, **2008**, 228(2), 200-211.

[111] Chou, L. Y., Fischer, H. C. *et al.* Visualizing Quantum Dots in Biological Samples Using Silver Staining. *Anal Chem,* **2009**, 81(11), 4560-4565.

[112] Ottensmeyer, F. P. & Andrew, J. W. High-Resolution Microanalysis of Biological Specimens by Electron Energy Loss Spectroscopy and by Electron Spectroscopic Imaging. *J Ultrastruct Res,* **1980**, 72(3), 336-348.

[113] Cross, S. E., Innes, B. *et al.* Human Skin Penetration of Sunscreen Nanoparticles: In-Vitro Assessment of a Novel Micronized Zinc Oxide Formulation. *Skin Pharmacol Physiol,* **2007**, 20(3), 148-154.

[114] St Croix, C. M., Leelavaninchkul, K. *et al.* Nitric Oxide and Zinc Homeostasis in Acute Lung Injury. *Proc Am Thorac Soc,* **2005**, 2(3), 236-242.

[115] Mardyani, S. & Chan, W. C. W. Quantification of Quantum Dots Using Phage Display Screening and Assay. *Journal of Materials Chemistry*, **2009**, 19(35), 6321-6323.

[116] Nygaard, U. C., Hansen, J. S. *et al.* Single-Walled and Multi-Walled Carbon Nanotubes Promote Allergic Immune Responses in Mice. *Toxicol Sci,* **2009**, 109(1), 113-123.

[117] Schanen, B. C., Karakoti, A. S. *et al.* Exposure to Titanium Dioxide Nanomaterials Provokes Inflammation of an in Vitro Human Immune Construct. *ACS Nano,* **2009**, 3(9), 2523-2532.

[118] Bassindale, A. R., Codina-Barrios, A. *et al.* An Improved Phage Display Methodology for Inorganic Nanoparticle Fabrication. *Chemical Communications*, **2007**, (28), 2956-2958.

[119] Chen, H., Su, X. *et al.* Qcm-D Analysis of Binding Mechanism of Phage Particles Displaying a Constrained Heptapeptide with Specific Affinity to Sio2 and Tio2. *Anal Chem,* **2006**, 78(14), 4872-4879.

[120] Wang, L. F. & Yu, M. Epitope Mapping Using Phage-Display Random Fragment Libraries. *Methods Mol Biol,* **2009**, 524, 315-332.

[121] Chen, B. X., Wilson, S. R. *et al.* Antigenicity of Fullerenes: Antibodies Specific for Fullerenes and Their Characteristics. *Proc Natl Acad Sci U S A,* **1998**, 95(18), 10809-10813.

[122] Izhaky, D. & Pecht, I. What Else Can the Immune System Recognize? *Proc Natl Acad Sci U S A*, **1998**, 95(20), 11509-11510.

[123] Arap, M. A. Phage Display Technology - Applications and Innovations. *Genetics and Molecular Biology*, **2005**, 28(1), 1-9.

[124] Bass, S., Greene, R. & Wells, J. A. Hormone Phage: An Enrichment Method for Variant Proteins with Altered Binding Properties. *Proteins*, **1990**, 8(4), 309-314.

[125] McCafferty, J., Griffiths, A. D. *et al.* Phage Antibodies: Filamentous Phage Displaying Antibody Variable Domains. *Nature*, **1990**, 348(6301), 552-554.

[126] Smith, G. P. & Petrenko, V. A. Phage Display. *Chem Rev*, **1997**, 97(2), 391-410.

[127] Caberoy, N. B., Zhou, Y. *et al.* Efficient Identification of Tubby-Binding Proteins by an Improved System of T7 Phage Display. *J Mol Recognit*, **2010**, 23(1), 74-83.

[128] Fuh, G. & Sidhu, S. S. Efficient Phage Display of Polypeptides Fused to the Carboxy-Terminus of the M13 Gene-3 Minor Coat Protein. *FEBS Lett*, **2000**, 480(2-3), 231-234.

[129] James, K. J., Hancock, M. A. *et al.* Tonb Interacts with Btuf, the Escherichia Coli Periplasmic Binding Protein for Cyanocobalamin. *Biochemistry*, **2009**, 48(39), 9212-9220.

[130] Pande, J., Szewczyk, M. M. & Grover, A. K. Phage Display: Concept, Innovations, Applications and Future. *Biotechnol Adv*, **2010**, 28(6), 849-858.

[131] Diamond, S. L. Methods for Mapping Protease Specificity. *Curr Opin Chem Biol*, **2007**, 11(1), 46-51.

[132] Kay, B. K., Kasanov, J. & Yamabhai, M. Screening Phage-Displayed Combinatorial Peptide Libraries. *Methods*, **2001**, 24(3), 240-246.

[133] Vanwetswinkel, S., Avalle, B. & Fastrez, J. Selection of Beta-Lactamases and Penicillin Binding Mutants from a Library of Phage Displayed Tem-1 Beta-Lactamase Randomly Mutated in the Active Site Omega-Loop. *J Mol Biol*, **2000**, 295(3), 527-540.

[134] Finucane, M. D., Tuna, M. *et al.* Core-Directed Protein Design. I. An Experimental Method for Selecting Stable Proteins from Combinatorial Libraries. *Biochemistry*, **1999**, 38(36), 11604-11612.

[135] Basha, S., Rai, P. *et al.* Polyvalent Inhibitors of Anthrax Toxin That Target Host Receptors. *Proc Natl Acad Sci U S A*, **2006**, 103(36), 13509-13513.

[136] Scott, J. K. & Smith, G. P. Searching for Peptide Ligands with an Epitope Library. *Science*, **1990**, 249(4967), 386-390.

[137] Wang, S., Humphreys, E. S. *et al.* Peptides with Selective Affinity for Carbon Nanotubes. *Nat Mater*, **2003**, 2(3), 196-200.

[138] Fack, F., Hugle-Dorr, B. *et al.* Epitope Mapping by Phage Display: Random Versus Gene-Fragment Libraries. *Journal of immunological methods*, **1997**, 206(1-2), 43-52.

[139] Bonetto, S., Carlavan, I. & Baty, D. Isolation and Characterization of Antagonist and Agonist Peptides to the Human Melanocortin 1 Receptor. *Peptides*, **2005**, 26(11), 2302-2313.

[140] Whaley, S. R., English, D. S. *et al.* Selection of Peptides with Semiconductor Binding Specificity for Directed Nanocrystal Assembly. *Nature*, **2000**, 405(6787), 665-668.

[141] Dang, X., Yi, H. *et al.* Virus-Templated Self-Assembled Single-Walled Carbon Nanotubes for Highly Efficient Electron Collection in Photovoltaic Devices. *Nat Nanotechnol*, **2011**, 6(6), 377-384.

[142] Kay, B. K., Adey, N. B. *et al.* An M13 Phage Library Displaying Random 38-Amino-Acid Peptides as a Source of Novel Sequences with Affinity to Selected Targets. *Gene*, **1993**, 128(1), 59-65.

[143] Naik, R. R., Stringer, S. J. *et al.* Biomimetic Synthesis and Patterning of Silver Nanoparticles. *Nat Mater*, **2002**, 1(3), 169-172.

[144] Flynn CE, L. S., Peele BR, Belcher AM. Viruses as Vehicles for Growth, Organization and Assembly of Materials. *Acta Materialia*, **2003**, 51, 5867-5880.

[145] Bradbury, A. R. & Marks, J. D. Antibodies from Phage Antibody Libraries. *Journal of immunological methods*, **2004**, 290(1-2), 29-49.

[146] Hammers, C. M. & Stanley, J. R. Antibody Phage Display: Technique and Applications. *J Invest Dermatol*, **2014**, 134(2), e17.

[147] Kim, J., Stroud, R. M. & Craik, C. S. Rapid Identification of Recombinant Fabs That Bind to Membrane Proteins. *Methods*, **2011**, 55(4), 303-309.

[148] Bostrom, J., Lee, C. V. *et al.* Improving Antibody Binding Affinity and Specificity for Therapeutic Development. *Methods Mol Biol*, **2009**, 525, 353-376, xiii.

[149] Liang, W. C., Dennis, M. S. *et al.* Function Blocking Antibodies to Neuropilin-1 Generated from a Designed Human Synthetic Antibody Phage Library. *J Mol Biol*, **2007**, 366(3), 815-829.

[150] Carmen, S. & Jermutus, L. Concepts in Antibody Phage Display. *Brief Funct Genomic Proteomic*, **2002**, 1(2), 189-203.

[151] Vaughan, T. J., Williams, A. J. *et al.* Human Antibodies with Sub-Nanomolar Affinities Isolated from a Large Non-Immunized Phage Display Library. *Nat Biotechnol*, **1996**, 14(3), 309-314.

[152] Krug, H. F. Nanosafety Research--Are We on the Right Track? *Angew Chem Int Ed Engl*, **2014**, 53(46), 12304-12319.

[153] Sambrook, J. a. R., D. W. Eds. 3rd edn, **2001**. (Cold Spring Harbour Laboratory Press,).

[154] Holliger, P. & Riechmann, L. A Conserved Infection Pathway for Filamentous Bacteriophages Is Suggested by the Structure of the Membrane Penetration Domain of the Minor Coat Protein G3p from Phage Fd. *Structure*, **1997**, 5(2), 265-275.

[155] Lubkowski, J., Hennecke, F. *et al.* The Structural Basis of Phage Display Elucidated by the Crystal Structure of the N-Terminal Domains of G3p. *Nat Struct Biol*, **1998**, 5(2), 140-147.

[156] Endemann, H., Gailus, V. & Rasched, I. Interchangeability of the Adsorption Proteins of Bacteriophages Ff and Ike. *J Virol*, **1993**, 67(6), 3332-3337.

[157] Russel, M. Filamentous Phage Assembly. *Mol Microbiol*, **1991**, 5(7), 1607-1613.

[158] Kretzschmar, T. & Geiser, M. Evaluation of Antibodies Fused to Minor Coat Protein Iii and Major Coat Protein Viii of Bacteriophage M13. *Gene,* **1995**, 155(1), 61-65.

# Chapter 2

*Identification of Phage Clones that Bind QDs and $TiO_2$ NPs, and Verification of Binding in vitro*

# 2.1 Biopanning

Antibody phage display is robust, highly versatile and a simple-to-use platform technology, where the antibody selection process can be done on a multitude of targets including proteins, inorganic materials, whole cells, tissues and animals[1]. The basic antibody phage selection process or biopanning on a target involves 5 steps[2]: i) preparation of library or amplification of existing library ii) exposure of phage library to target iii) removal of non-specific binders by repeated washing iv) recovery of target bound phage by elution v) back to step (i) three to four more times. The ultimate goal of the selection process is to discover phages that bind to the target (antigen) with high affinity from the large starting library of phage clones (~$10^9$ unique clones) of phages, the majority of which do not bind or have very low affinity[3]. Although ideally, only one round of selection would be required, iterative rounds of selection and amplification are required to eliminate background non-binders and select the best binders to the target from the library[1].

## 2.1.1 Phage Exposure to Target

The screening protocols in phage display can be tailored to meet the needs of the specific target. The most widely used method is to immobilize the target on a solid support and expose phage solutions to the immobilized target. Successful panning strategies have included immobilization of targets to plastic plates, on surface of magnetic beads, surface modified tubes (eg. MaxiSorp™)[4,5], and even targets on whole fixed or living cells, tissue sections or animals[6,7]. In addition, biopanning has been performed on BIAcore

sensorchips[8] and on biotinylated antigen in solution and capturing phage-bound antigen on streptavidin-coated surfaces[9]. However, a known problem with physical methods of selection such as those described above is that the epitope may be partially denatured after immobilization which may lead to selection of antibodies that do not recognize or bind to the native antigen (off-target antibodies)[10]. Moreover, a potential problem with using biotinylated antigen is that upon using streptavidin beads to isolate phage bound to antigen-biotin complex, antibodies to streptavidin are also isolated, especially in non-immune libraries. In this thesis work, panning was done on antigen (nanoparticles) dispersed in solution to mitigate some of these off-target effects described above.

### 2.1.2 Washing, Elution and Amplification Steps

Next, it is important to perform the selection in the presence of a blocking agent to hinder phage non-specific binding. Milk powder, bovine serum albumin (BSA), and casein are common blocking agents[10]. Selection is usually performed at room temperature. Excessive washing to remove unbound phage and weakly bound phage is also done in presence of a detergent (eg. 0.05-0.5% Tween-20) to minimize non-specificity. The target is rinsed 5-10 times in a suitable buffer solution (tris-buffered saline (TBS)) containing Tween-20 (TBST). Washing in the first cycle when the phage copies are in a low number (for a 1% display system, only ~100 copies of each phage is present) should be less stringent, after which more stringent wash conditions are used since phages are present at much higher copies post amplification in bacterial cells[10]. After washing the phages bound to the target are eluted using one of several mechanism that include: introducing a dramatic drop in pH[10], or a reducing agent, or enzymatic cleavage reaction[5,11]. In this

thesis we drop the pH using a 0.1 M glycine (pH 2.2) solution. Following elution of the bound phage, they are collected and used to infect *E.coli* host cells, which amplify them. The amplicons are collected and form the input pool for the next round of biopanning. The number of rounds required is not predicted in advance, but is dependent on the degree of enrichment in the selection method and also on affinities of the antibodies in the population. The degree of enrichment is the ratio of binders to non-binders before and after selection[10]. This typically varies between 5 and 1000-fold depending on the target (NPs in this thesis). The diversity and thereby the enrichment if any, is monitored after a couple of rounds using BstN1 endonuclease fingerprinting analysis of the immunoglobulin genes where the presence of repeating patterns was considered to be an evidence of clonal abundance and enrichment[12]. This method first involves amplifying scFv antibody sequences from the colonies using PCR, and subsequent digestion of the product using BstN1 enzyme, gives different band patterns unique to each scFv on an agarose gel. Amino acid sequencing of the clone is done once binders if any, have been identified using the BstN1 fingerprinting analysis to reduce the number of clones to a manageable amount.

This thesis describes a novel approach of panning in solution to obtain antibodies that are reactive with intact, dispersed NPs, namely QDs and $TiO_2$ NPs as opposed to immobilizing them on a solid support. Binders to NPs were selected from a phage library consisting of ~$2x10^9$ unique scFvs derived from natural antibody variable region sequences, each displayed monovalently on the minor coat gIIIp of M13 filamentous

phage. This library has been previously used to generate antibodies against a wide variety of proteins, haptens and cell surface antigens[12-15].

# 2.2 Materials and Methods

## 2.2.1 Nanoparticle Preparation and Characterization

QDs were used as a model NP to first develop antibodies and validate binding. Commercially available CdSe/ZnS core/shell QDs capped with octadecylamine (ODA) (NN-Labs, 5.8 nm core diameter, and 620 nm emission wavelength (Figure 2.1)) was purchased. Previously described[16] ligand exchange methods were used to prepare water-soluble GSH-QDs. Briefly, 300 µL of ODA-QDs were precipitated by the addition of 1:1 methanol: acetone and separated by centrifugation at 14,000 rpm for 5 min (Eppendorf 5417 C). The ODA-QD pellet was re-suspended in 300 µL tetrahydrofuran (THF). Next, 30 mg GSH (Calbiochem, Cat. number 3541) was added to 1 mL methanol, and the solution was adjusted to a pH of 11.0 with the addition of tetramethylammonium hydroxide pentahydrate powder (Sigma Aldrich Inc.). The ODA-QD-THF solution was slowly added drop-wise to the GSH-methanol solution while stirring in a 4 mL glass vial (VWR) immersed in a mineral oil bath at 60 °C for 2 h on a hotplate/stirrer (VWR), after which they are stirred overnight at room temperature. The QDs were precipitated by the addition of excess ether (1-2 mL) and centrifuged at 14,000 rpm for 5 min at room temperature. The supernatant was discarded and GSH-QDs were re-suspended in 300 µL of a 0.01 N NaOH and dialyzed using a 5 kD molecular weight cutoff DispoDialyzer filter (Harvard Apparatus Inc.) against excess deionized water (pH=6.5, 50 mL water,

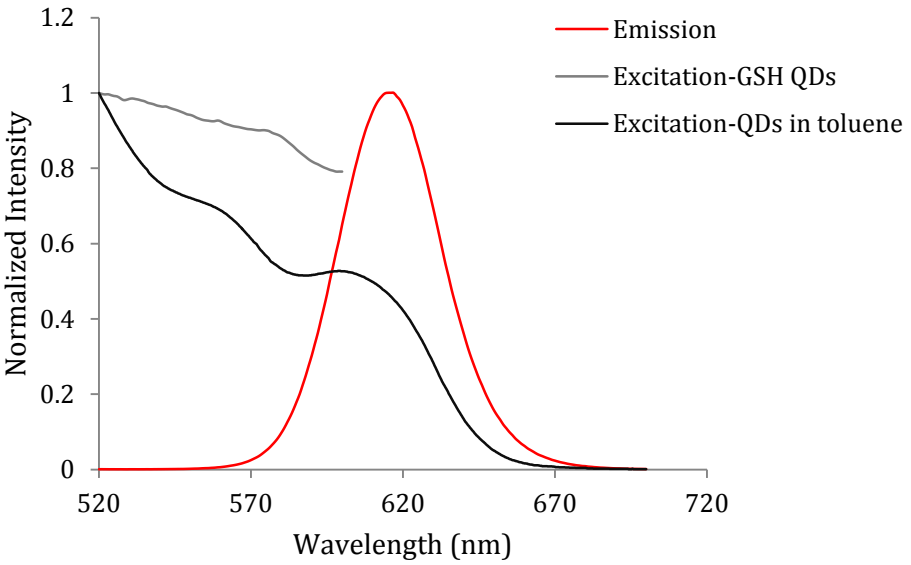


**Figure 2.1: QD Excitation and Emission Spectra**

Excitation (grey) and emission (red) spectra of CdSe/ZnS core/shell GSH-functionalized QDs with an emission peak of 620 nm. The excitation spectrum of organic QDs in toluene is shown in black.

changed once) for 48 h. The concentration of prepared GSH-QDs was determined by measuring the UV-vis absorbance previously described[17]. Briefly, the absorption at first exciton was measured and an excitation coefficient value was used from Yu et al., to calculate the concentration using Beer-Lambert's law. The hydrodynamic diameter was measured by dynamic light scattering (DLS) and the surface charge was determined from zeta potential measurements in water (pH=6.7) using a Malvern Zetasizer Nano ZS (Malvern Instruments Inc.) prior to all experiments.

## 2.2.2 Phage Library Construction

Detailed description of phage library construction is described elsewhere[12,13]. The bacterial host strain used for all antibody selection and expression was TG1[13] (Agilent). Briefly, a large human naïve antibody library was constructed by using PCR amplification of cDNA derived from peripheral blood lymphocytes of a pool (>100) of donors (Sullivan Lab, University of Rochester Medical Centre, (URMC)). Primers were designed to amplify human light and heavy chain variable regions. The amplified regions were cloned as scFvs with an amino acid linker region (amino acid sequence EGKSSGSGSESKAS) between $V_L$ and $V_H$ domains. The phagemid vector used was pAP-$III_6$, which is a derivative of pAP-$III_\Delta$[18]. This vector expresses the scFv-M13gIIIp fusion protein under the control of *E.coli* alkaline phosphatase (AP) promoter[12]. This specific promoter was chosen to allow a low level expression of fusion protein in standard LB medium (high in phosphate) to favor monovalent display[19]. Upon removal of the viral gIIIp fragment, by restriction digestion and re-ligation, His and FLAG-tagged scFvs can be expressed after growth in low-phosphate growth medium[20]. The diversity

of the library is approximately $2x10^9$ unique clones.

### 2.2.3 BstN1 Fingerprinting

This method involves picking randomly chosen single colonies (~12-20) from the titer plates after panning 'round 4' into a PCR master mix with primers designed to amplify the scFv insert. The primers used were ompA (TCGCGATTGCAGTGGCACT) and -266: (CCCCTTATTAGCGTTTGCCATCTT). A 2-step PCR was run: 30 s at 95 °C, 1'30''at 60 °C, for 25 cycles followed by 5' at 72 °C. The PCR products of ~1,000 bp were digested with MvaI restriction endonuclease, which is an isoschizomer of the widely used BstN1 (termed BstN1 fingerprinting) and loaded onto a 1.8-2% agarose gel for electrophoresis, after which the gel was photographed. The selected clones were sequenced at the University of Rochester Functional Genomics Core Facility or at GeneWiz. The complementarity determining regions (CDRs) are identified according to Kabat et al[21].

### 2.2.4 Phage Stock Preparation

Individual phage stocks and phage pools for enrichment rounds were prepared following infection with a helper phage by PEG precipitation. Phage cultures were centrifuged for 5 min, and phages in the supernatant were precipitated by addition of PEG 6000 and NaCl to final concentrations of 4% and 0.5 M, respectively. After incubation at room temperature for 60 min, the solution was then centrifuged (14,000 rpm, 10 min) to obtain the phage pellet, which was then re-suspended in TBS with 0.5% casein (Blocker™, Pierce). Fresh phage pools were used for enrichment whenever possible; 15% glycerol

was added to the phage stocks before freezing them at -80 °C to ensure stable antibody display for future use.

### 2.2.5 TEM Analysis

Briefly[22], 10 µL of the sample (phage with NPs) was placed into a carbon coated nickel grid and 10 µL of 2% phosphotungstic acid was added and allowed for 2-5 min. Excess fluid was wicked off and samples were allowed to air-dry. The samples were imaged using a Hitachi 7650 Transmission Electron Microscope and an attached Gatan 11 megapixel Erlangshen digital camera system (Electron Microscopy Core, URMC).

## 2.3 Results

### 2.3.1 Selection of Binders to QDs and $TiO_2$ NPs

#### 2.3.1.1 NP selection criteria and pre-panning considerations

We used GSH-QDs (CdSe/ZnS core/shell) and $TiO_2$ NPs (Evonik/Degussa P25, 80% anatase and 20% rutile crystal, ~21 nm primary particle size). GSH-QDs were selected for their superior stability to resist agglomeration in water and buffer systems compared to other commonly used water soluble coatings such as DHLA (Appendix A, Figure A1). The hydrodynamic diameter and polydispersity of the GSH-QDs measured in water using DLS were 14.1±2.5 nm and 0.33±0.06 respectively, and they were negatively charged (-22.82 mV) as determined from zeta potential measurements (pH= 5.3-5.6). The Evonik $TiO_2$ was selected because of its wide use in commercial skin care products. $TiO_2$ NPs dispersed in water form aggregates that range from ~100 nm to ~1.5 µm when visualized

under TEM (Appendix A, Figure A1). DLS was not used since $TiO_2$ NPs cannot be dispersed in water. Prior to performing panning, the NPs were tested for their dispersion and pelleting properties using centrifugation in the absence of phage but in the phage buffer systems (TBS, TBST) at NP concentrations that would be used during enrichment. This was done in order to define protocols for successful pelleting and re-suspension of the NPs for solution-phase panning. Due to their small size and solution stability the GSH-QDs required extremely high speeds (83,000 g and above) to pellet out of solution. In contrast, due to their tendency to aggregate, $TiO_2$ NPs were pelleted using much lower speeds on the order of 1200-1500 g (Sorvall Biofuge centrifuge). Through experimentation, an optimal speed of 83,000 g (55,000 rpm, Optima TLX ultracentrifuge, Beckman Coulter) was determined for pelleting GSH-QDs, which allowed minimized phage pelleting and easy re-suspension of the formed pellet; although higher speeds could have also yielded visible pellets. Minimizing amount of phage pelleting was important in order to ensure that phages did not pellet along with NPs as an artifact of centrifugation but by virtue of a potential binding interaction.

#### 2.3.1.2 NP panning process

The GSH-QDs (400 µL, 100 nM) and $TiO_2$ NPs (400 µL, 0.5 mg/mL) were diluted in TBS mixed with the phage library ($10^{12}$ phages/mL, 100 µL) present in diluted TBS plus 0.5% casein with gentle agitation for 2 h at room temperature. For GSH-QDs panning, the input phage stock was pre-centrifuged to pellet phage agglomerates at 116,000 g (65,000 rpm). After incubation to allow binding of phage to QDs, the QD/phage mixture was centrifuged at 83,000 g (55,000 rpm) for 10 min and the $TiO_2$/phage mixture was

centrifuged at 1300 g (4000 rpm) for 5 min to pellet phage-bound NPs. The unbound phage-containing supernatant was removed and the phage-bound NP pellet was re-suspended in TBST and centrifuged. This wash cycle was repeated 5 times, after which the pellet was washed once with deionized water. After washing the bound phages were eluted from the NPs using 200 µL of 0.1 M glycine (pH 2.2, containing 0.01% BSA) and neutralized using 12 µL of 2 M Tris base (3 µL per 50 µL of glycine). The titer of the eluted phages was quantified by transduction of serial dilutions of the phage into TG1 cells to ampicillin resistance and the resulting colonies on the plates were manually counted. A phage pool for 'round 2' of enrichment was generated by transduction of 100% of the eluate from the first round. The transductants were grown at 37 °C, infected with VCS M13 helper phage and grown overnight at 30 °C. The phage stocks were prepared on the following day by PEG precipitation. Typically, after four rounds of enrichment a BstN1 fingerprinting analysis was carried out to identify binders if any, through the presence of identical restriction enzyme patterns among the clones tested, taken as an evidence of specific enrichment as previously shown[12]. Upon performing BstN1 fingerprinting of 12 randomly selected clones, it was found that following 4 rounds of panning on GSH-QDs and $TiO_2$ NPs, phage clones termed GSH43ϕ and Ti49ϕ respectively, showed a clonal abundance of 17-25% (Figure 2.2). These individual phage clones were then tested for binding to GSH-QDs and $TiO_2$ NPs using various custom-designed assays described below.

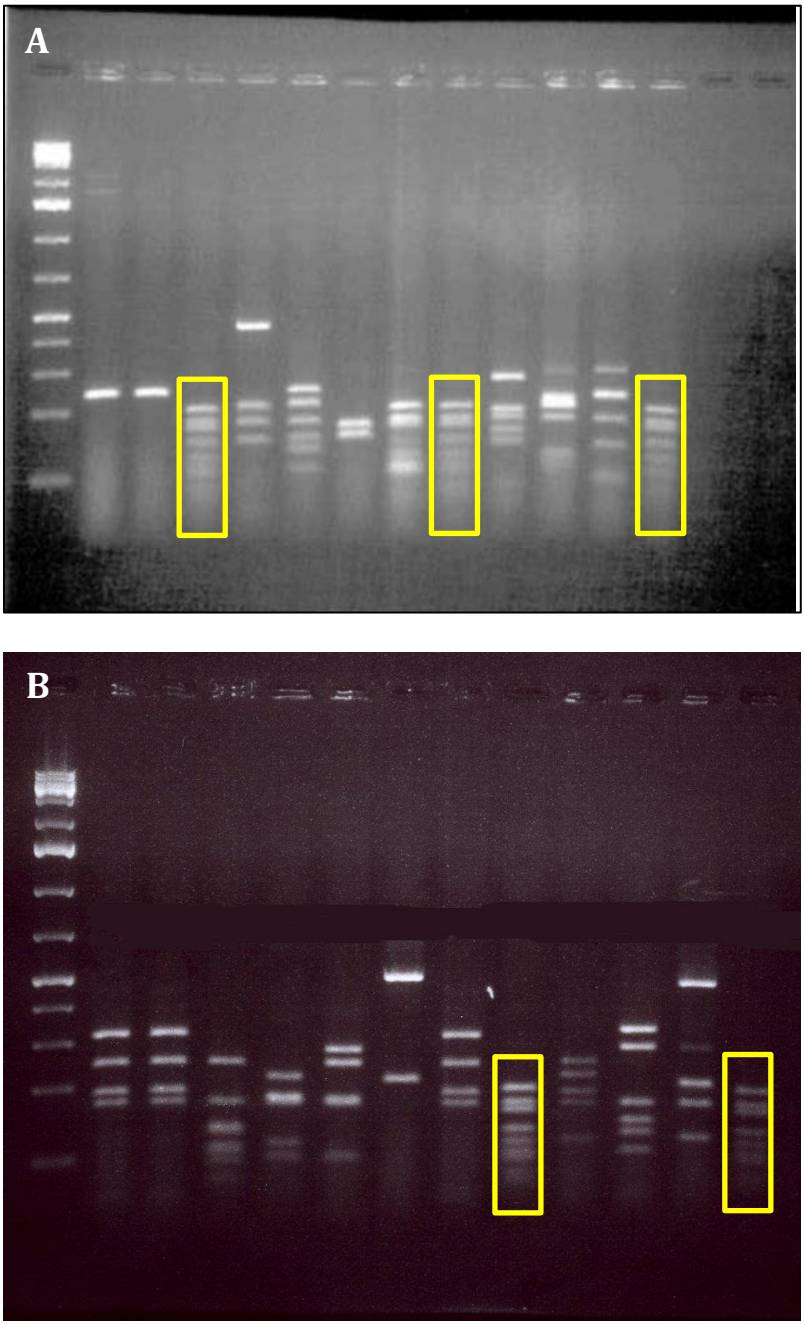


**Figure 2.2: BstN1 fingerprinting images for GSH-QDs and $TiO_2$ NPs**

BstN1 fingerprinting analysis showing unique scFv patterns for A) GSH-QDs at the end of 4 rounds of panning. Yellow boxes represent an example of repeating patterns (GSH43) and B) $TiO_2$ NPs showing presence of multiple pattern repeats out of which Ti49 was selected ($9^{th}$ clone from left).

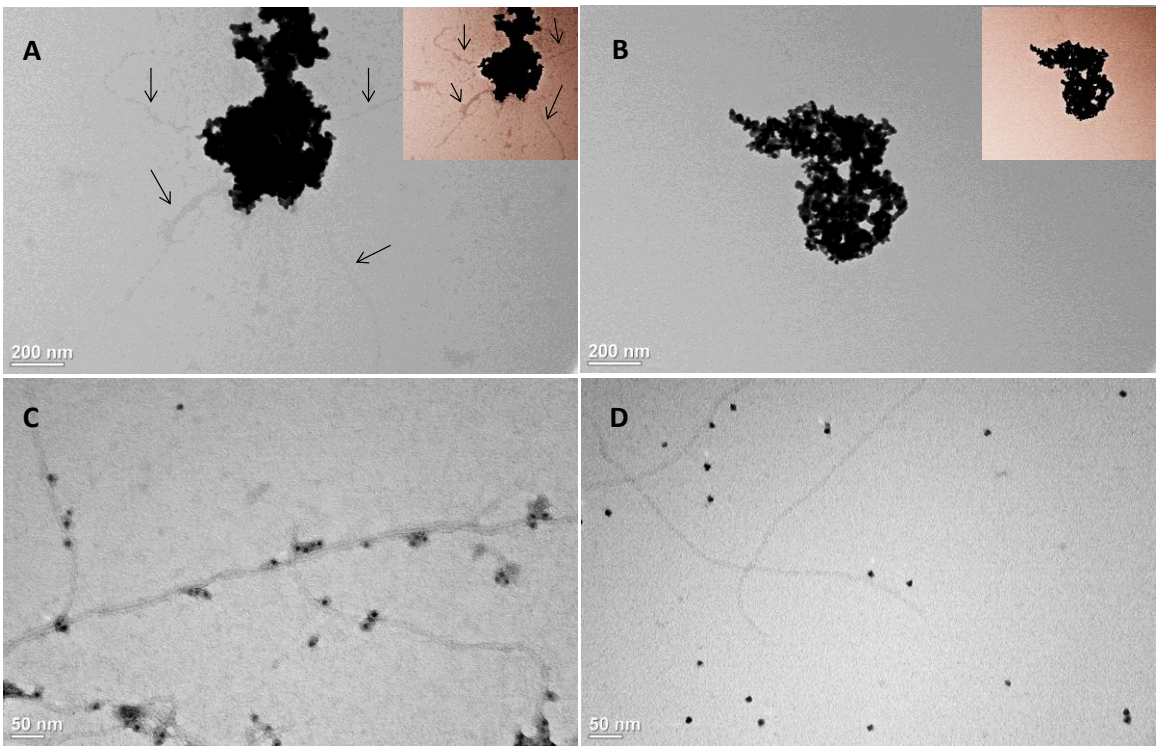


**Figure 2.3: TEM Images of Phage binding NPs**

TEM images showing (A) Ti49ϕ (black arrows) binding $TiO_2$ NPs whereas (B) there is no evidence for IL-12ϕ (negative control) to bind $TiO_2$ NPs. Scale bar=200 nm. Insets are images enhanced to highlight the phage. (C) GSH43ϕ exhibit strong association and clustering with GSH-QDs whereas (D) the negative control IL-12ϕ shows no affinity for the GSH-QD, which appear highly dispersed. Scale bar=50 nm.

**A**

| CLONE | CDR1 | CDR2 | CDR3 |
|---|---|---|---|
| GSH43 | LPVLTQPPSASGSPGQRVTISCSGS **SSNIGSNTVN** | WYQQLPGTAPKLLIY **SNNQRPS** | GVPDRFSGSKSGTSASLAISGLRSEDEADYYCAA **WDDSLNG** | WVFGGGTKLTVLG |
| Ti49 | SSELTQDPAVSVALGQTVRITC **QGDSLRSYYAS** | WYQQKPGQAPVLVIY **GKNNRPS** | GIPDRFSGSSSGNTASLTITGAQAEDEAEYYCYS **RDRSGNR** | VIFGGGTKVTVLG |

**B**

| CLONE | CDR1 | CDR2 | CDR3 |
|---|---|---|---|
| GSH43 | QVQLQSGAEVKKPGASVKVSCKASGYTFN **THGFS** | WVRQAPGQGLEWMGW **ISASNGNTKYPQNLQG** | RVTMTVDTFTTTAYLELRSLRSDDTAVYYCVR **DRTDYYVPGTFDPLYGPFDY** | WGQGTLVTVSS |
| Ti49 | QVQLESGPGLVKPSETLSLACTVSGGSIT **SSSYYWG** | WIRQPPGKGLEWIG **SMSYRGTTYYNPSLES** | RAIISADTAKNQFSLNLNSVTAADTAVYYCAR **WHCSSSMCYDLDY** | WGPGTLVTVSS |

## Figure 2.4: Amino Acid Sequences of GSH43 and Ti49

Amino acid sequences of A) light and B) heavy chain of GSH43 and Ti49 clones. The CDRs in each sequence are in bold type face and underlined.

## 2.3.2 Validation of Phage Clones Binding to NPs *in vitro*

*In vitro* binding and TEM assays were conducted to validate the binding of phage clones isolated after four rounds of panning to GSH-QDs and $TiO_2$ NPs. Appropriate negative controls such as an arbitrary phage clone from the library were included in each experiment. In these experiments, phage clone against interleukin-12 (IL-12ϕ) was used as a negative control.

### 2.3.2.1 *In vitro* binding assay

Binding to NPs *in vitro* was tested using a panning assay. Here, the GSH43ϕ and IL-12ϕ were mixed with GSH-QDs in separate tubes at room temperature for 2 h with gentle agitation. Similarly, Ti49ϕ was incubated with $TiO_2$ NPs along with IL-12ϕ with $TiO_2$ NPs in a separate tube. Following centrifugation using appropriate speeds for each NP as described above, the unbound phages from the supernatant were removed, the pellet containing bound phages to NPs was washed multiple times and the phages eluted. Upon evaluating phage titers as described above, we found that GSH43ϕ bound GSH-QDs and Ti49ϕ bound $TiO_2$ NPs 10-fold and ~150-fold more than negative control (IL-12ϕ), respectively (Appendix A, Figure A2).

### 2.3.2.2 *In vitro* TEM binding assay

To further confirm phage binding to their target NPs, we used TEM analysis. In this assay, GSH-QDs were mixed individually with GSH43ϕ and IL-12ϕ , and $TiO_2$ NPs were mixed separately with Ti49ϕ and IL-12ϕ. After a 2 h incubation period with gentle agitation, the samples were washed to remove unbound phages using the above described

procedure. The pellets after the final wash were re-suspended in TBS buffer, and prepared for TEM imaging. Results showed evidence for binding of Ti49ϕ with $TiO_2$ NPs (Figure 2.3A) while IL-12ϕ did not (Figure 2.3B) and GSH43ϕ binding to GSH-QDs causing formation of phage clusters (Figure 2.3C) whereas IL-12ϕ did not (Figure 2.3D).

# 2.4 Conclusions

We have shown that binders to GSH-QDs and $TiO_2$ NPs namely GSH43 and Ti49 can be isolated using phage display from a naïve human scFv library. The phage clones GSH43ϕ and Ti49ϕ bind their respective targets 10 and 150-fold more than a negative control phage. The lower enrichment value observed for GSH43ϕ is likely a result of precipitation of unbound phage during ultracentrifugation causing higher background colony counts despite our efforts to pre-clear the phage prior to exposure to NPs. The high speed used in order to separate the QDs from solution is a potential cause for this low level of enrichment due to high background (non-specifically binding phage). Nonetheless, these values are in accordance with an 8-fold enrichment value reported in literature for the isolation of peptides against solid ZnO susbtrates using phage display technology[23]. The complementarity determining regions (CDR) of both the antibodies (GSH43, Ti49) isolated are comprised of a high percentage of polar uncharged amino acids (serine and asparagine), 30% and 32%, respectively. More strikingly, the CDRs lack a preponderance of cysteines (<3%) and histidines (<1%), which typically are the ones enriched in metal ion binding peptides (Figure 2.4). This suggests an alternate mechanism involved in binding to NPs. In the next section, the binding of purified scFvs

has been investigated using various custom-designed *in vitro* assays. Moreover, binding of GSH43ϕ and Ti49ϕ clones to similar materials (same core composition but a different coating) and dissimilar materials were tested to better understand the mechanism of scFv binding/recognition of NPs, which is discussed in the next chapter.

# References

[1] Hoogenboom, H. R. Selecting and Screening Recombinant Antibody Libraries. *Nat Biotechnol,* **2005**, 23(9), 1105-1116.

[2] Arap, M. A. Phage Display Technology - Applications and Innovations. *Genetics and Molecular Biology,* **2005**, 28(1), 1-9.

[3] Smith, J., Kontermann, R. E. *et al.* Antibody Phage Display Technologies with Special Reference to Angiogenesis. *FASEB J,* **2005**, 19(3), 331-341.

[4] Nissim, A., Hoogenboom, H. R. *et al.* Antibody Fragments from a 'Single Pot' Phage Display Library as Immunochemical Reagents. *EMBO J,* **1994**, 13(3), 692-698.

[5] Willats, W. G. Phage Display: Practicalities and Prospects. *Plant Mol Biol,* **2002**, 50(6), 837-854.

[6] Johns, M., George, A. J. & Ritter, M. A. In Vivo Selection of Sfv from Phage Display Libraries. *Journal of immunological methods*, **2000**, 239(1-2), 137-151.

[7] Watters, J. M., Telleman, P. & Junghans, R. P. An Optimized Method for Cell-Based Phage Display Panning. *Immunotechnology,* **1997**, 3(1), 21-29.

[8] Malmborg, A. C., Duenas, M. *et al.* Selection of Binders from Phage Displayed Antibody Libraries Using the Biacore Biosensor. *Journal of immunological methods,* **1996**, 198(1), 51-57.

[9] Hawkins, R. E., Russell, S. J. & Winter, G. Selection of Phage Antibodies by Binding Affinity. Mimicking Affinity Maturation. *J Mol Biol,* **1992**, 226(3), 889-896.

[10] Bradbury, A. R. & Marks, J. D. Antibodies from Phage Antibody Libraries. *Journal of immunological methods,* **2004**, 290(1-2), 29-49.

[11] Ward, R. L., Clark, M. A. *et al.* Retrieval of Human Antibodies from Phage-Display Libraries Using Enzymatic Cleavage. *Journal of immunological methods,* **1996**, 189(1), 73-82.

[12] Haidaris, C. G., Malone, J. *et al.* Recombinant Human Antibody Single Chain Variable Fragments Reactive with Candida Albicans Surface Antigens. *Journal of immunological methods*, **2001**, 257(1-2), 185-202.

[13] Shea, C., Bloedorn, L. & Sullivan, M. A. Rapid Isolation of Single-Chain Antibodies for Structural Genomics. *Journal of structural and functional genomics*, **2005**, 6(2-3), 171-175.

[14] Denny, P., Hagen, F. K. *et al.* The Proteomes of Human Parotid and Submandibular/Sublingual Gland Salivas Collected as the Ductal Secretions. *J Proteome Res*, **2008**, 7(5), 1994-2006.

[15] Wuertzer, C. A., Sullivan, M. A. *et al.* Cns Delivery of Vectored Prion-Specific Single-Chain Antibodies Delays Disease Onset. *Molecular therapy : the journal of the American Society of Gene Therapy*, **2008**, 16(3), 481-486.

[16] Zheng, H., Mortensen, L. J. & DeLouise, L. A. Thiol Antioxidant-Functionalized Cdse/Zns Quantum Dots: Synthesis, Characterization, Cytotoxicity. *J Biomed Nanotechnol*, **2013**, 9(3), 382-392.

[17] Yu, W. W., Qu, L. *et al.* Experimental Determination of the Extinction Coefficient of Cdte, Cdse, and Cds Nanocrystals. *Chemistry of Materials*, **2003**, 15(14), 2854-2860.

[18] Malone, J. & Sullivan, M. A. Analysis of Antibody Selection by Phage Display Utilizing Anti-Phenobarbital Antibodies. *J Mol Recognit*, **1996**, 9(5-6), 738-745.

[19] Bass, S., Greene, R. & Wells, J. A. Hormone Phage: An Enrichment Method for Variant Proteins with Altered Binding Properties. *Proteins*, **1990**, 8(4), 309-314.

[20] Simmons, L. C., Reilly, D. *et al.* Expression of Full-Length Immunoglobulins in Escherichia Coli: Rapid and Efficient Production of Aglycosylated Antibodies. *Journal of immunological methods*, **2002**, 263(1-2), 133-147.

[21] Kabat, E. A. & Wu, T. T. Identical V Region Amino Acid Sequences and Segments of Sequences in Antibodies of Different Specificities. Relative Contributions of Vh and Vl Genes, Minigenes, and Complementarity-Determining Regions to Binding of Antibody-Combining Sites. *J Immunol*, **1991**, 147(5), 1709-1719.

[22] Horne, R. W. & Wildy, P. Virus Structure Revealed by Negative Staining. *Adv Virus Res*, **1963**, 10, 101-170.

[23] Rothenstein, D., Claasen, B. *et al.* Isolation of Zno-Binding 12-Mer Peptides and Determination of Their Binding Epitopes by Nmr Spectroscopy. *J Am Chem Soc*, **2012**, 134(30), 12547-12556.

# Chapter 3

*In vitro Verification of Binding of Isolated scFvs with Affinity to QDs and $TiO_2$ NPs*

# 3.1 Introduction

As the global production and use of NPs have increased and are projected to be over half a million tons by 2020[1], the potential for release of engineered nanomaterials into the environment is only going to increase[2]. NPs predominantly interact with the environment as aggregates[2]. Many studies pertaining to NP aggregation-state exists, and bring to light that the NP surface and the localized environment around that surface are critical to NP transformation in the environment. Transformations including aggregation/agglomeration can effect redox state reactions with biomacromolecules, which can affect NP transport, fate and toxicity[2]. For example, the surface of silver (Ag) NP, in addition to containing surface adsorbed molecules, is susceptible to reaction with oxygen, making it unlikely that Ag is the primary element on the surface. Similarly, it is unlikely that free $Ag^+$ is present in high concentration, as they have a tendency to form Ag complexes. This property of dissolution and aggregation can affect the physiochemical properties of the NP, how it interacts in biological systems and ultimately its fate, transport and toxicity[3]. Current analytical methods give a limited insight to these transformations; therefore more sensitive techniques are required[2] to yield information about NP state and presence in both, the environment and biological systems.

There is very little known about the ability of the immune system to recognize NPs[4,5]. We have proved in the previous chapter that it is possible to obtain antibodies recognizing and binding NPs using phage display technology without the need for NP immunogenicity. Our work is novel in panning against NPs in solution in order to obtain antibodies recognizing intact dispersed NPs as all other prior work published employed

NP immobilization strategies, which is limiting as discussed in Chapter 5[6,7]. Although for a successful proof-of-concept demonstration, we will need to test the binding of scFvs to NPs in a tissue environment, where the NPs interact with biomacromolecules such as proteins, the *in vitro* tests described in this chapter nevertheless give us the confidence that purified scFvs can be used as reagents to detect NPs, and even transformed NPs in the biological environment. In this chapter we present work done with many types of similar and dissimilar NPs to study the cross-reactivity and binding behavior of the scFvs GSH43 and Ti49. All the assays are custom-designed as there is no literature evidence on the existence of antibodies (scFvs or otherwise) against NPs. Appropriate negative controls such as 'no-NP' samples and arbitrary clones from the scFv library have been included in all experiments. The negative control scFvs used in the assay described in this chapter include human GRP78 (BiP), neurotrophin-3 (NT3) and a 15 amino acid (PVSP(ps)SQKLKRKAEEDPE) peptide (Npep). These controls were chosen simply based on ease of availability. Detailed descriptions of each assay are given below.

# 3.2 Materials and Methods

## 3.2.1 Protein (scFv) Synthesis and Purification

Preparation of the scFv protein from positive binders and negative controls was performed by removing the gene III fragment from the display vector by digestion of the plasmid with SalI and XhoI, followed by re-ligation of the compatible ends. This manipulation also appends a hexa-histidine tag to the carboxy terminus of the scFv to permit affinity purification of the protein on an immobilized $Ni^{2+}$ resin. The scFvs also

contain a FLAG epitope (DYKDDDDKL) at the amino terminus of the light chain domain to enable secondary detection with an anti-FLAG antibody. After removal of the M13 gene III fragment, scFvs were prepared by growth of the cultures in medium with limiting inorganic phosphate to induce expression from the *phoA* promoter. The cell pellets were lysed with BugBuster™ (Novagen) and the His-tagged scFvs were purified on $Ni^{+2}$ magnetic beads using a Thermo KingFisher instrument to automate bead washing. The scFvs were eluted from the washed beads using PBS containing 250 mM imidazole, dialyzed against PBS and stored at 4 °C. Prior to using scFvs in experiments, SDS-PAGE gel was used to confirm presence of scFvs in the sample. The gel was stained with Coomasie Blue (Simply Blue, Invitrogen) and photographed. The approximate concentration of the scFv purified was determined by measuring the absorbance at 280 nm and normalizing it with the reading for pure imidazole used during the above mentioned elution step.

### 3.2.2 Dot Blot Assay

In this assay 1 µL of each NP was spotted onto three pieces of nitrocellulose membrane (Optitran BA-S83, Whatman, Germany). The membrane was blocked with 5% non-fat milk (LabScientific Inc.) in wash buffer (0.15 NaCl, 10 mL Tris HCl (pH=8), 1 mL Tween 20 in water) at room temperature for 1 h, after which it was incubated overnight at 4 °C with scFvs (GSH-43, negative control BiP and Ti49) at a concentration of 4 µg/mL in milk. The membrane was rinsed 3 times in wash buffer for 3 min each, and the anti-FLAG antibody conjugated to horse radish peroxidase (HRP) at a 0.5 µg/mL concentration was added in milk and incubated for 1 h at room temperature. For

chemiluminescent detection, the membrane was incubated in ECL substrate solution (Reagent A+B, Thermo Fisher Scientific) for HRP for 5 min and developed using an x-ray film (Phoenix).

### 3.2.3 DLS Assay

GSH43 and negative control (BiP)-scFvs were incubated with GSH-QDs (50 nM) for 2 h at room temperature with gentle agitation, after which the solution was centrifuged at 55,000 rpm (Optima TLX ultracentrifuge, Beckman Coulter) for 10 min and the pellet re-suspended in TBS. These samples were again re-suspended in deionized water to make a 1 mL solution for each sample. Hydrodynamic diameter of the NPs with and without scFvs (only GSH-QDs in TBS) was analyzed using a Malvern Zetasizer NanoZS (Malvern Instruments Inc.) by measuring dynamic light scattering properties of these NPs in solution.

### 3.2.4 Image Stream Flow Cytometry

#### 3.2.4.1 Cells

Squamous cell carcinoma cells (SCC cell line) were used for the experiment due to their ease of availability (Pentland Lab, URMC). Trypsin (Invitrogen) was added to cells to gently dislodge them from the flasks and fetal bovine serum (FBS, Invitrogen) was added to neutralize trypsin. Cells were spun to form a pellet and re-suspended with GSH-QDs (~1 µL in 300 µL phosphate buffer serum (PBS)) and allowed to uptake/associate with the QDs for 1 h at room temperature. Cells were washed once in PBS and blocked with rabbit serum (host of secondary antibody, Sigma Aldrich Inc.) diluted (1:10) in for 1 h in

an ice bath. GSH43 and BiP scFvs were added to two different cell samples containing GSH-QDs at 10 µg/mL concentrations in BSA, and allowed to incubate for 1 h (ice bath). The cells were washed twice with ice-cold PBS to remove excess scFvs. An anti-FLAG Alexa Fluor 647 -conjugated antibody (Cell Signaling Technologies) was added diluted in BSA (1:100) and allowed to incubate with the cells for 1 h in an ice bath. The cells were again washed in ice-cold PBS to remove excess secondary antibody. Cells were then fixed in 2% formaldehyde in PBS for 20 min at room temperature. The cells were spun and re-suspended in 60 µL PBS prior to analyzing them on Image Stream (Amnis ImageStream GenX, URMC Flow core) Compensation controls such as cells stained with only the secondary antibody or GSH-QDs and a 'no-scFV' control with GSH-QDs and secondary antibody were included in all experiments. Samples were run on the Image Stream instrument and images were collected under brightfield and florescence using appropriate lasers for GSH-QDs (laser 405) and secondary anti-FLAG antibody (laser 647) at a magnification of 40X.

#### 3.2.4.2 Beads

Anti-FLAG antibody coated commercially available beads (Sigma Aldrich Inc.) were used to coat GSH43 and BiP scFvs passively overnight at 4 °C. Beads were collected and centrifuged to remove excess scFvs. The beads were blocked in 2% BSA in TBS for 1 h at room temperature. GSH-QDs at a concentration of 50 nM were added to samples containing scFv-coated beads and to a sample of uncoated beads. QDs were not added to the 'beads only' control. QDs were allowed to incubate with the beads for 2 h at room temperature with gentle agitation, after which the beads were washed in TBS with

repeated centrifugation and re-suspension. The beads were finally re-suspended in 60 µL TBS and analyzed using Image Stream under brightfield and fluorescence using appropriate lasers for QDs. Images were analyzed using IDEAS Application software (version 6.0). A more comprehensive image analysis was done where the individual samples mentioned above were transferred to individual wells in a 96-well plate. All the wells were scanned using Celigo S Cell Cytometer (Nexcelom Bioscience) and analyzed using the in-built software. Brightfield and fluorescent images were obtained using appropriate threshold values.

### 3.2.5 Confocal Microscopy

To confirm Ti49-scFv binding, ~0.4 mg of $TiO_2$ NPs in water were dried at 100 °C overnight on glass slides (VWR), after which the spot was enclosed in a barrier (Appendix B, Figure B1A) using a hydrophobic pen (ImmEdge™ Pen, Vector Labs). Slides were blocked in normal goat serum (Sigma Aldrich Inc., 1:10 diluted in TBS) and incubated with Ti49 and negative control (Npep)-scFvs (5 µg/mL) overnight at 4 °C. Slides were then washed with TBST and incubated with fluorescein isothiocyanate (FITC)-conjugated anti-FLAG antibody (Abcam) for 1 h at room temperature. The slides were again washed with TBST and mounted using in-house prepared mowiol for imaging using confocal microscopy (Olympus IX81 inverted microscope, URMC) with appropriate filters for FITC using a 60x oil objective. For quantitative analysis (ImageJ), fluorescence intensity for negative control and Ti49 images was calculated by the formula, *Fluorescence Intensity=Integrated Density-(Area of ROI*Mean Background*

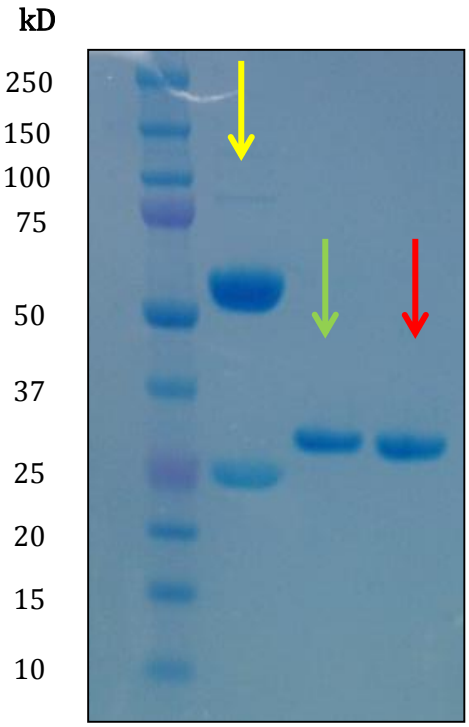


**Figure 3.1: Representative SDS-PAGE Gel**

Figure shows presence of purified GSH43-scFv (green arrow) and negative control (NT3, red arrow)-scFvs indicated by the blue bands (25 kD) compared to a whole antibody control (YerVoy antibody, yellow arrow).

*Fluorescence)* and plotted. A similar protocol was used to test binding of the GSH43-scFv compared to a negative control (Npep-scFv), where collagen (PureCol™, Invitrogen) was coated onto the slides (1:4 dilution in TBS) and allowed for 15 min. GSH-QDs (50 nM in sodium bicarbonate buffer) were incubated overnight at 4 °C. Slides were washed in TBST and blocked for 1 h with normal goat serum (1:10 in TBS) prior to staining. 5 µg/mL GSH43 and Npep-scFvs were added to the respective slides and incubated overnight at 4 °C. After thorough washing, FITC- conjugated anti-FLAG antibody was used to detect scFvs. Samples were mounted using mowiol and imaged using confocal microscopy (Olympus IX81 inverted microscope, URMC) using appropriate filters for FITC and QDs and a 60x oil objective. Image analysis was done using Olympus Fluoview Software (FV1000, Version 3.1b) and Pearson's coefficient of co-localization was found to be 0.65 (where, a value of -1=perfect exclusion, 0=random localization, 1=perfect co-localization).

# 3.3 Results

Upon confirming the presence of scFvs (expected MW=25kD) in the purified samples by SDS-PAGE gel analysis (Figure 3.1, green and red arrows) and determining their concentration of scFvs by absorption spectroscopy, different assays were used to confirm the binding and cross-reactivity properties of GSH43 and Ti49 scFvs to GSH-QDs and $TiO_2$ NPs respectively. Binding of GSH43-scFvs to similar and dissimilar materials with respect to GSH-QDs was tested using dot blots. For dissimilar materials, Au NPs (20 nm, citrated, Sigma Aldrich) and CNTs (multi-walled, MWSusp-100, NanoLab, Inc) w-

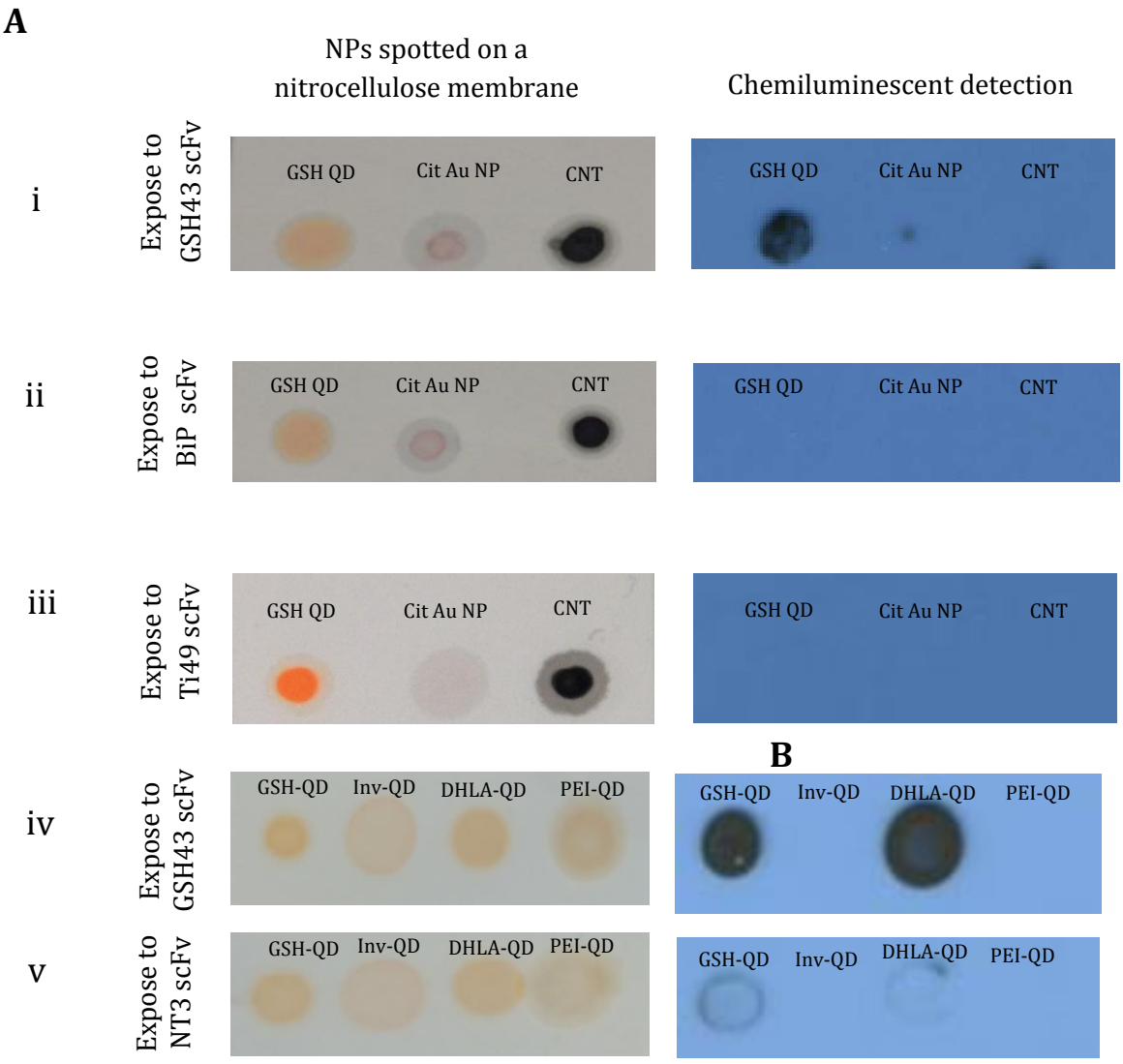


**Figure 3.2: Dot Blot Analysis**

Dot blots investigating scFvs (5 µg/mL) binding to similar and dissimilar materials. A) For dissimilar materials, spots on a nitrocellulose membrane (left column) showing GSH-QDs (orange), Au NPs (pink) and CNTs (black) spots. Chemiluminescence detection of scFv binding with HRP (right column). Results show that GSH43-scFv binds GSH-QDs but not Au NPs and CNTs (i), negative control BiP-scFv (ii) and Ti49-scFv (iii) do not bind any of the NPs. B) For similar materials, GSH-QDs, Inv-QDs, DHLA-QDs, and PEI QDs were spotted on a nitrocellulose membrane (left column). Upon chemiluminescence detection of scFv binding using HRP (right column), results show that GSH43-scFvs bind GSH-QDs and DHLA-QDs at 5 µg/mL, but not Inv-QDs and PEI-QDs (iv), whereas NT3 negative control scFvs (v) show faint background staining at the same concentration.

ere tested alongside GSH-QDs. Results showed strong binding of GSH43-scFvs to GSH QDs indicated by the formation of a dark chemiluminescent spot (Figure 3.2A(i)), whereas GSH43-scFvs did not bind Au NPs (pink spot) or the CNTs (black spot). In addition, negative control BiP-scFvs did not bind any of the NPs indicating specificity of GSH43-scFvs to GSH-QDs (Figure 3.2A(ii)). Moreover, Ti49-scFvs did not bind QDs, Au NPs or CNTs (Figure 3.2A(iii)). To test GSH43-scFV binding to materials similar to GSH-QDs, QDs with the same core/shell CdSe/ZnS composition but varying in surface coated ligands, either prepared in-house or obtained commercially were used. DHLA QDs (14 nm, negatively charged), polyethyleneimine (PEI)-coated QDs (23 nm, positively charged) and carboxylated QDs (565 nm emission, negatively charged, 10 nm, Invitrogen ITK 565™ (Inv-QDs)) were spotted on the membrane alongside GSH-QDs and tested for binding to GSH43-scFvs. Results showed that shows that GSH43-scFvs bind GSH-QDs and DHLA-QDs, but not Inv-QDs or PEI-QDs (Figure 3.2B(iv)). The negative control NT3-scFv showed only a faint background staining to all these QDs (Figure 3.2B(v)). This shows that GSH43-scFvs recognize QDs with a similar core/shell composition with different binding affinity likely modulated by the composition and lability of the surface ligand coating.

Next, we sought to measure the change in NP size upon scFv association as evidence for binding. GSH-QDs bound to GSH43-scFvs along with a negative control (BiP) and GSH-QDs alone in TBS in individual tubes were prepared as described above. The samples mixed with scFvs were pelleted using an ultracentrifuge and re-suspended in

**A**

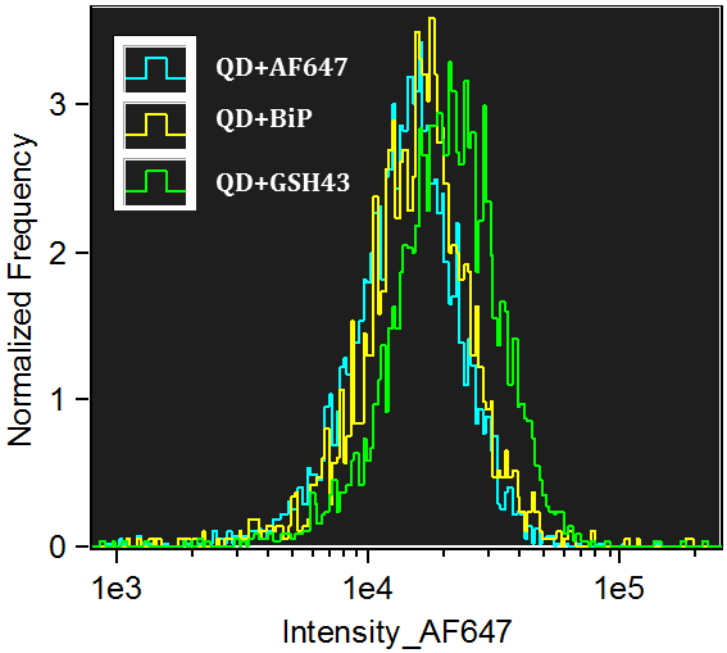


**B**

| Population | Count | % Gated | Median |
|---|---|---|---|
| QD+AF647_Cells&Focused | 4297 | 100 | 13945.94 |
| QD+BiP_Cells&Focused | 2149 | 100 | 15532.67 |
| QD+GSH43_Cells&Focused | 3809 | 100 | 20233.22 |

**Figure 3.3 Image Stream Experiment Using Cells**

A) Representative Image Stream histogram data using SCC cells showing intensity of Alexa Fluor 647-conjugated anti-FLAG antibody in QD+AF647 (no scFv), QD+BiP and QD+GSH43 samples. QD+GSH43 cell samples show a shift in the median intensity of Alexa Fluor 647 indicating binding of QDs to GSH43 which in turn binds to AF647 conjugated anti-FLAG antibody, compared to negative control scFv containing sample and sample without scFvs. B) Table showing values of median intensity for the three samples, the highest being GSH43 containing cells stained with GSH-QDs.

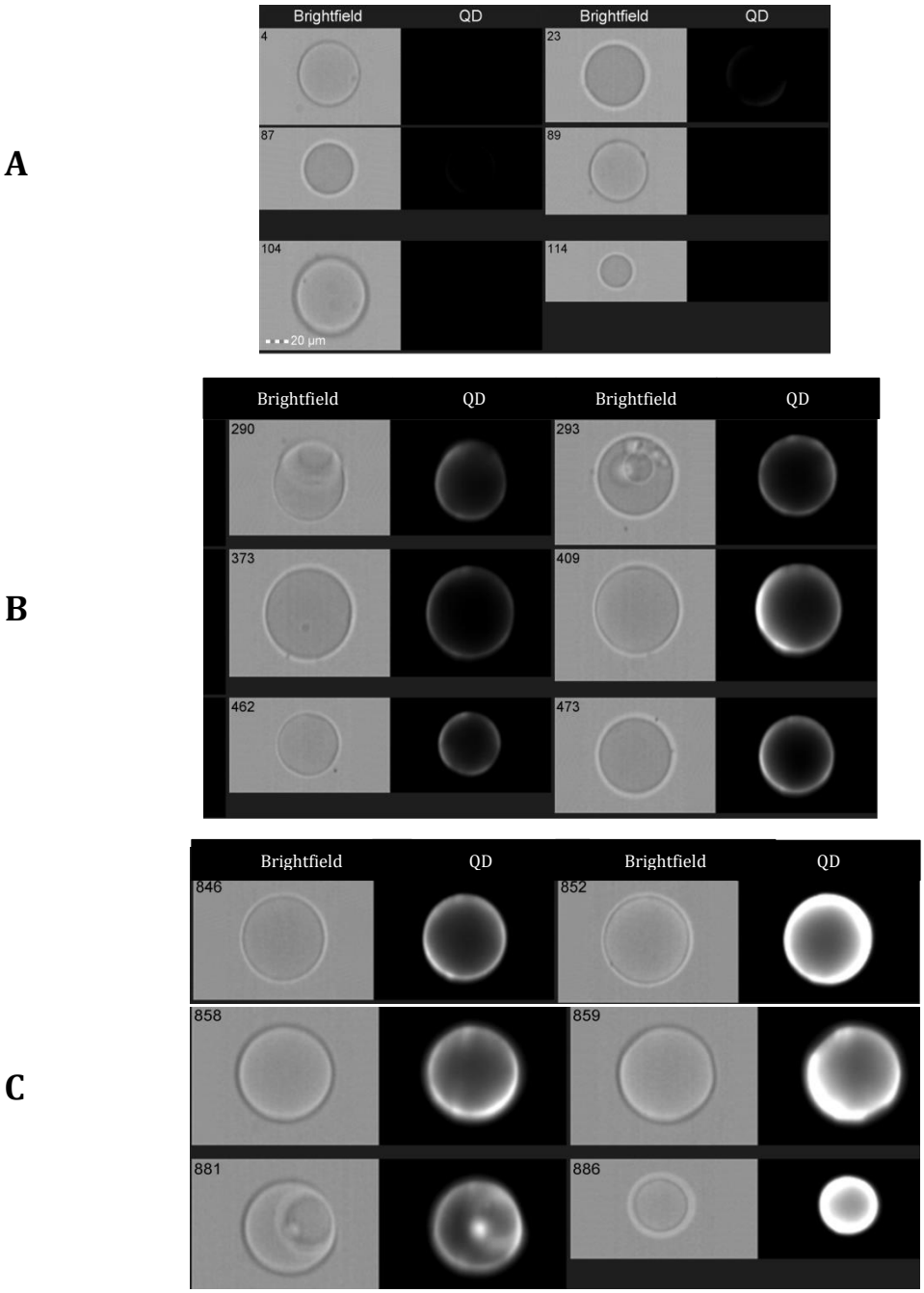


## Figure 3.4 Image Stream Experiment Using Beads

Representative images showing brightfield and QD channels of beads flowing through Image Stream flow cytometer where A) represents beads not coated with scFvs but treated with GSH-QDs. No QD fluorescence is seen in the images as they did not bind anti-FLAG coated agarose beads. However, upon coating beads with B) negative control BiP-scFv shows weak background QD binding and upon coating beads with C) GSH43-scFv, QD fluorescence is visibly higher due to binding of GSH-QDs to GSH43-scFvs. Scale bar=20 µm.

TBS. The control sample (GSH-QDs in TBS) was also taken through the whole process for comparison. It was found that the hydrodynamic diameter (Appendix B, Figure B1) of GSH-QDs bound to GSH43-scFvs (~651 nm) was 1.5-fold larger than that of BiP-associated GSH-QDs ($p<0.05$, one-way ANOVA) and 2.5-fold larger than GSH-QDs alone in TBS with statistical significance ($p<0.01$, one-way ANOVA).

To further confirm scFv binding, we conducted image stream experiments outlined in Section 3.2.4 employing a comprehensive gating scheme. First, the events which were not in focus were excluded in the analysis. Within the population of events in focus, the 'cells' were selected based on aspect ratio and area. The population of cells containing QDs and stained with anti-FLAG Alexa Fluor 647 were analyzed for co-localization of the fluorophores which was taken as an evidence of binding of GSH43-scFv to GSH-QDs. Results showed that there was an increase in the median intensity (Figure 3.3) of anti-FLAG Alexa Fluor 647 in the cell populations containing QDs and GSH43-scFv (median=20233.22) represented by a slight shift in the histogram compared to a negative control (BiP-scFv containing cells, median=15532.67), and cell samples containing no scFvs (containing GSH-QDs and stained with anti-FLAG Alexa Fluor antibody, median=13945.94). Since only a 30% increase in intensity was observed, we attributed this to the potential varying QD uptake behavior in cells.

To eliminate these cell-to-cell differences in QD uptake, anti-FLAG antibody coated agarose beads were used to perform the experiment. Upon binding scFvs to these beads, GSH-QD binding to GSH43-scFvs was analyzed comparing it to beads coated with a negative control scFv (BiP) and stained with GSH-QDs, and beads not coated with

scFvs but stained with GSH-QDs (Figure 3.4). Results again showed an increase in QD fluorescence intensity of beads coated with GSH43-scFv and stained with GSH-QDs demonstrating a 2-fold increase in intensity compared to BiP-coated beads and a 3-fold increase compared uncoated beads (Appendix B, Figure B2). This is almost a 10-fold increase in QD intensity upon binding to GSH43-scFv coated beads compared to beads coated with BiP-scFv. The observed increase in QD intensity on beads coated with GSH43-scFv compared to the negative control scFv coated beads was found to be statistically significant (student's unpaired t-test, $p=0.035$). A potential issue was the occasional clogging of the flow channels due to the heterogeneity in the size of the beads and this was confirmed by observing the bead samples in a 96-well plate using brightfield and fluorescence filters (Celigo Instrument). Results again showed greater QD fluorescence intensity in the wells containing beads coated with GSH43-scFv compared to BiP coated beads (Appendix B, Figure B3).

To test the binding of Ti49-scFvs to $TiO_2$ NPs we could not use dot blot analysis since the presence of $TiO_2$ NPs on the nitrocellulose membrane could not be verified by color. Hence to confirm Ti49-scFv binding to $TiO_2$ NPs, we dried the NPs on to a glass slide and used confocal microscopy to quantify presence of FITC-conjugated anti-FLAG reporter. Images were captured both under brightfield and fluorescence. ImageJ was used for the analysis of line profiles of three regions of interest (ROIs) and the results averaged. A control slide without $TiO_2$ NPs (Appendix B, Figure B4A) treated with scFvs and anti-FLAG antibody shows no background staining (Appendix B, Figure B4B). Figure 3.5A (row 2) shows binding of Ti49-scFv to $TiO_2$ NPs as it can be

determined by the fluorescence signal from FITC-conjugated anti-FLAG antibody. Although a slight background signal was detected for negative control treated (Npep-scFv) on $TiO_2$ (Figure 3.5A, row 1), the quantification data (Figure 3.5B) clearly shows a statistically significant difference in the level of binding of Ti49-scFvs to $TiO_2$ NPs showing the ability of these scFv antibodies to detect NPs *in vitro*. A similar experiment was done with GSH- QDs where they were immobilized on the glass slide using a collagen coating (Appendix B, Figure B5A) and tested binding to GSH43-scFvs relative to a negative control (Npep-scFv) using confocal microscopy. A strong specific binding of GSH43-scFvs to GSH-QDs (Appendix B, Figure B5B) was observed as indicated by the co-localization signal from FITC-conjugated anti-FLAG antibody and GSH-QDs (Pearson's co-localization coefficient=0.65, Appendix B, Figure B5C).

# 3.4 Conclusions

We have demonstrated that scFvs can be used successfully as reagents to detect NPs employing standard immunolabeling using various custom-designed *in vitro* assays. GSH43 and Ti49-scFvs show binding to GSH-QDs and $TiO_2$ NPs respectively over negative control scFvs included in all experiments. The scFvs did not show binding to other materials used in the experiments such as collagen or glass proving ability to recognize NPs in a laboratory setting. Low numbers of events in the case of using beads to verify QD binding to scFvs is due to the potential aggregation of anti-FLAG antibody coated agarose beads causing blockage and a substantial decrease in the regular flow of beads in the instrument thereby requiring longer times to collect all the beads in the sam-

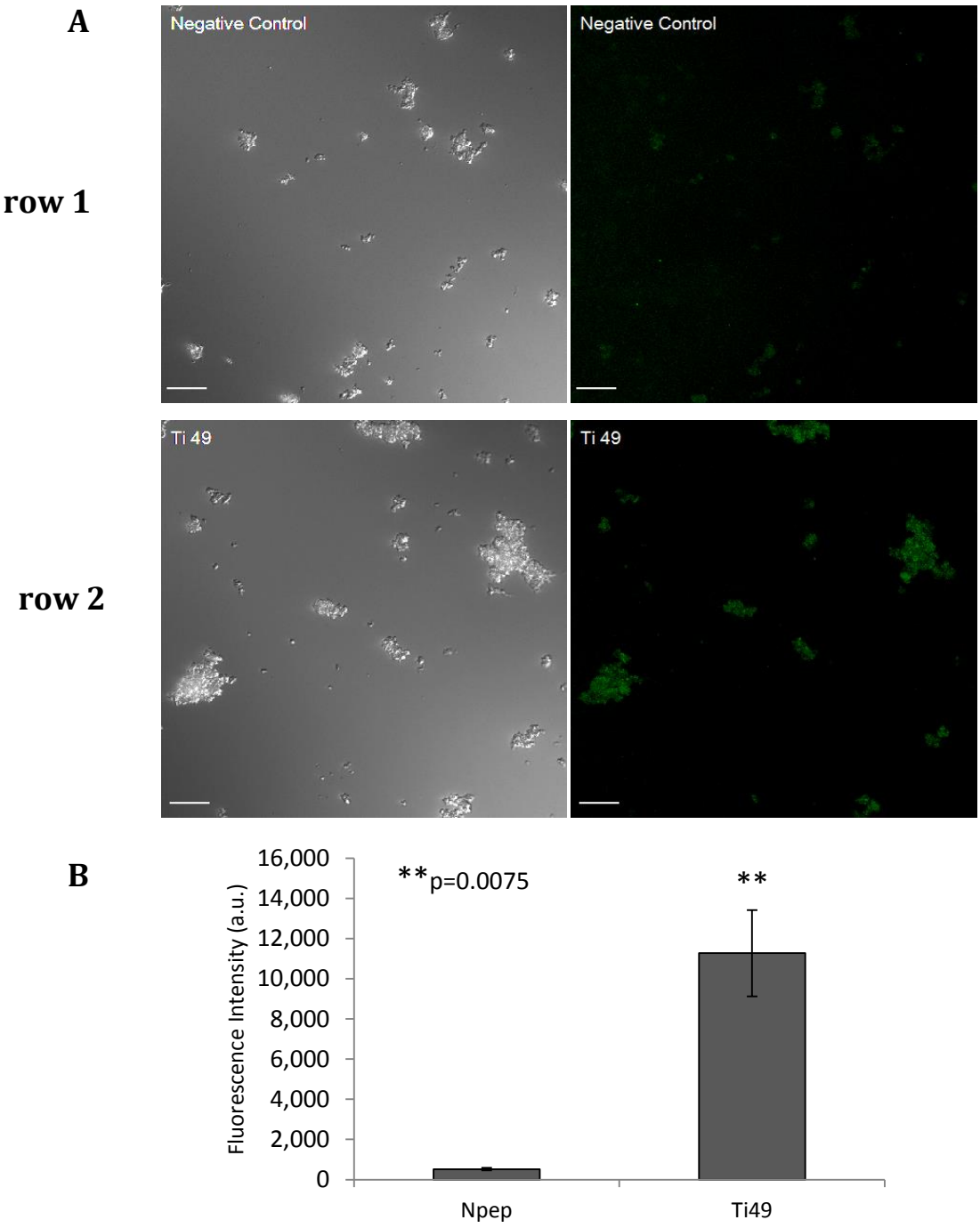


**Figure 3.5: Confocal Microscopy**

Brightfield and fluorescence images investigating the binding of Ti49-scFvs to $TiO_2$ NPs immobilized on a glass slide using FITC-conjugated anti-FLAG secondary antibody detection. A) Representative images of negative control Npep-scFv showing minimal binding to $TiO_2$ NPs (row 1), whereas Ti49-scFvs shows strong binding to $TiO_2$ NPs (row 2). Scale bar=20 μm. B) Quantitative analysis of the integrated fluorescence intensity shows significant difference in the Ti49-scFv treated sample compared to negative control Npep-scFv. Data shown is average of three ROIs from the images. Error bars indicate SEM. **p=0.0075 using student's unpaired t-test.

ple. However, representative data from all the experiments performed (n=3 for cells and beads) show evidence for scFv binding over the control samples included. It was also demonstrated that these scFv antibodies could be used to detect NPs using standard assays that can further be custom-designed for future applications such as to detect NPs in environmental samples including water and soil samples. This is the first time to our knowledge that antibodies against GSH-QDs and $TiO_2$ NPs have been developed using phage display and have been shown to bind these NPs with good specificity. In the next chapter, the functionality of these antibodies in their detecting of fluorescent and non-fluorescent NPs in a biological milieu has been investigated.

# References

[1] Robichaud, C. O., Uyar, A. E. *et al.* Estimates of Upper Bounds and Trends in Nano-Tio2 Production as a Basis for Exposure Assessment. *Environ Sci Technol*, **2009**, 43(12), 4227-4233.

[2] Maurer-Jones, M. A., Gunsolus, I. L. *et al.* Toxicity of Engineered Nanoparticles in the Environment. *Anal Chem*, **2013**, 85(6), 3036-3049.

[3] Levard, C., Hotze, E. M. *et al.* Environmental Transformations of Silver Nanoparticles: Impact on Stability and Toxicity. *Environ Sci Technol*, **2012**, 46(13), 6900-6914.

[4] Chen, B. X., Wilson, S. R. *et al.* Antigenicity of Fullerenes: Antibodies Specific for Fullerenes and Their Characteristics. *Proc Natl Acad Sci U S A*, **1998**, 95(18), 10809-10813.

[5] Izhaky, D. & Pecht, I. What Else Can the Immune System Recognize? *Proc Natl Acad Sci U S A*, **1998**, 95(20), 11509-11510.

[6] Mardyani, S. & Chan, W. C. W. Quantification of Quantum Dots Using Phage Display Screening and Assay. *Journal of Materials Chemistry*, **2009**, 19(35), 6321-6323.

[7] Rothenstein, D., Claasen, B. *et al.* Isolation of Zno-Binding 12-Mer Peptides and Determination of Their Binding Epitopes by Nmr Spectroscopy. *J Am Chem Soc*, **2012**, 134(30), 12547-12556.

# Chapter 4

*Verification of Binding of scFvs to NPs in a Biological Milieu*

# 4.1 Introduction

As discussed in the previous sections of this dissertation, humans are increasingly susceptible to interaction and subsequent contact with nanomaterials by the day, due to the increased use of NPs/nanomaterials in the fields of engineering, oncology, dermatology and chemistry to name a few[1]. Skin is the first point of contact for nanoparticles-from topical applications, clothing, sports goods and domestic utensils[2], although the respiratory and the gastrointestinal system are the other modes of NP entry into the body. Researchers focusing on NP-skin penetration often report data based on the use of a high acute dose of NP in animal models, which is unlikely to occur in an ambient or occupational setting, which is more likely to be chronic low dose exposure. Diseases such as cancer can take years to develop following low dose chronic exposure to chemical carcinogens such as cigarette smoke[3] and asbestos[4]. The acute model is generally preferred in order to obtain a high signal to noise ratio; however, adverse outcomes if any in humans and in the environment are dependent upon real-life exposures at toxicologically relevant doses[5].

One of factors limiting our ability to predict the fate and transport of NPs in a biological environment is the lack of sensitive analytical instrumentation to detect low doses of NPs in the tissue. Quantification of NP dose in order to correctly understand NP fate and effects on tissues and organs is vital and many techniques have been developed in this regard. However, techniques such as atomic absorption spectroscopy (AAS) currently used to quantify presence of NPs in organs and tissues, despite having good sensitivities, fail to distinguish between metals in the elemental form (eg. free ion) or in

the NP form. This can especially be crucial for drawing conclusions about NP localization in the body. Proteins present in the biological milieu may also confound NP fate, translocation and detection. Proteins may play the role of a stabilizing agent by forming a protein corona on the surface of NPs[6]. The adsorbed proteins likely dictate the initial biological responses to the presence of the NPs. These 'transformed' NPs may have altered physiochemical properties such as surface charge[6] and size, which may change over time posing further challenges in detecting them and elucidating their biological impact. Therefore, new sensitive methods must be developed in order to detect transformed NPs and understand conditions under which NPs may enter the body and be transported into systemic circulation.

In this chapter, the scFvs identified against GSH-QDs and $TiO_2$ NPs have been tested for their functionality in binding to those NPs in a biological milieu using an *ex vivo* human skin tissue model. Of the existing biomedical applied nanotechnologies to date, the use of CdSe/ZnS core/shell nanocrystals (semiconductor QDs) has been at the forefront of biomedical research[7,8], and thus will be the choice of NP for the proof-of-concept studies described in this chapter. Their unique fluorescence signature will enable tracking them and thereby verify their binding to the scFv antibody using commonly used detection techniques in these proof-of-concept studies. Following studies with GSH-QDs, the ability of the scFvs isolated against $TiO_2$ NPs (P25 form) will be tested for the detection of non-fluorescent $TiO_2$ NPs in a human skin model. Immunohistochemistry (IHC) was used where the scFvs binding the NPs were detected using a secondary

enzyme-conjugated anti-FLAG antibody, which yields a distinct color based on the substrate used in the assay.

# 4.2 Materials and Methods

## 4.2.1 Skin Processing

All *ex vivo* studies were performed on fresh viable human skin obtained hours within an abdominoplasty or mammoplasty (Strong and Highland Hospitals, University of Rochester, NY). Ethical approval was obtained from the University of Rochester Research Subjects Review Board (RSRB00031804). The skin was washed three times with 1X phosphate buffered saline (PBS) and treated with 5 μg/mL fungizone (Invitrogen) in 25 mL sterile PBS for 10 min. It was then rinsed thoroughly with 1X PBS three times to remove excess fungizone before tissue processing. In a HEPA-filtered tissue culture hood (SterileGARD III Advance), using a sterile blade (Bard-Parker, BD Acute Care, NJ, USA) and a scalpel (Fisher Scientific Inc.), the subcutaneous fat was removed and the dermal layer was thinned down leaving the epidermis intact. The blades were changed in regular intervals. For all experiments, skin pieces of ~5-6 $cm^2$ were cut from the donor sample. In the case where skin barrier disruption was required to allow NP penetration as a positive control, skin samples were tape stripped (Scotch 3M 3750 clear packing tape, USA) ten times prior to NP application by pressing a fresh piece of tape firmly on to the skin and removed prior to the application of the next piece of tape.

### 4.2.2 Nanoparticle Application to Skin

Skin samples were placed on gauze in a sterile petri-dish filled with media (RPMI media, Invitrogen, 5-8 mL) to keep the skin viable during the course of the experiment. GSH-QDs and $TiO_2$ NPs in water were applied on to the skin in quantities less than those routinely used for cosmetic testing. Typically sunscreens are tested at 2 mg/cm$^2$. Hence, for a sunscreen with 5% w/w $TiO_2$ NPs this would be 0.1 mg/cm$^2$ NPs applied. In our studies we applied 0.01 mg/cm$^2$ $TiO_2$ NPs and GSH-QDs by pipetting and spreading them evenly on the epidermal side of the skin. GSH-QDs were also applied to the dermis side of skin or injected (50 μL in 100 μL deionized water) using an insulin needle (skin rested with stratum corneum facing upwards) from epidermis to dermis where positive control samples were required. $TiO_2$ NPs in water were applied to dermis when positive control samples were desired, and a $TiO_2$ NP-containing sunscreen (Eucerin SPF15) was applied to skin samples (at 2 mg/cm$^2$, 8 mg total) for validating Ti49-scFvs to detect $TiO_2$ NPs in the sunscreen. Skin samples were placed in the sterile hood for 24 h, after which excess NPs were wiped off the skin surface gently using gauze dipped in sterile 1X PBS. All the skin samples post NP application were stored at -80 °C until analysis.

### 4.2.3 Immunohistochemistry

Frozen skin was mounted using TEK OCT compound, after which they were sectioned (5 μm thickness) on to microscope slides (VWR) using a cryostat (Thermo Scientific). The epidermis and the dermis were sectioned simultaneously to prevent accidental transfer of NPs to the blade. Blades were changed between sections at regular intervals to prevent

accidental transfer of NPs on the blade to the skin surface. The slides were fixed in methanol (-20 °C, 10 min) prior to the experiment and dipped in water (Ultrapure™ water, Invitrogen) to remove the excess OCT compound. The slides were washed twice with 1X TBS to wash off excess methanol and a hydrophobic pen was used to create a water-repellent barrier to keep reagents localized on the tissue specimen. The slides were blocked with normal mouse serum for 30 min (Sigma Aldrich) at room temperature, after which GSH43-scFvs were added to the slides, diluted in 1% BSA in TBS (10 µg/mL) and allowed to incubate overnight at 4 °C in a humidified chamber. The slides were washed thrice with 1X TBST and incubated with anti-FLAG antibody conjugated to alkaline phosphate (AP) (Sigma-Aldrich Inc.) for 1 h at room temperature at a 0.1-0.5 µg/mL concentration. After removing excess antibodies by washing, the slides were incubated with BCIP/NBT (KPL) substrate for AP with the addition of levamisole (Vector laboratories Inc., CA) for 5 min at room temperature. Levamisole is an endogenous AP inhibitor that enables visualization of AP staining due to the binding of scFv-anti-FLAG AP-tagged antibody alone. Excess substrate solution was washed away with deionized water and mowiol (Fluka, #81381, Sigma Aldrich Inc., prepared in-house) was used as a mounting medium for imaging. The samples were analyzed under a fluorescent microscope (Nikon Eclipse E800 with a Spot RTS Camera) at 40x magnification. Images were captured using brightfield and appropriate fluorescence filters (for QDs), and analyzed using ImageJ (NIH).

### 4.2.4 Laser Capture Microdissection/Atomic Absorption Spectroscopy

Samples (frozen sections post-IHC on glass slides) prepared for Laser Capture Microdissection (LCM, Zeiss, Palmbeam) using the IHC method described above were imaged under brightfield for AP staining and fluorescence using an appropriate filter for QDs (exposure: 800 ms). Both, brightfield and fluorescence images were captured at 40x magnification before laser catapult (cut) and after cut, and the skin sections collected onto AdhesiveCap™ (Zeiss) microfuge tubes were analyzed using AAS for presence of cadmium (Cd) for both QD containing samples and control specimens not containing QDs. A total of three ROIs for positive control studies with GSH-QDs injected in skin and two ROIs from control tissue sections were collected for AAS analysis. Cd concentration analysis was performed using a Perkin-Elmer PinAAcle 900Z atomic absorption spectrometer equipped with longitudinal Zeeman background correction and a transverse heated graphite furnace (Perkin-Elmer Life and Analytical Sciences, Shelton, CT 06484 USA). Cd absorption was measured at 228.8 nm using an electrodeless discharge lamp source. A mixed matrix modifier of ammonium phosphate and magnesium nitrate was used to stabilize Cd during the pyrolysis step. Both, positive controls as described above and GSH-QDs (applied on the epidermis) samples were prepared for AAS by adding 200 µL of 4% ultrapure nitric acid (PlasmaPure Nitric Acid, SCP Science, NY) to the microfuge tube. The tube was then capped and inverted for 3 h to dissolve the sample on the cap. After vortexing the tube, 100 µL was taken for AA analysis.

### 4.2.5 Scanning Electron Microscopy

Prior to imaging skin sections, $TiO_2$ detection limit quantification on the Zeiss Supra 40VP Field Emission SEM (University of Rochester) was done by preparing coverslips with 50 μL each of 1, 0.1 and 0.01 mg/mL $TiO_2$ in water pipetted onto an area of 1 $cm^2$. EDX spectra were obtained for each of the samples where a discernable peak for Ti was observed for 1 (50 μg/$cm^2$ $TiO_2$) and 0.1 mg/mL (5 μg/$cm^2$ $TiO_2$) samples but not for 0.01 mg/mL (0.5 μg/$cm^2$ $TiO_2$) sample (Appendix C, Figure C1).

Human skin sections containing $TiO_2$ NPs applied to the dermis or the epidermis were cryosectioned on quartz coverslips to ensure an absence of inherent Ti contained in the coverslips. Following IHC staining procedures described above, regions of AP staining were visualized and marked for SEM imaging using the brightfield settings in a light microscope.

## 4.3 Results

### 4.3.1 Validating GSH43-scFv Binding to QDs

The ability of GSH43-scFvs to bind to GSH-QDs in skin was verified using *ex vivo* human skin. NPs were applied using previously established protocols[9]. Following skin exposure to NPs, the tissue was cryosectioned for IHC analysis using scFvs and a secondary anti-FLAG reporter conjugated to alkaline phosphatase (AP). Skin slices were treated with levamisole (1 drop for every 200 μL of substrate) during incubation with BCIP/NBT substrate for AP in order to eliminate endogenous phosphatase activity and allow for visualization of only those bluish-purple regions formed due to binding of

scFvs-anti-FLAG conjugate to NPs. Prior to experiments control skin samples (without NPs) were tested for endogenous phosphatase activity and absence of AP staining was ensured with the addition of levamisole.

Figure 4.1 shows bright-field and fluorescent images of a skin section following a 24 h application of GSH-QDs to the stratum corneum and a control sample (no QD exposure). The control sample shows negligible AP staining (Figure 4.1A), indicating the absence of non-specific GSH43-scFv binding to the skin sections. In contrast, the skin sample exposed to GSH-QDs shows numerous punctate areas of strong AP staining in brightfield (Figure 4.1B). Observation of this skin section under fluorescence imaging shows a dense cluster of QDs (Figure 4.1C) that co-localizes with AP staining (blue arrows, Figure 4.1B, inset). However, based on fluorescence imaging (Figure 4.1C) the detection of GSH-QD presence in skin is suggested to be far less than that suggested by AP staining. Using ImageJ software, the fluorescence image can be threshold enhanced (Figure 4.1D), which reveals many more potential instances of QDs in the skin tissue; but as previously noted[10] it is difficult to unambiguously distinguish the QDs from tissue autofluorescence artifacts. Results from AP staining (Figure 4.1B) however, clearly demonstrate the utility of GSH43-scFvs to overcome this challenge. The AP staining identifies many areas that co-localize with high fluorescence (black arrows, Figure 4.1B and 4.1D). Additionally, we observed regions with strong AP staining with corresponding regions that do not show presence of QD fluorescence (red arrows, Figure 4.1B and 4.1D) suggesting that scFvs can be used to identify QDs whose fluorescence cannot be detected over background.

In order to validate that the fluorescent regions co-localizing with AP staining indeed contain QDs, we used the LCM technique to isolate portions of tissue by cutting and catapulting them on to an AdhesiveCap™ microfuge tubes placed directly over the specimen using a designed laser pulse. Downstream analysis of the specimens in the tubes involved use of AAS technique to assay for elemental Cd presence. Detection of Cd implies presence of GSH-QDs in the samples, as Cd was part of the core composition of the QDs used in the study. Initial studies were conducted on a skin sample with a high QD presence introduced by dermal injection to ensure Cd levels exceeded the AAS detection limit of detection (LOD) equal to 7 pg/ml. The control skin sample (no QDs, Figure 4.2) again showed no discernable AP staining and no visible fluorescence QD signal (exposure time: 800 ms). In contrast, strong AP staining is seen under bright-field in the dermis where GSH-QDs were injected as shown in Figure 4.3A with the corresponding QD fluorescence before dissection shown in Figure 4.3B. The portion of the skin marked for dissection is enclosed in the blue dotted area (Figure 4.3C). The portion remaining after catapult is shown in Figure 4.3D. AAS analysis of the tissue areas where strong QD fluorescence was co-localized with AP staining was performed to confirm the presence of Cd. Since the mass of tissue was too low to be quantified, results were expressed as concentration of Cd, which was found to be 214 ng/mL of Cd.

Having demonstrated the ability of the LCM/AAS techniques to detect QD presence in the positive control sample, we proceeded to use this methodology to confirm the presence of QDs in epidermal regions that exhibit strong AP staining following their topical application on tape stripped skin (Figure 4.4). Initial measurements of individual

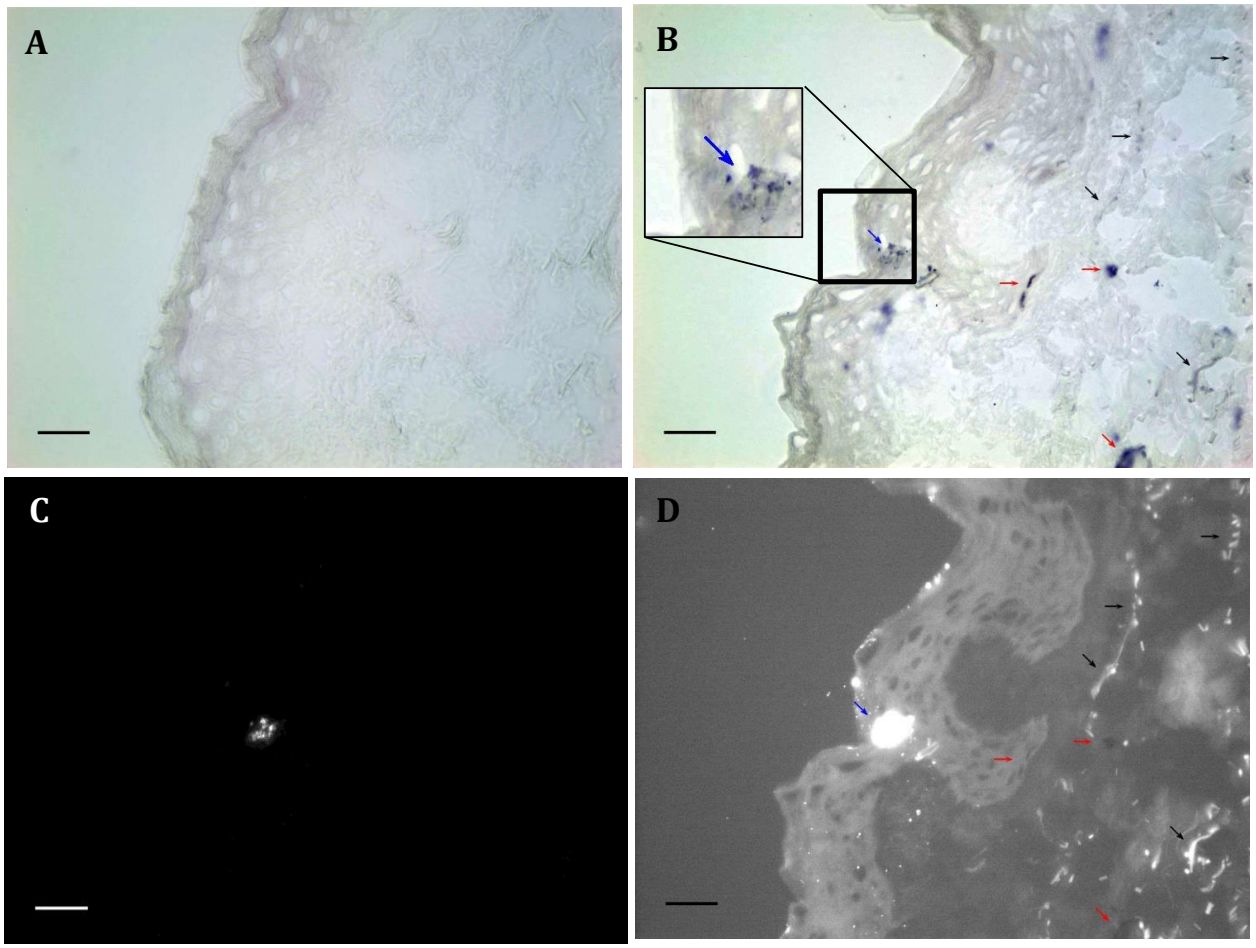


**Figure 4.1: QD Detection in *ex vivo* Human Skin using GSH43-scFv**

Representative skin images under brightfield and fluorescence. A) Control skin sample without GSH-QD exposure showing an absence of AP staining indicating absence of non-specific binding of GSH43-scFv to skin. B) Brightfield image of skin sample exposed to GSH-QDs for 24 h showing numerous areas with strong AP staining (black, blue, and red arrows). Inset shows an area of high AP staining (blue arrow) in the epidermis that correlates with high QD presence as seen under C) fluorescence imaging, exposure 1.642 s. D) Applying a threshold to enhance the fluorescent signal shows that some of the areas with strong AP staining (black arrows) co-localize with QD fluorescence, whereas other areas (red arrows) indicate potential presence of QDs that are not visible under the fluorescence exposure conditions used. This suggests the ability of GSH43-scFv to detect the presence of QDs that may otherwise being undetectable in skin. This was confirmed with LCM studies. Scale bar=50 μm.

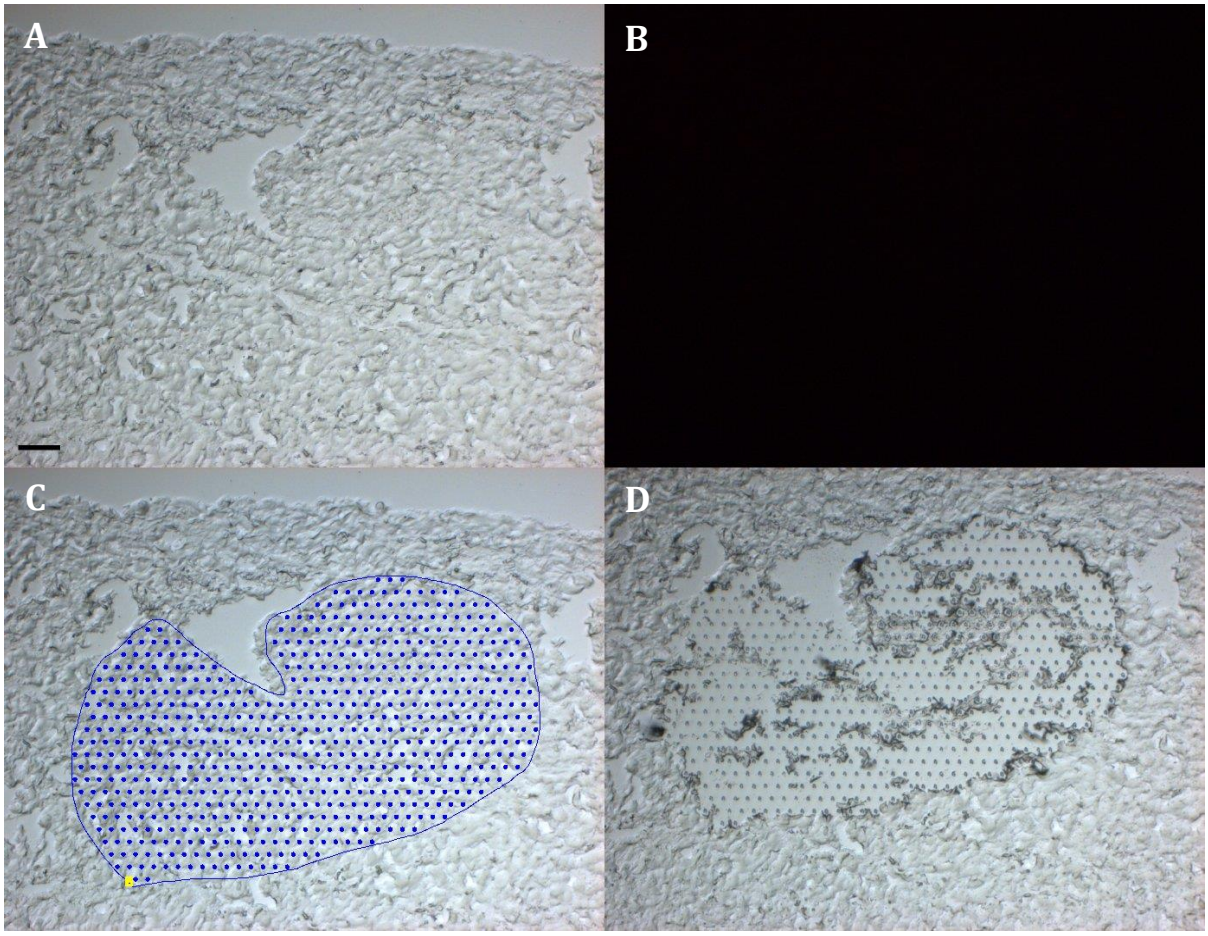


**Figure 4.2: LCM Imaging of Control 'no QD' Sample in Dermis of Skin**

Representative control sample showing A) no AP staining indicating lack of binding of GSH43-scFvs to GSH-QDs. B) Complete absence of GSH-QDs (no fluorescence). C) Portions of tissue sections were marked for cut and captured onto adhesive tube caps using LCM, and processed for AAS. D) The portion of skin remaining after capture is shown. Scale bar=50 μm.

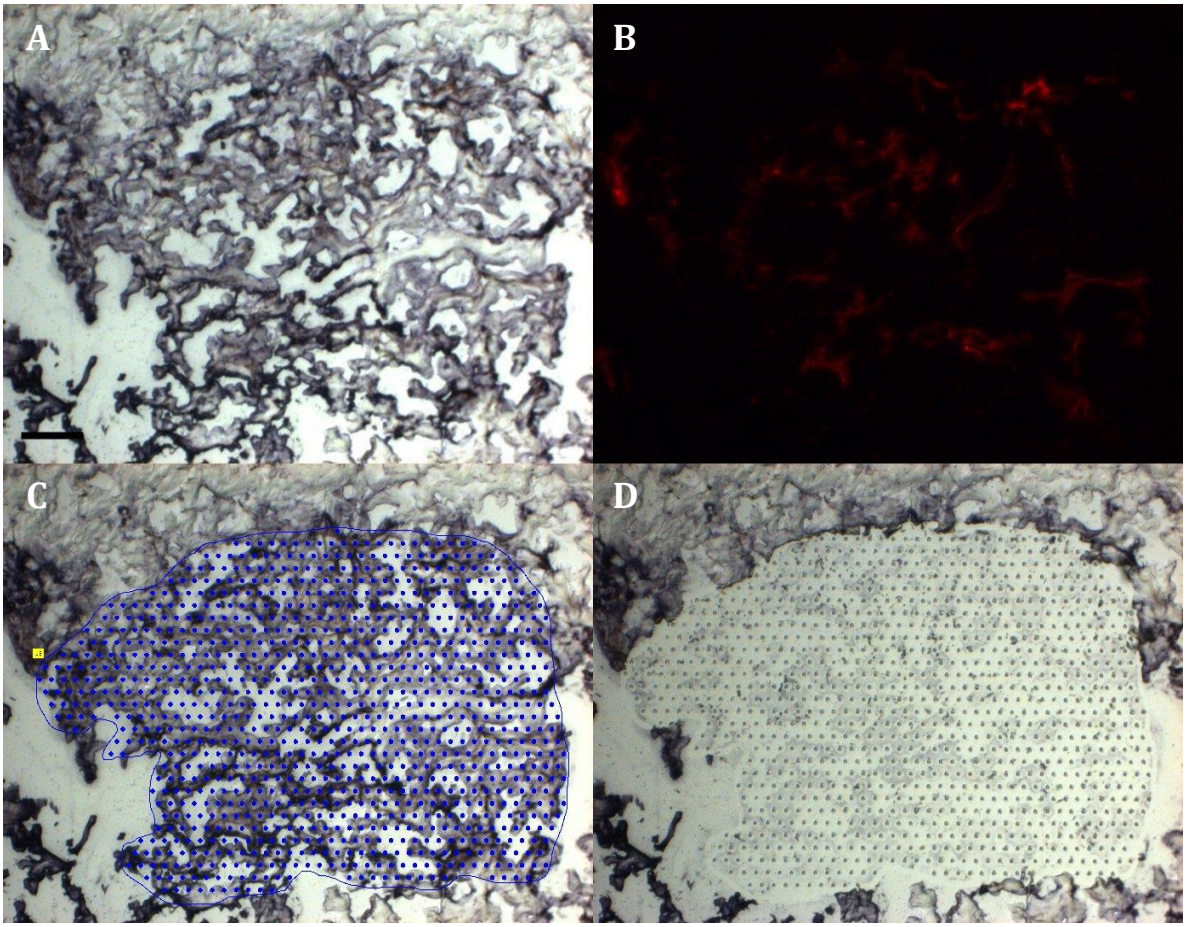


**Figure 4.3: LCM Imaging to Confirm Presence of QDs in Dermis**

Representative skin sample containing QDs injected showing A) dark bluish-purple staining indicating binding of GSH43-scFvs detected by AP. B) Fluorescence image of skin sample before dissection showing QD presence. C) Portions of stained areas were marked for cut and captured onto adhesive tube caps using LCM, and processed for AAS. D) The portion of skin remaining after capture. Scale bar=50 μm.

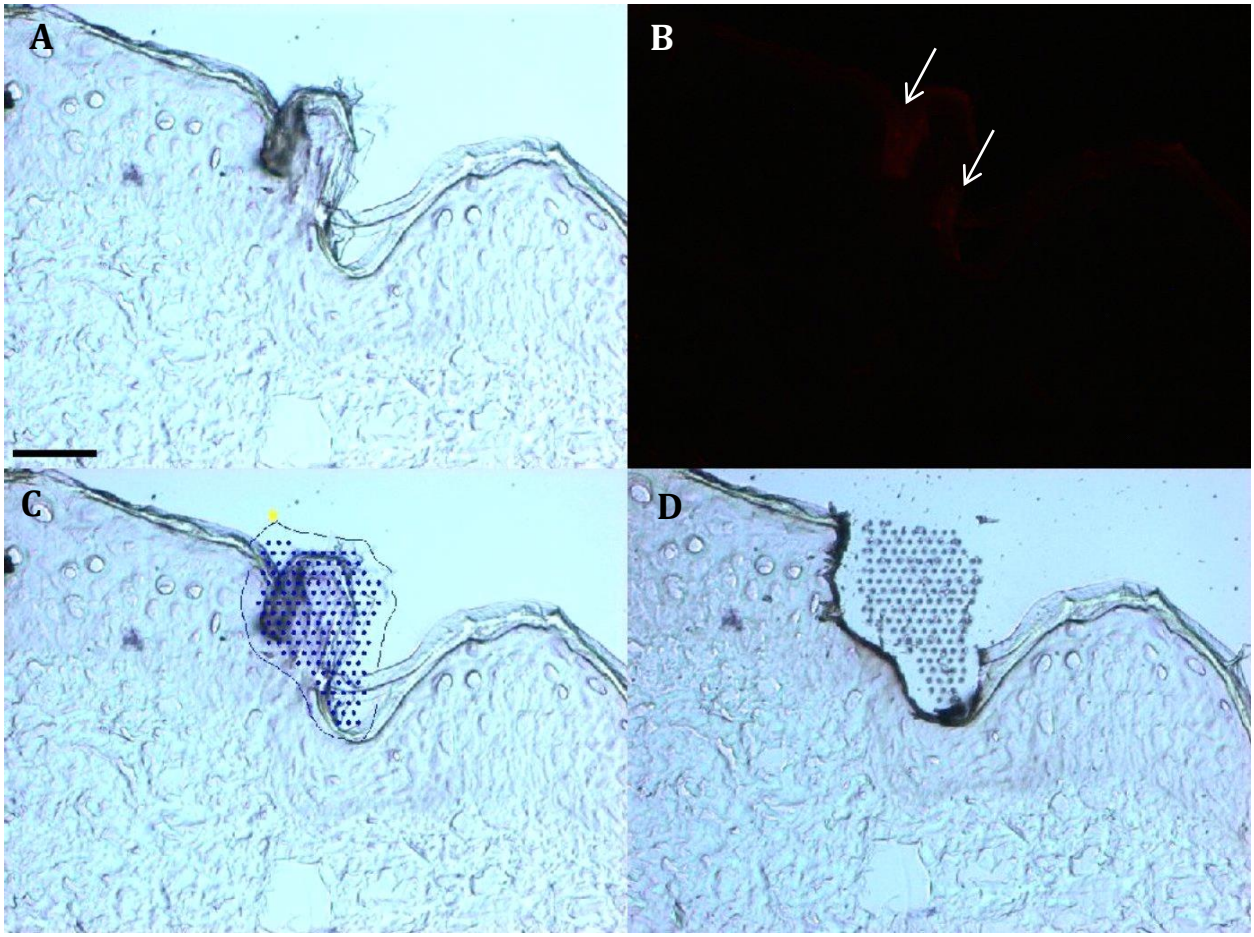


**Figure 4.4: LCM Imaging of QDs Applied on Epidermis of Skin**

Representative skin image showing A) AP staining on epidermis due to binding of GSH43-scFvs to GSH-QDs applied on epidermis. A portion with visible staining and B) fluorescence (white arrows) was C) marked for cut and D) captured for AAS analysis. Cd levels were found to be 0.108 ng/mL, which was above instrument LOD (0.007 ng/mL) proving presence of QDs. Scale bar=50 μm.

ROIs in tissue sections showed levels of Cd <LOD using AAS. However by combining six ROIs with strong AP staining we measured 108 pg/mL of Cd concentration, which is ~100 times above the LOD indicating the presence of QDs in these regions. The Cd level measured from six random ROI collected and combined from the control sample (no QD, Figure 4.5) was 8.5 pg/mL, which is near the instrument LOD (7 pg/ml) and may indicate the presence of endogenous Cd derived from dietary sources which is more readily detected in the liver[11,12]. In addition, we collected and combined six ROIs with strong AP staining (Figure 4.6A) that lacked discernible QD signal under fluorescence imaging (Figure 4.6B). AAS analysis measured 18 pg/mL of Cd, which is above the instrument LOD and ~10 times higher than the endogenous Cd measured in the skin of the control (no QDs). These results demonstrate a proof-of-principle that GSH43- scFvs can enable the detection of GSH-QDs (strong AP staining in bright field) present at low levels using the standard IHC technique.

### 4.3.2 Validating Ti49-scFv Binding to $TiO_2$ NPs

$TiO_2$ NPs (Evonik, P25) were applied in water on the skin and a $TiO_2$ NP-containing commercial sunscreen (Eucerin SPF15) was also tested to determine presence and penetration if any, of these NPs through skin. Results from IHC based on Ti49-scFv-anti-FLAG AP staining show $TiO_2$ NPs when applied in water to be predominantly localized in the upper layers of the SC (Figure 4.7A, red arrows) in intact skin relative to control skin sections (no $TiO_2$ NPs, Figure 4.7B) which showed an absence of AP staining. Some

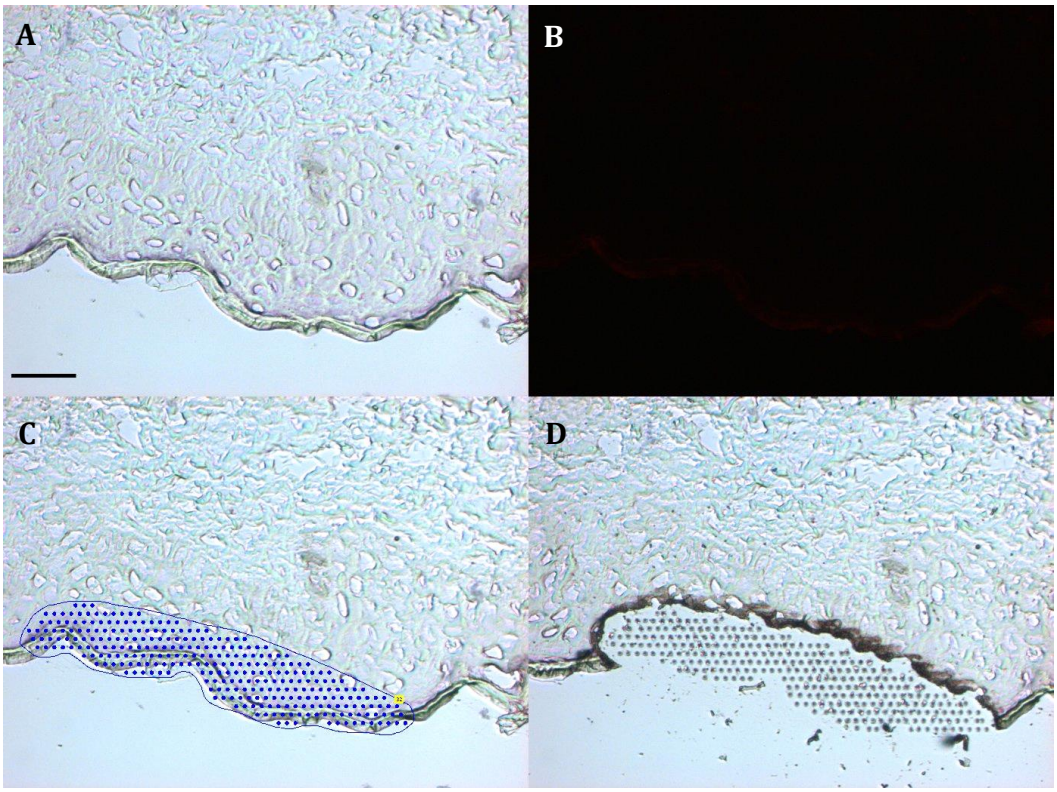


**Figure 4.5: LCM Imaging of Epidermis of Control 'no QD' Skin Sample**

Representative control skin (no QDs) image showing A) absence of AP staining in brightfield and B) no fluorescence. Upon using LCM to C) cut and D) capture portions of skin for AAS analysis, Cd levels (0.0085 ng/mL) were found to be near instrument LOD levels (0.007 ng/mL). Scale bar=50 μm.

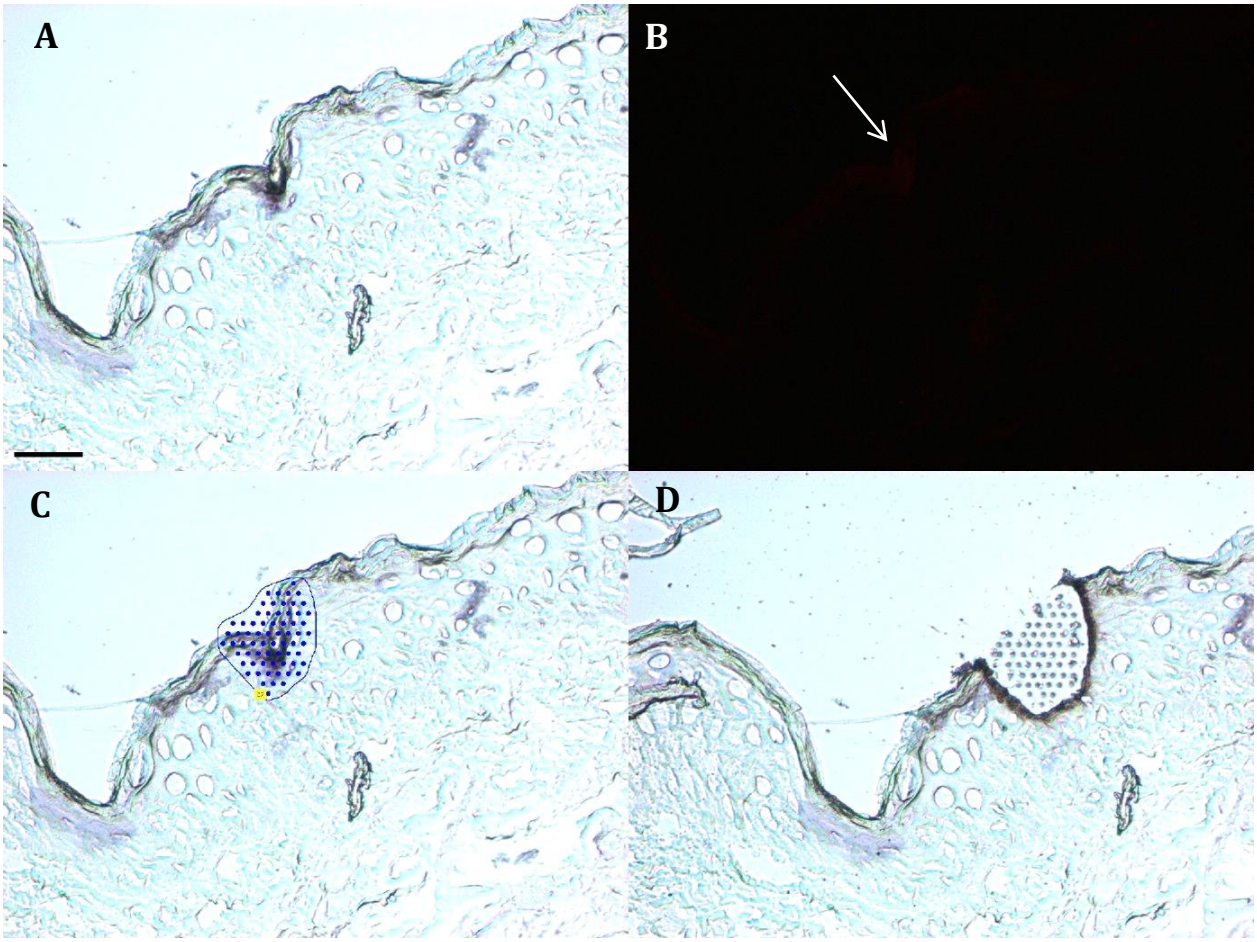


**Figure 4.6: LCM Imaging to Detect QDs in Areas without Fluorescence in Epidermis of Skin**

Representative images showing A) areas where AP staining was visible but B) not fluorescence (white arrow). However, when sample C) was marked for cut and D) captured using LCM, and analyzed using AAS, Cd levels were found to be 0.018 ng/mL, which was greater than control (0.0085 ng/mL) indicating QD presence in the stained areas. Scale bar=50 μm.

samples showed the presence of a mild punctuate AP staining beneath the SC, potentially suggesting occasional translocation of the NPs to the epidermal layers of skin (Figure 4.7A, blue arrows). However, AAS could not be used to prove that these occurrences indeed contain $TiO_2$ NPs due to the difficulties associated with dissolving $TiO_2$ NPs and a poor AAS detection sensitivity for Ti ions. Therefore the areas of skin (cryosectioned on a quartz coverslip) exhibiting bluish-purple staining in a positive control sample (Figure 4.8A, $TiO_2$ NPs applied to the dermis of skin) were analyzed to visualize the morphology of the $TiO_2$ NPs in skin. The individual particles in these samples were easily discernable as part of large aggregates of NPs when examined for the presence of $TiO_2$ NPs using SEM (Figure 4.8B, 4.8C). However, upon examining several samples exhibiting AP staining in the epidermis and the dermis, it was found that it was harder to discern individual NPs in the aggregates. Moreover, SEM/EDX spectra did not show presence of Ti ions in the AP stained regions. This was expected, as we estimate $TiO_2$ EDX detection limit to be 0.5-5 $\mu g/cm^2$, which likely far exceeds the $TiO_2$ NP presence in these skin samples.

Results from IHC experiments on sunscreen-treated skin samples showed that Ti49-scFvs were able to detect $TiO_2$ NPs localized in the upper layers of the SC (Figure 4.9A), whereas Ti49-scFvs-treated control samples (not containing sunscreen application) did not show any AP staining (Figure 4.9B). Based on the SEM/EDX results above, the areas of staining in the sunscreen-treated skin samples, not visible in control samples can be concluded to likely contain $TiO_2$ NPs.

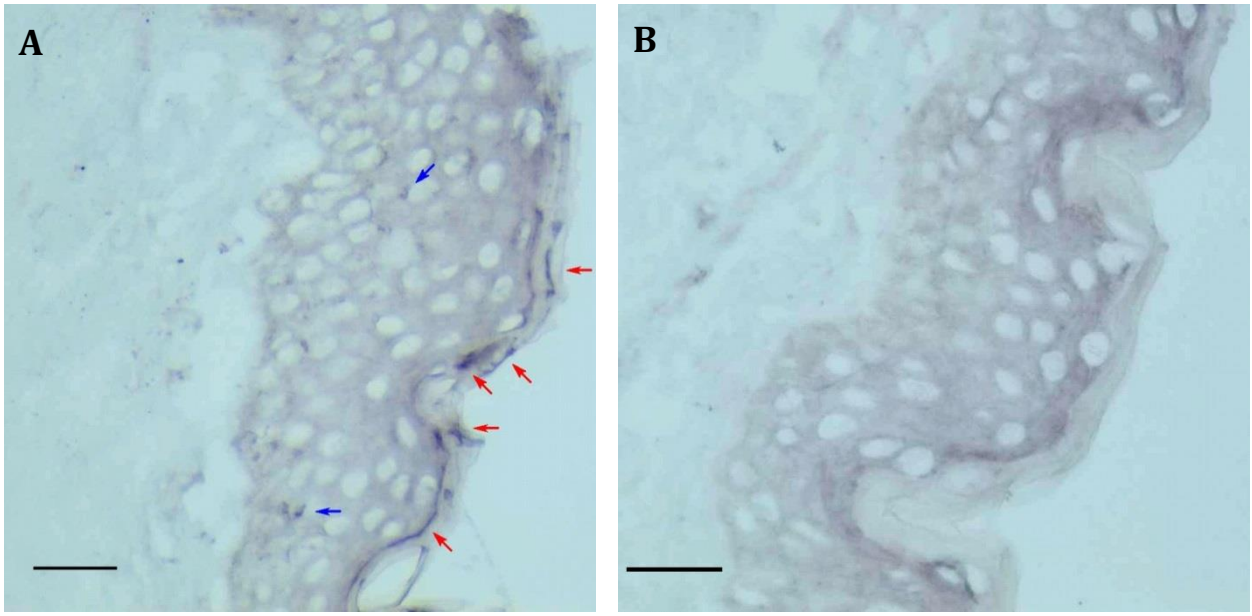


**Figure 4.7: Detection of $TiO_2$ Applied on Epidermis of Skin Using Ti49-scFv**

Representative images of A) $TiO_2$ applied on epidermis of intact skin, red arrows indicate AP staining due to binding of Ti49-scFv to $TiO_2$ NPs. Blue arrows indicate AP staining, which could potentially be $TiO_2$ particles penetrated through skin to the dermis. B) Control sample with no $TiO_2$ applied and upon exposure to Ti49-scFvs, no non-specific binding (no AP staining) was observed. Scale bar=50 μm.

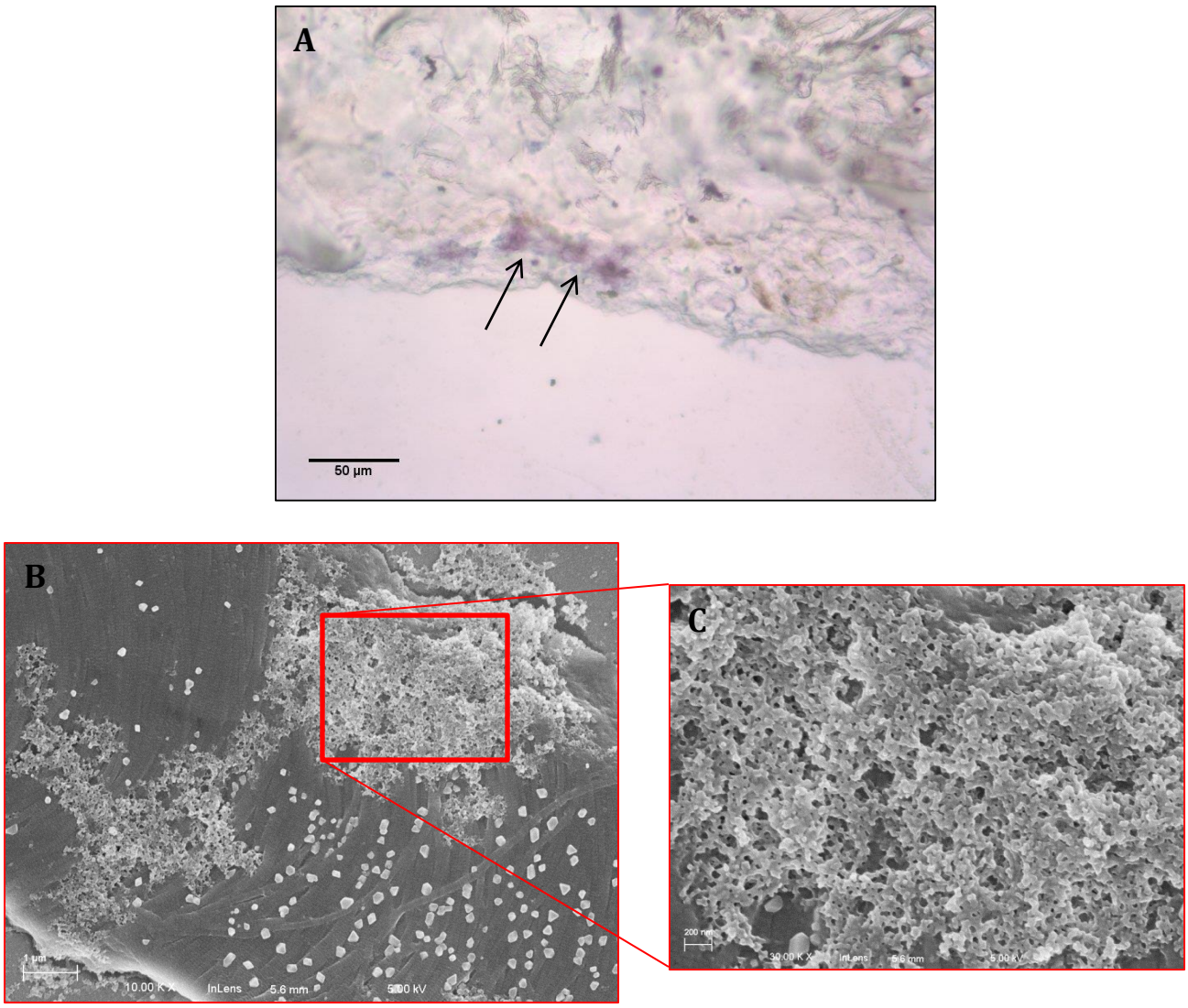


**Figure 4.8: SEM/EDX to Validate Presence of $TiO_2$ NPs in the AP Stained Areas**

Positive control human *ex vivo* skin treated with $TiO_2$ NPs in the dermis of skin. IHC was performed with Ti49-scFvs to prove presence of $TiO_2$ NPs. A) Bright-field image showing AP staining (black arrows) with the use of Ti49-scFvs in an *ex vivo* human skin sample upon application of 1 mg/mL $TiO_2$ NPs in the dermis, scale bar=50 µm. B) SEM image showing $TiO_2$ NPs, scale bar=1 µm and C) magnified image of the $TiO_2$ NPs in skin hence proving presence of NPs in the corresponding stained areas, scale bar=200 µm.

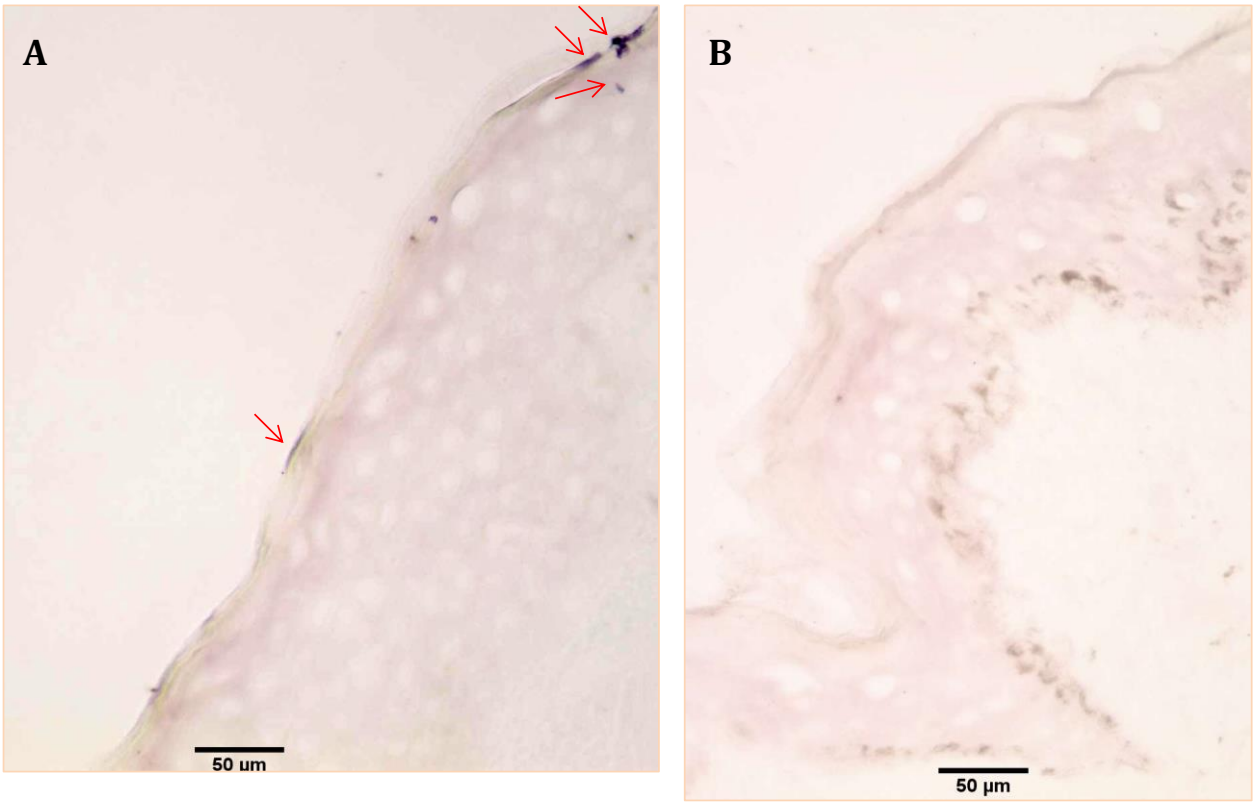


**Figure 4.9: Detection of $TiO_2$ NPs in Sunscreen Application to Epidermis**

Representative image of Ti49 scFvs detecting $TiO_2$ in sunscreen (Eucerin SPF15) applied to skin. A) AP staining upon due to binding of Ti49-scFv to $TiO_2$ NPs in sunscreen is indicated using red arrows. B) Control skin sample without $TiO_2$ NPs showing no AP staining upon treating with Ti49-scFvs. Scale bar=50 µm.

# 4.4 Conclusions

The functionality of the scFvs isolated using phage display was demonstrated by their utilization for the detection of NPs in an *ex vivo* human skin model. Areas with visible AP staining proved to contain GSH-QDs in them and the fluorescence in these regions were not tissue autofluorescence as confirmed by LCM/AAS studies. GSH43-scFv was capable of detecting low levels of NPs present in the epidermal layers of skin as demonstrated in the proof-of-concept study using fluorescent QDs. QDs were used a model NP in this study since the presence of QDs in a sample with visible AP staining can be validated using fluorescence. The LCM/AAS studies showed presence of QDs using AAS (~10-fold above control) in areas with visible AP staining but no observable fluorescence.

We were able to detect non-fluorescent $TiO_2$ NPs in the upper layers of the SC in intact skin using Ti49-scFvs, and this result was in accordance to those reported in literature, where $TiO_2$ was confined to the SC and the upper layers of the SC shown using various animal models[13-15]. The high tendency of $TiO_2$ NPs to agglomerate is a likely contributing factor in the hindrance to $TiO_2$ penetration beyond the SC in skin. A mild staining was observed beneath the SC for $TiO_2$ in water and $TiO_2$-containing sunscreen treated skin samples. However, efforts to detect the elemental Ti (EDX) proved inconclusive. While LCM studies proved presence of NPs (QDs) in areas with no discernable fluorescence, occurrences of $TiO_2$ NPs therefore, albeit less frequent that QD-containing samples beneath the SC can potentially be concluded to be NP ($TiO_2$)

presence, suggesting the occasional translocation of $TiO_2$ NPs to the epidermal layers through the defects in the SC.

Phage display was successfully used to isolate scFv antibodies against GSH-QDs and $TiO_2$ NPs. These antibodies bind these NPs in skin as confirmed by a variety of techniques used in conjunction with IHC including LCM, AAS and SEM/EDX. Since antibodies cannot be raised and selected against molecules too small (eg. metal ions)[16], we can conclude that the scFvs bind intact QDs and $TiO_2$ NPs as opposed to Cd or Ti ions that might have leeched during the translocation process through skin. Therefore, the use of scFvs to detect whole, intact NPs in tissue will comprise an expansive tool kit when used in conjuncture with other quantitative techniques currently available to provide accurate information both about the NP form (whether intact particle or soluble ion) and presence, regardless of the amount of NPs in any biological environment.

# References

[1] Antonio, J. R., Antonio, C. R. *et al.* Nanotechnology in Dermatology. *An Bras Dermatol*, **2014**, 89(1), 126-136.

[2] Nasir, A. Nanotechnology and Dermatology: Part I--Potential of Nanotechnology. *Clin Dermatol*, **2010**, 28(4), 458-466.

[3] Mauderly, J. L., Gigliotti, A. P. *et al.* Chronic Inhalation Exposure to Mainstream Cigarette Smoke Increases Lung and Nasal Tumor Incidence in Rats. *Toxicol Sci*, **2004**, 81(2), 280-292.

[4] Gustavsson, P., Nyberg, F. *et al.* Low-Dose Exposure to Asbestos and Lung Cancer: Dose-Response Relations and Interaction with Smoking in a Population-Based Case-Referent Study in Stockholm, Sweden. *Am J Epidemiol,* **2002**, 155(11), 1016-1022.

[5] Nel, A., Xia, T. *et al.* Nanomaterial Toxicity Testing in the 21st Century: Use of a Predictive Toxicological Approach and High-Throughput Screening. *Acc Chem Res*, **2013**, 46(3), 607-621.

[6] Casals, E., Pfaller, T. *et al.* Time Evolution of the Nanoparticle Protein Corona. *ACS Nano*, **2010**, 4(7), 3623-3632.

[7] Jiang, W., Papa, E. *et al.* Semiconductor Quantum Dots as Contrast Agents for Whole Animal Imaging. *Trends Biotechnol*, **2004**, 22(12), 607-609.

[8] Medintz, I. L., Uyeda, H. T. *et al.* Quantum Dot Bioconjugates for Imaging, Labelling and Sensing. *Nat Mater*, **2005**, 4(6), 435-446.

[9] Ravichandran, S., Mortensen, L. J. & DeLouise, L. A. Quantification of Human Skin Barrier Function and Susceptibility to Quantum Dot Skin Penetration. *Nanotoxicology*, **2011**, 5, 675-686.

[10] Mortensen, L. J., Ravichandran, S. *et al.* Progress and Challenges in Quantifying Skin Permeability to Nanoparticles Using a Quantum Dot Model. *J Biomed Nanotechnol*, **2010**, 6(5), 596-604.

[11] Gopee, N. V., Roberts, D. W. *et al.* Quantitative Determination of Skin Penetration of Peg-Coated Cdse Quantum Dots in Dermabraded but Not Intact Skh-1 Hairless Mouse Skin. *Toxicol Sci*, **2009**, 111(1), 37-48.

[12] Mortensen, L. J., Jatana, S. *et al.* Quantification of Quantum Dot Murine Skin Penetration with Uvr Barrier Impairment. *Nanotoxicology*, **2013**, 7(8), 1386-1398.

[13] Gamer, A. O., Leibold, E. & van Ravenzwaay, B. The in Vitro Absorption of Microfine Zinc Oxide and Titanium Dioxide through Porcine Skin. *Toxicol In Vitro*, **2006**, 20(3), 301-307.

[14] Ryman-Rasmussen, J. P., Riviere, J. E. & Monteiro-Riviere, N. A. Penetration of Intact Skin by Quantum Dots with Diverse Physicochemical Properties. *Toxicol Sci*, **2006**, 91(1), 159-165.

[15] Sadrieh, N., Wokovich, A. M. *et al.* Lack of Significant Dermal Penetration of Titanium Dioxide from Sunscreen Formulations Containing Nano- and Submicron-Size Tio2 Particles. *Toxicol Sci*, **2010**, 115(1), 156-166.

[16] Street, A., Sustich, R. *et al. Nanotechnology Applications for Clean Water: Solutions for Improving Water Quality*. **2014**. (Elsevier Science).

# Chapter 5

*Characterization of Binders and Challenges Associated with Discovery of Binders to NPs*

# 5.1 Introduction

An unimmunized scFv phage display library consisting of $2x10^9$ unique clones was used to isolate antibodies against GSH-QDs and $TiO_2$ NPs. The utility of these scFvs was established in the previous chapters where they were used to detect the respective NPs in *in vitro* assays as well as in a biological milieu using an *ex vivo* human skin model. We have demonstrated for the first time detection of NPs using a chromogenic reporter where the enzyme activity can be used to amplify the signal over time, thereby allowing detection of NPs present even in low quantities in tissue. Although phage display technology can allow for selection of antibodies *in vitro*, antibodies selected through phage display often need to have higher affinities for their targets. Even *in vivo* antibodies initially generated undergo an editing process called affinity maturation to generate antibodies with higher affinities and higher selectivity to the antigens. This affinity maturation process that occurs *in vivo* (in germinal centers), typically involves the introduction of a small number of mutations via somatic hypermutation during B cell maturation[1]. These mutations can affect affinity by influencing positioning of side chains contacting the antigen[2] or replacing 'low affinity' residues with contact residues with more favorable energetics[1]. Affinity maturation can be mimicked *in vitro* using a variety of techniques described in the literature such as the use of mutator strains[3], error-prone PCR[4], chain shuffling[5,6], DNA shuffling[7], and oligonucleotide-directed mutagenesis[6,8-10].

In this thesis, chain shuffling was investigated to attempt to increase binding affinity of the clone isolated against QDs. In this strategy, the $V_H$ gene of the best phage

antibody isolated is kept constant and is paired with a library of light chains followed by selection for binding to the target to find $V_H$-$V_L$ pairs with the improved affinity to the target. Other enrichment methods such as immobilizing the target antigen onto a substrate[11], which is widely used for biopanning in phage display has also been investigated in this thesis. While this work describes the isolation of antibodies to NPs using phage display and biopanning on NPs dispersed in solution, a more typical approach for phage display employs target antigens immobilized via chemical coupling[12] or non-covalent absorption[13] to a hydrophobic surface for biopanning. A previous study[14] has reported isolation of peptides using phage display that bind QDs immobilized on protein (gelatin)-coated polystyrene plates. Although other studies[15] have reported similar modest enrichment levels (~8-fold binding over control) of peptides isolated against inorganic materials such as solid ZnO substrates, we sought to investigate panning on QDs immobilized on a solid substrate to isolate binders with potentially greater binding ability to QDs than from biopanning in solution (i.e. more than 10-fold over background). A potential concern for using ultracentrifugation as described previously in this thesis is the unintended precipitation of unbound phage, thereby increasing background levels resulting in false positives in analyzing cross-reactivity properties of the scFvs. To this end, we investigated a salt precipitation method which allows use of lower centrifugal forces to separate phage bound to NPs as well as panning on NPs immobilized on a surface. To examine cross-reactivity binding of the clones isolated to materials, we conducted both phage panning in solution and on polystyrene plates. Various proteins were used to immobilize QDs on the surface of polystyrene well

plates including collagen, gelatin, BSA, human serum albumin (HSA), lactoferrin (LF) and ovalbumin (OVA) based on the procedure described by Mardyani et al.[14].

We first discuss the use of salt precipitation to pellet NPs during biopanning at lower speeds to prevent unbound phage precipitation associated with higher speeds in the ultracentrifuge. Next, biopanning on QDs immobilized on protein-coated wells and the associated challenges have been examined. For $TiO_2$ NPs, others binders screened for from the population of binders after Round 4 of biopanning were studied. Additionally, cross-reactive behavior of the binders obtained using one or more of the techniques described above (target antigen dispersed or immobilized) were examined using various NPs of different compositions in order to understand an underlying mechanism of binding of the scFv antibodies to NPs. This chapter finally discusses the use of a library formed by chain shuffling of GSH43 clone as described above to pan against GSH-QDs both in solution and in the immobilized form in order to select for the best $V_H$-$V_L$ pair from the library with the highest affinity to the target.

# 5.2 Materials and Methods

## 5.2.1 Centrifugation Titer Assay

In this assay, individual phage stocks either freshly prepared or previously prepared and stored at -80 °C with 15% glycerol were diluted at a 1:5 in TBS (500 µL total volume) and mixed with NPs (QDs, all $TiO_2$ NPs (0.5 mg/mL), Au NPs (20 nm, 0.025 mg/mL), Au powder (0.5 mg/mL) or CNTs (0.2 mg/mL). After 2 h of incubation with gentle agitation at room temperature, the unbound phages were separated by centrifugation

(55,000 rpm without salt for QDs, 29,000 rpm with addition of salt (1 M $MgCl_2.6H_2O$) for QDs, 1300 g for all $TiO_2$ NPs, 29,000 rpm for Au NPs (20 nm), 4000 g for Au powder, 29,000 rpm for CNTs) and the NP-phage pellet was washed 5 times in TBST and once in deionized water before eluting with glycine containing 0.01% BSA (pH 2.2). The titer of the eluted phages was quantified by transduction of serial dilutions of the phage into TG1 cells to ampicillin resistance and the resulting colonies on the agar plate were counted manually. A binder clone to Au powder (designated VHH) outlined in Hattori et al.,[16] was selected as a positive control clone in our experiments and was sequenced (Integrated DNA Technologies®) and engineered into our phage display system. A fold change was assessed in the case of each experiment with respect to controls included (negative control clone or positive control VHH clone for Au powder).

### 5.2.2 Enrichment on Wells

Enrichment on QDs immobilized on the plate was performed according to a method described in Mardyani et al.,[14] (referred to as plate titer assay). For immobilization of QDs, plates were coated with 2% BSA in TBS for 1 h at room temperature. The wells were then washed 3 times with deionized water to remove any excess BSA. GSH-QDs at a 50 nM concentration (50 µL per well) for testing binding or cross-reactivity were added in sodium bicarbonate buffer ($NaHCO_3$, 0.1 M) and allowed to incubate overnight at 4 °C with gentle agitation. The excess QDs were removed by washing the wells gently with TBST. After confirming presence of QDs using a hand-held UVR lamp source prior to each experiment, the wells were blocked with TBS+0.5 % casein for 1 h at room temperature prior to the addition of appropriate individual phage stocks, which were

added either freshly prepared (no dilution) or frozen (1:5 dilution in TBS, 50 µL total volume) and allowed to incubate for 2 h at room temperature with gentle agitation. The unbound phages were then removed and the wells were washed 7 times with TBST and once with deionized water. After elution with glycine containing 0.01% BSA (pH 2.2), the titer of the eluted phages was quantified by transduction of serial dilutions of the phage into TG1 cells to ampicillin resistance and the resulting colonies on the agar plate were counted manually. A fold change was assessed in the case of each experiment with respect to controls included and plotted. A similar protocol was used in the case of GSH-coated wells used as a target for the cross-reactivity studies discussed below.

### 5.2.3 Phage ELISA with GSH-QD Immobilization

2 % BSA diluted in TBS was coated for 30 min at room temperature and washed 3 times with deionized water. 50 nM of GSH-QDs (50 µL in $NaHCO_3$ buffer) were incubated overnight at 4 °C with gentle agitation. Excess QDs were washed off with TBST. The plate was blocked with TBS+0.5 % casein for 1 h at room temperature, following which GSH43ϕ and negative control Npepϕ were incubated at a series of dilutions (1:1, 1:2, 1:3, 1:4) in TBS containing 0.5 % casein. The plates were washed 5 times with TBST and 5 times with TBS, and anti-M13 HRP antibody (GE Healthcare) was added diluted in TBS (0.5 µg/mL) and incubated for 1 h at room temperature. Following thorough washing (10 washes as above), the plate was incubated with Sure Blue™ TMB substrate (KPL) and the absorbance was measured at 450 nm after stopping the reaction with 1 N HCl. Results were plotted and analyzed.

### 5.2.4 Phage ELISA on GSH-coated Wells

Commercially available pre-blocked GSH-coated well strips (Pierce™, Life technologies, Cat. number 15140) were used. Strips were blocked with TBS+0.5% casein for ~30 min at room temperature. GSH43ϕ and negative control 'empty vector' phages (containing a truncated gene III fragment with the N-terminal FLAG, but no scFv) phages were incubated in a series of dilutions in TBS containing 0.5% casein (1:1, 1:2, 1:4, 1:8,…., 1:64). A 'no phage' well was also incorporated where the well was incubated with TBS+0.5% casein solution alone. After 1 h of incubation at room temperature, the wells were washed 5 times with TBST and 5 times with TBS. Secondary anti-M13 HRP antibody was added diluted in TBS (0.5 µg/mL) and incubated for 1 h at room temperature. Following thorough washing (10 washes as above), the plate was incubated with Sure Blue™ TMB substrate and the absorbance was measured at 450 nm after stopping the reaction with 1 N HCl. Results were plotted and analyzed.

### 5.2.5 Swap-L Library Construction and Panning

A plasmid preparation made from ~$1x10^9$ transductants of the human library was digested with Hind III and Nhe I and the repertoire of light chain ($V_L$) fragments was isolated after agarose gele electrophoresis. The $V_L$ pool fragment was extracted and purified using a Qiagen Min Elite gel extraction kit. Similarly, the GSH43 heavy chain fragment ($V_H$) was isolated from Nhe I and Sal I digested phagemid DNA. The $V_L$ and GSH43 $V_H$ fragments were ligated to Hind III + Sal I digested AP-III6 display vector overnight with T4 ligase (New England Biolabs) and ethanol precipitated. The ligated

DNA was re-suspended in 10 µL of water and electroporated in a BioRad Gene Pulser in a 1 mm cuvette. After outgrowth for 1 h in SOC medium, the cells were plated on a single 25 cm Lb+ ampicillin plate and incubated overnight at 37 °C. Approximately $5x10^7$ transformants were obtained (titer was determined by serial dilution and transduction before plating). The cells were scraped and re-suspended in 5 ml of LB medium and an aliquot containing approximately $1x10^9$ cells was innoculated into 40 ml of LB medium, grown at 37 °C for 2.5 h and infected with helper phage. The infected cells were grown at 30 °C overnight in the presence of ampicillin and kanamycin. Phages were harvested and purified by PEG precipitation and re-suspended in 1 ml of TBS 0.5% casein.

The GSH-QDs (400 µL, 50 nM) were diluted in TBS mixed with the above-mentioned swap-L phage library ($10^{12}$ phages/mL, 100 µL) present in diluted in TBS plus 0.5% casein with gentle agitation for 2 h at room temperature. After incubation to allow binding of phage to QDs, the QD/phage mixture was centrifuged at 83,000 g (55,000 rpm) for 10 min and the unbound phage-containing supernatant was removed and the phage-bound NP pellet was re-suspended in TBST and centrifuged. This wash cycle was repeated 5 times, after which the pellet was washed once with deionized water. After washing the bound phages were eluted from the NPs using 0.1 M glycine (pH 2.2, containing 0.01% BSA) and neutralized using 200 µL of 2 M Tris base. Phage pools for subsequent rounds were prepared as described in Chapter 2. For rounds 3 and 4, the input phage pool was pre-centrifuged to pellet phage agglomerates at 116,000 g (65,000 rpm) to pellet phage agglomerates and reduce high background levels of binding.

# 5.3 Results

## 5.3.1 Use of Salt to Precipitate QDs

Prior to selection using the phage library, different salts were tested for their ability to precipitate QDs at a lower speed than that used for the initial enrichment (55,000 rpm). Salts including NaCl and $MgCl_2.6H_20$ were tested at 1 and 5 M concentrations. A final concentration of 1 M $MgCl_2.6H_20$ was selected as optimal due to the dispersion and pelleting properties imparted to GSH-QDs. As described previously in Chapter 2, the phage library ($10^{12}$ phages/mL, 100 µL) was mixed with GSH-QDs diluted in TBS (100 nM, 400 µL) for 2 h at room temperature with gentle agitation. Next, 120 µL of $MgCl_2.6H_2O$ was added to the QD-phage solution (1 M final salt concentration), after which the solution was centrifuged at 29,000 rpm instead of 55,000 rpm originally used for 10 min to pellet phage-bound QDs. The pellet was then washed and phages were eluted as previously described. Upon 4 rounds of panning, a BstN1 analysis of 12 randomly selected clones showed the presence of three clones HS2, HS3 and HS4, which were identified based on repeating patterns of each of the clones observed on the digest (Appendix D, Figure D1). The phage clones showed a clonal abundance of 16% each. The amino acid sequences of these clones are shown in Appendix D, Table D1. These clones were further tested for their binding to GSH-QDs and cross-reactivity to various other NPs and compared to GSH43 clone generated without the use of salt and characterized in Chapter 2.

## 5.3.2 Validation of Binding of HS2, 3, 4 Clones

### 5.3.2.1 Validation of binding *in vitro* using phage clones

Binding to QDs *in vitro* was tested using a panning assay. Here, the HS2, 3, 4ϕ and IL-12ϕ were mixed with GSH-QDs in separate tubes at room temperature for 2 h with gentle agitation. Following centrifugation using salt at a speed of 29,000 rpm the unbound phages from the supernatant were removed, after which the pellet containing bound phages was washed 6 times (5 times with TBST, once with deionized water) and eluted using glycine. The HS2, 3, 4ϕ were found to bind GSH-QDs ~100-fold more than the negative control IL12ϕ (Appendix D, Figure D2). This is in contrast to the 10-fold above background binding to GSH-QDs exhibited by GSH43ϕ. TEM was further used to verify binding of the phage clones to GSH-QDs using a protocol described in Chapter 2 with the addition of salt solution to precipitate QDs. It was found that HS2, 3, 4ϕ clones bound GSH-QDs but negative control LFϕ did not (Appendix D, Figure D3).

### 5.3.2.2 Validation of binding *in vitro* using scFvs

The clones HS2, 3, 4 were prepared as purified scFvs to validate their binding *in vitro* to GSH-QDs and to GSH-QDs in human skin. A dot blot assay was used to verify binding of these clones to GSH-QDs and it was found that HS 2, 3, 4-scFvs bound GSH-QDs indicated by the formation of a black spot in the chemiluminescent assay, whereas a negative control scFv (NT3) did not (Appendix D, Figure D4). Moreover, the HS2, 3, 4-scFvs did not bind Au NPs (tannic acid coated, 5 nm), DHLA-QDs or Inv-QDs tested alongside showing specific recognition of GSH-QDs (Appendix D, Figure D4). Since

upon sequencing, the clones were found to contain the same heavy chain with different light chains, we proceeded with one of the clones (HS2) for validation of their QD binding functionality in a biological milieu. Results from IHC showed ability of HS2-scFv to bind to QDs as seen in Figure 5.1B indicated by areas of bluish-purple AP staining (red arrows) in brightfield whereas a control skin sample without QDs does not show any staining (Figure 5.1A). These areas also showed presence of punctuate spots when observed using appropriate filters for QDs (Figure 5.1C). Additionally, areas of AP staining indicated by yellow arrows do not show presence of QD fluorescence, which suggests potential detection of those QDs not visible using common fluorescence microscopy (Figure 5.1B). This suggests that HS2 clone obtained by panning on GSH-QDs using lower speeds of centrifugation with the addition of salt to precipitate NPs recognizes GSH-QDs both *in vitro* and in an *ex vivo* human skin model.

## 5.3.3 Cross-reactivity Assessment of Clones against GSH-QDs

### 5.3.3.1 GSH43ϕ cross-reactivity

Cross-reactivity properties of GSH43 clone in both the phage and scFv forms were studied using various assays. For the phage form, both panning in solution, and phage ELISA and panning assays on GSH-QDs immobilized on polystyrene plates were performed. Upon panning on QDs with different surface coatings such as DHLA and PEG-QDs in solution, GSH43ϕ was found to bind ~3 and 4-fold more than control (IL-12ϕ) and 100-fold more than control to magnetic beads (His Mag™ agarose beads, Novagen, Appendix D, Figure D5A) compared to a negative control clone. GSH43ϕ was

also found to bind Au in a powder form ~80-fold more than control (IL-12ϕ) albeit ~20-fold less than a positive control (clone reported as a binder in Hattori et al.[16]) and bind silica particles (100 nm) ~5-fold more than control (IL-12ϕ) (Appendix D, Figure D5B). Unexpectedly, GSH43ϕ also showed ~100-fold more binding to $TiO_2$ NPs than control (Appendix D, Figure D5C). While we do not fully understand the origin of cross-reactivity behavior exhibited by GSH43ϕ it is unlikely to be a random event or driven by electrostatics. We exchanged the light chain of GSH43ϕ clone with the light chain of IL-12ϕ and the hybrid clone was tested for binding to the GSH-QDs and $TiO_2$ NPs. This manipulation reduced the hybrid GSH43ϕ binding to the GSH-QDs by ~4-fold and it reduced the cross-reactivity binding to the $TiO_2$ NPs to background (IL-12ϕ) levels. Hence, this finding suggests that the cross-reactivity binding observed may result from a shape complementarity effect linked to the biopanning process. This was further investigated by panning on QDs immobilized on polystyrene plates to exclude any potential artifacts associated with the high speeds used in ultracentrifugation, which may result in the unwanted pelleting of phage. Prior to performing cross-reactivity studies, a phage stock not displaying the scFv (‘empty’ phage) was prepared in order to evaluate if the high background observed in the centrifugation titer assay was an artifact of phage pelleting during the centrifugation process.

A plate titer assay was employed to minimize artifact during panning, where QDs were immobilized on high binding 96-well plates as previously reported[14] coated with 2% BSA prior to QD deposition. Upon panning, it was found that phages not displaying scFvs (empty vector phage) showed no binding to QDs whereas GSH43ϕ displayed a 200

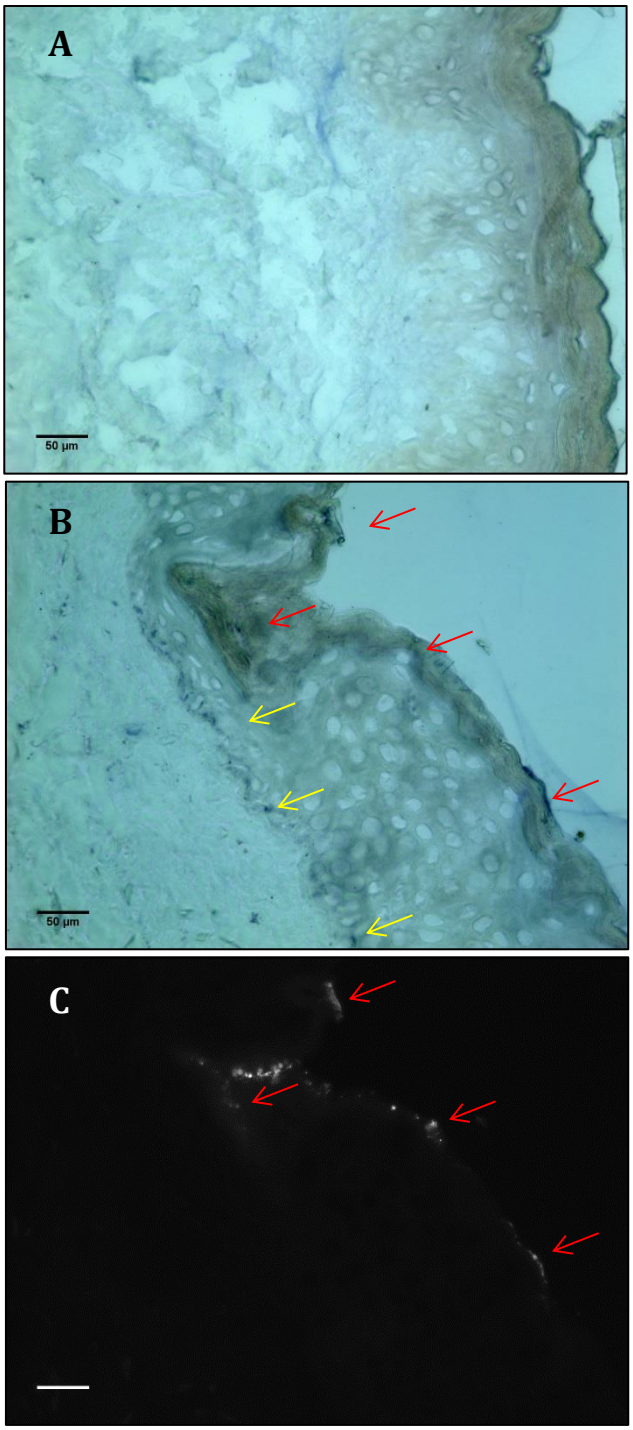


**Figure 5.1: QD Detection Using HS2-scFv in an *ex vivo* Human Skin Model**

Representative skin images under brightfield and fluorescence. A) Control skin sample without GSH-QD exposure showing an absence of AP staining indicating absence of non-specific binding of HS2-scFv to skin. B) Brightfield image of skin sample exposed to GSH-QDs for 24 h showing numerous areas with strong AP staining (red and yellow arrows) due to HS2 binding detected by anti-FLAG AP antibody that correlates with high QD presence. C) Fluorescence image showing punctuate areas of QD presence co-localizing with areas of AP staining (red arrows) due to binding of HS2-scFv. Scale bar=50 µm.

-fold more binding to GSH-QDs (Appendix D, Figure D6). Hence, we resorted to the plate titer method to assess cross-reactivity of the GSH43ϕ to QDs with the CdSe/ZnS core/shell but different surface chemistries. A plate titer assay was employed where GSH43ϕ showed binding to GSH-QDs in a concentration dependent manner (presence of QDs immobilized on BSA shown in Figure 5.2A), which was significantly higher than binding (Figure 5.2B, Figure 5.3A) of a negative control phage clone (Npepϕ) or GSH43ϕ binding wells without QDs (BSA only). Upon assessing different QDs, results from the plate titer assay (Figure 5.3B) show that GSH43ϕ (upon elution with glycine pH 2.2) binds to GSH-QDs (25.2 nm and negatively charged), Invitrogen QDs (Inv-QD, Invitrogen ITK™ 565-QDs, 10 nm and negatively charged), and PEI-QD (23 nm and positively charged[17]) but minimal binding was observed to the DHLA-QD (14 nm and negatively charged). The lack of binding of GSH43-scFv to the PEI-QDs (Figure 3.2) is in contrast to the strong binding observed in the phage format (Figure 5.3B). We attribute this to non-specific binding of the positive PEI-QDs to the M13 phages which carry a high negative surface charge[18]. The lack of GSH43-scFv binding to the negative charged Inv-QDs (Figure 3.2) is also in contrast to the results observed using the phage format of the clone GSH43ϕ (Figure 5.3B). We attribute this to differences in binding affinity, as from dot blot concentration studies we did observe strong binding of the GSH-scFv to the Inv-QD with increasing GSH-scFv concentration (5-20 μg/mL) with a continued absence of binding to PEI-QDs (Appendix D, Figure D6). These data suggest that QD binding in the phage format is not specific to the GSH coating or to surface charge. Although we cannot control for the amount of QDs that bind

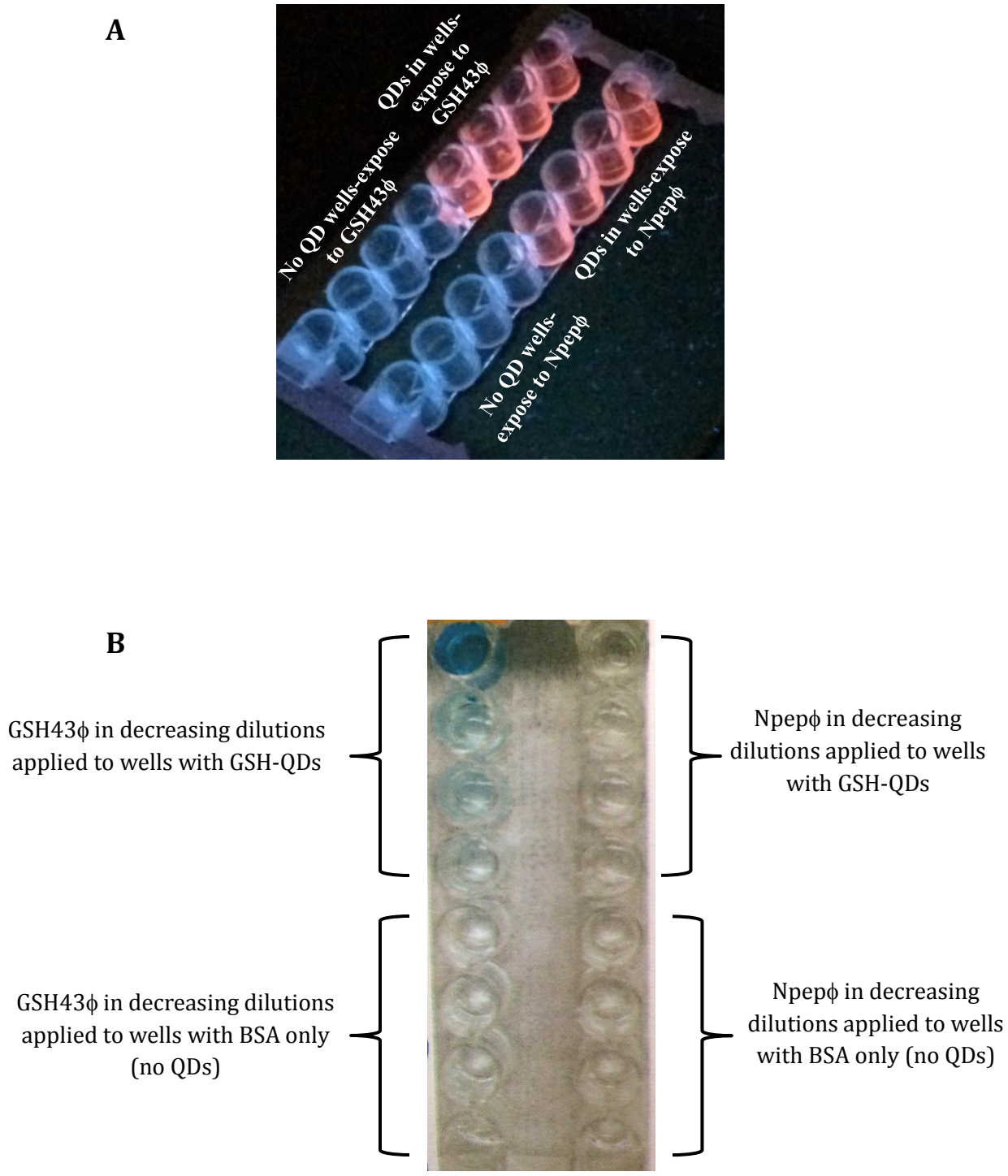


**Figure 5.2: Representative Phage ELISA with GSH-QDs as Target**

A) Representative image showing GSH-QDs immobilized on BSA coated wells. Fluorescence is indicative of QD presence as seen under a hand-held UVR lamp source. B) Representative phage ELISA showing binding observed via the blue color formed after addition of TMB substrate. Image was captured prior to addition of stop solution and measuring absorbance. GSH43ϕ binds GSH-QDs in a dose dependent manner seen by the changes in blue color of substrate but not BSA wells showing specificity to QDs. Negative control Npepϕ does not bind GSH-QDs or BSA.

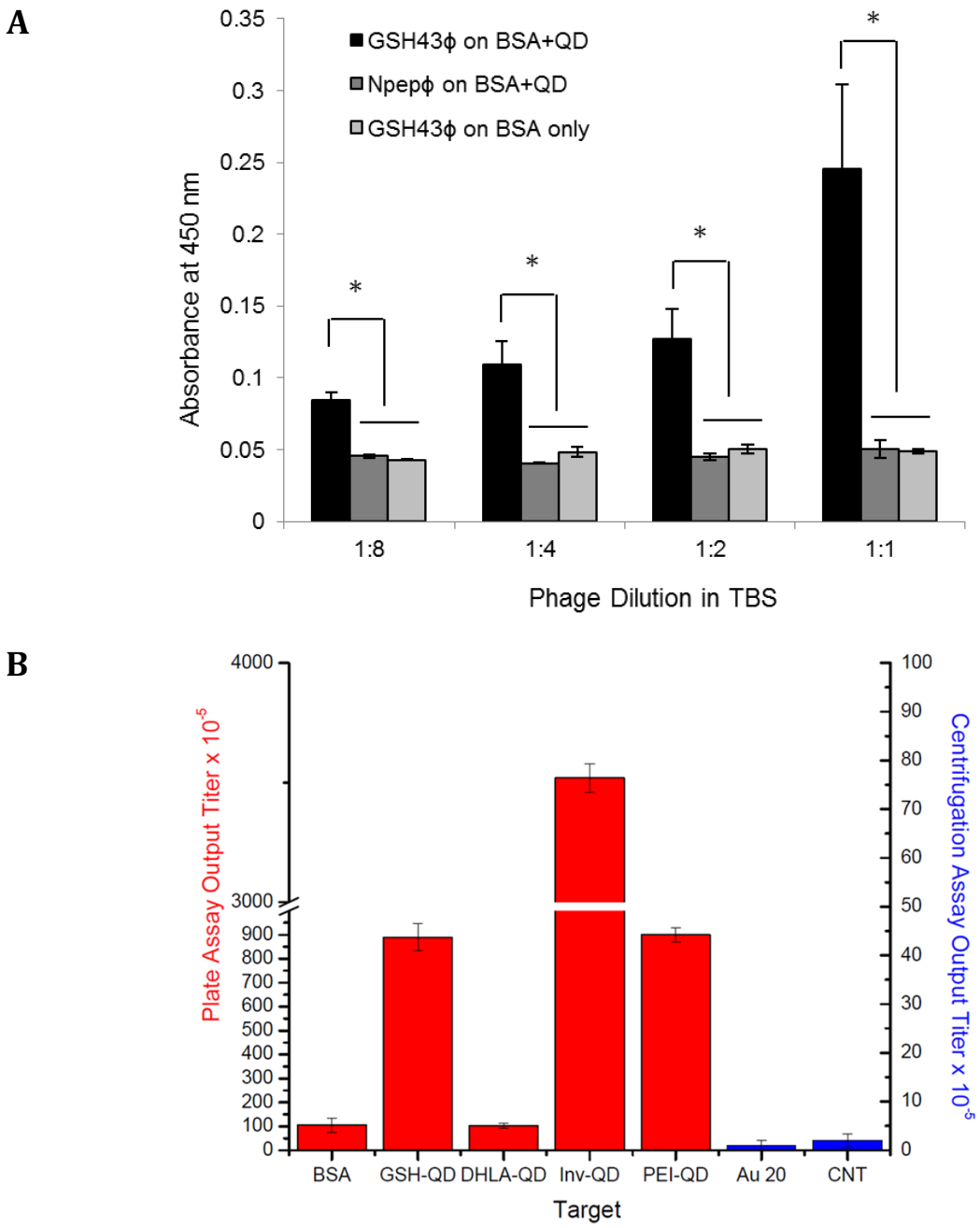


**Figure 5.3: Binding and Cross-reactivity Behavior of GSH43ϕ**

Binding behavior of GSH43ϕ in A) phage ELISA assay showing that with an increasing concentration of phage, significantly more binding (*$p<0.05$) of GSH43ϕ to GSH-QDs occurs when detected using TMB substrate at 450 nm, compared to negative control Npepϕ and GSH43ϕ interacting with wells containing BSA alone (no QDs). Values are average of three independent experiments and error bars represent SEM. B) Cross-reactivity to QDs with different surface coatings measured using a plate titer assay has been shown in red bars. GSH43ϕ binds GSH-QDs and exhibits cross-reactivity to Inv-QDs and PEI QDs. Negligible binding was observed using a centrifugation titer assay to Au NPs and CNTs (blue bars). Error bars are (number of colonies)$^{1/2}$.

to the wells coated with BSA, the presence of QDs on the plate before and after the washing steps (7 TBST washes, 1 water wash) could be verified using a UVR lamp source. For this reason, none of the NPs described above except QDs were tested to assess GSH43ϕ cross-reactivity using this method obtained from literature[14], but were instead tested using a centrifugation titer assay. The GSH43ϕ did not bind CNTs or Au NPs (20 nm) as observed through a centrifugation titer assay consistent with GSH43-scFv behavior as described in Chapter 3.

#### 5.3.3.2 GSH43ϕ recognition of epitopes on QDs

In order to gain a better idea about the mechanism of recognition of GSH-QDs by the GSH43 clone, whether core/shell or surface coating, we used commercially available pre-blocked, GSH-coated polystyrene well-strips to test binding to GSH43ϕ. A phage ELISA assay with GSH43ϕ along with phages not displaying an antibody incubated in a series of dilutions was used. Results showed that GSH43ϕ bound GSH-coated wells ~8-fold over background binding of empty vector phages which was significant up to three dilution ranges (Figure 5.4, student's unpaired t-test, $p<0.015$). This suggests that GSH was indeed recognized by the GSH43 clone and is potentially a mechanism by which GSH43ϕ bind GSH-QDs. This was further confirmed by panning of GSH43ϕ on GSH-coated well strips in a plate titer assay, where GSH43ϕ bound GSH-coated wells above background (almost negligible) binding of empty vector phages (Appendix D, Figure D7).

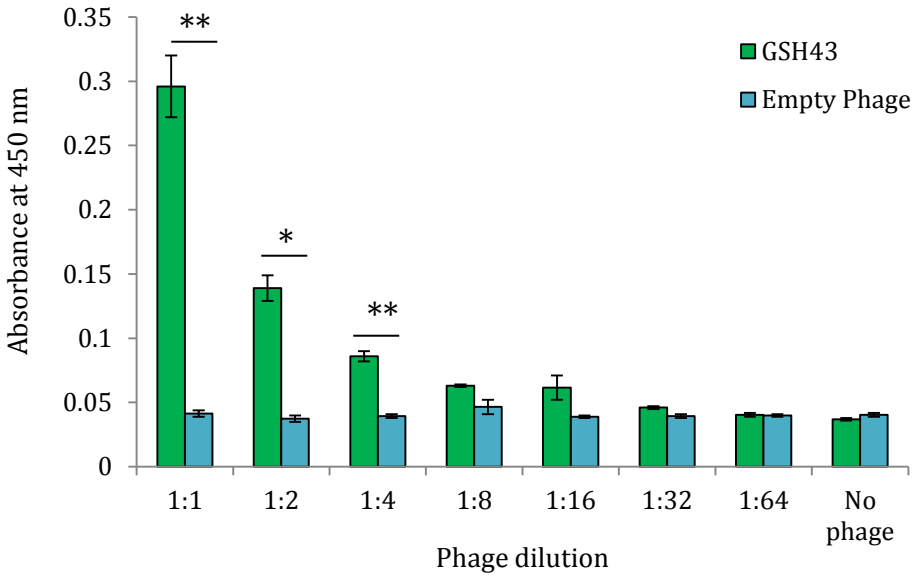


**Figure 5.4: GSH43ϕ Binding GSH**

Plot showing binding of GSH43ϕ to GSH-coated wells in a phage ELISA assay. GSH43ϕ binds GSH (green bars) significantly over background binding exhibited by negative control phage (blue bars). A student's unpaired t-test was used to determine significance, **$p<0.01$, *$p=0.01$. Data plotted are average of two independent experiments and error bars represent SEM.

#### 5.3.3.3 HS2, 3, 4ϕ cross-reactivity

HS3ϕ as a representative clone from this set of binders discovered against GSH-QDs was selected for testing cross-reactivity to other NPs including CNTs, Au (20 nm), $TiO_2$, DHLA- QDs, PEG-QDs and Inv-QDs using the centrifugation titer assay. We found that the clone exhibited a ~100-fold more binding (Appendix D, Figure D8) to all NPs except CNTs (~10-fold) compared to a negative control clone included in each panning experiment (IL-12ϕ, LFϕ). Further studies were not pursued with these clones due to the unexpected high cross-reactive binding observed to almost all NPs tested. The clones were also found not to bind or recognize GSH-coated wells strips when tested using a phage ELISA assay.

### 5.3.4 Additional Binders to $TiO_2$ NPs

Upon screening 16 additional colonies after round 4 of panning on $TiO_2$ NPs using BstN1 fingerprinting, two additional clones were found to be abundant as indicated by pattern repeats (Appendix D, Figure D9). The clones designated Ti6 and Ti15 were found to bind $TiO_2$ NPs ~130-fold more than negative control clones tested alongside. Ti6 was chosen for further studies as the clone exhibited negligible cross-reactivity to Au powder compared to Ti15 clone (Appendix D, Figure D10), which exhibited high cross-reactivity comparable to the binder isolated against Au powder (positive control) described elsewhere[16]. The amino acid sequence of Ti6 clone is shown in Appendix D, Table D2. Phage clones Ti6 and Ti49 were also tested with $TiO_2$ NPs varying in compositions and obtained from different vendors (Appendix D, Figure D11) than the original $TiO_2$ NPs

(Evonik/Degussa, 80% anatase and 20% rutile crystal, ~21 nm primary particle size) used as a target to obtain these clones. These include $TiO_2$ NPs with 1% manganese as dopant ($TiO_2$-Mn, nanopowder, <100 nm size, Sigma Aldrich Inc.), $TiO_2$ NPs composed of 100% anatase form ($TiO_2$-A NPs, ~32 nm, Alfa Aesar, Cat. number 39953) and $TiO_2$ NPs composed of 100% rutile form ($TiO_2$-R NPs, DuPont, Cat. number R101). Figure 5.5A shows results from panning on these particles using a centrifugation titer assay where Ti6ϕ and Ti49ϕ bound the original target $TiO_2$ NPs (anatase+rutile) and $TiO_2$-Mn NPs ~400 and 150-fold respectively. Interestingly, both Ti6ϕ and Ti49ϕ bound $TiO_2$-R NPs 3 and 4-fold more, and bound $TiO_2$-A NPs ~1.5-fold than the original target $TiO_2$ NPs (anatase+rutile) themselves. While the reason for the differences in binding intensity is not fully understood, the clones were found to universally bind the $TiO_2$ NPs tested in this thesis.

### Ti49ϕ cross-reactivity

Ti49ϕ was tested with Au particles in a powder form, Au NP (20 nm) and CNTs using a centrifugation titer assay (blue bars). Figure 5.5B shows that Ti49ϕ did not bind Au powder (100-fold less binding compared to the binder (VHH clone) included as a positive control in the experiment. Moreover, Ti49ϕ did not exhibit cross-reactivity to NPs or CNTs. When tested using a centrifugation titer assay, Ti49ϕ bound GSH-QDs more than background levels (Appendix D, Figure D12A). To ensure minimizing any artifacts due to the high speeds used in ultracentrifugation to pellet GSH-QDs, a plate titer assay (Figure 5.5B, red bar) was used where the QDs were immobilized using 2% BSA coated onto polystyrene plates. It was found that Ti49ϕ only exhibited background levels (App-

endix D, Figure D12B) of binding to GSH-QDs comparable to an arbitrary negative control clone from the library using this assay. The apparent binding as seen in the centrifugation titer assay, therefore, could indeed be concluded to be an artifact of ultracentrifugation.

### 5.3.5 Other Enrichment Protocols using GSH-QDs as Targets

As described in this Chapter 3 and this chapter, the low signal to noise ratio with GSH43 clone exhibited through various assays and the high background levels of phage binding observed during the panning process using centrifugation led us to consider immobilization of GSH-QDs as a target polystyrene well plates. As described above and using a procedure outlined by Mardyani et al.,[14] various proteins including gelatin, BSA, human serum albumin (HSA), lactoferrin (LF) and ovalbumin (OVA) were used to immobilize QDs. Presence of QDs post- immobilization and removal of excess QDs was confirmed using a hand-held UVR lamp source prior to addition of phage for enrichment.

In the first enrichment, gelatin was used to immobilize GSH-QDs for the first two rounds of panning after which collagen was used to coat the wells for round 3 and 4. Upon performing a BstN1 fingerprinting (Appendix D, Figure D13A), we found 1 dominant clone (Clone 13) and 4 unique clones. A phage ELISA with the individual phage stocks for each clone prepared was used to verify binding to GSH-QDs coated on gelatin, collagen and cross-reactivity to gelatin and collagen-coated wells alone (no QD). Results showed that all the five clones were cross-reactive to gelatin and collagen and no specific binding to GSH-QDs coated in the wells above the background binding could be discerned (Appendix D, Figure D13B). This could be due to potential enrichment of bin-

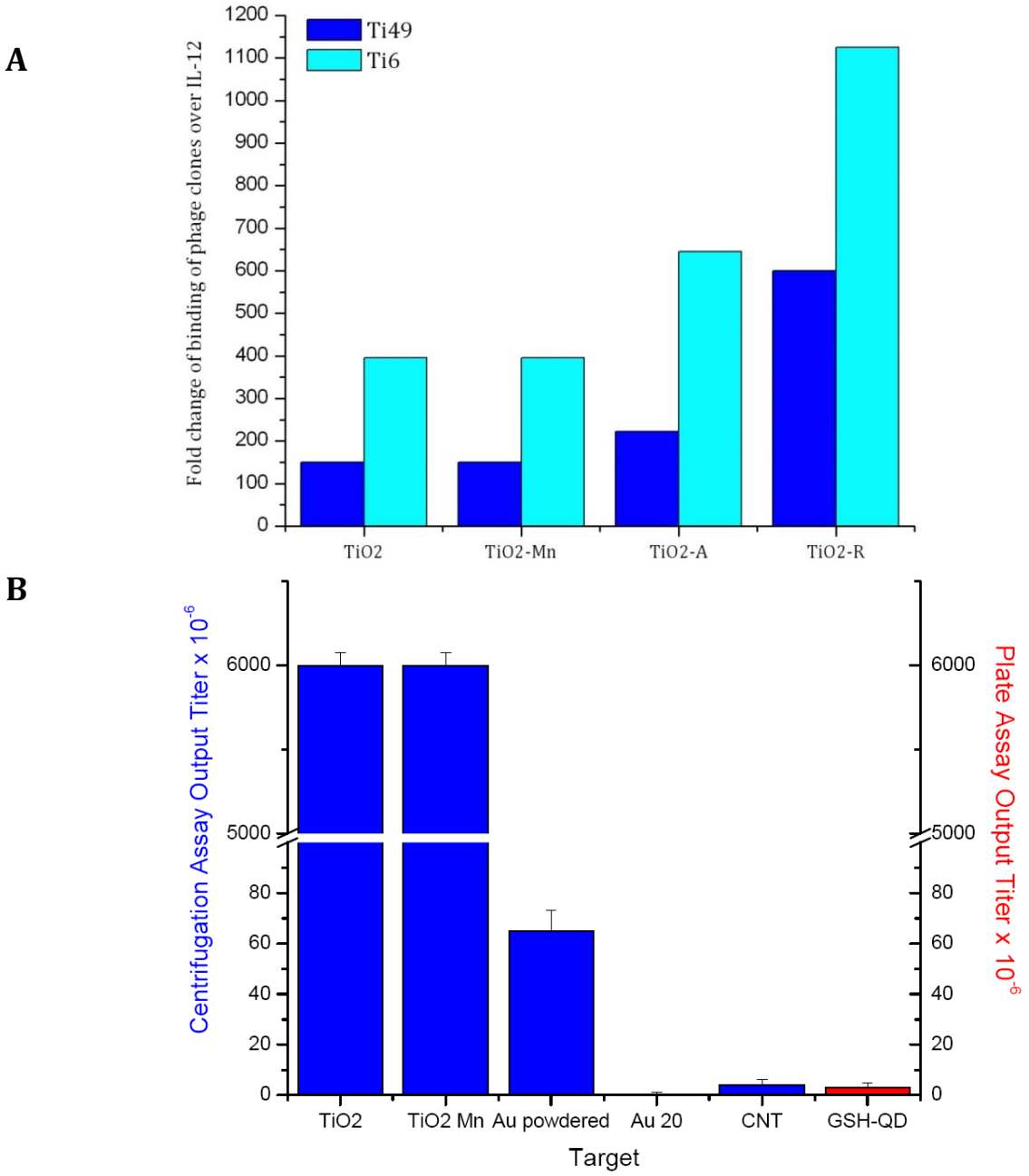


**Figure 5.5: Binding and Cross-reactivity of Ti49ϕ and Ti6ϕ**

Binding of Ti49ϕ and Ti6ϕ to different $TiO_2$ NPs varying in composition and source and cross-reactivity of Ti49ϕ to other NPs. A) Using a centrifugation titer assay, Ti49ϕ and Ti6ϕ was found to bind $TiO_2$-Mn (Sigma Aldrich Inc.) similar to $TiO_2$ NPs (Evonik, P25) with Ti6ϕ having a greater affinity (~2.6-fold) to $TiO_2$ NPs. Both phage clones bound $TiO_2$-R higher (Ti49ϕ by 3-fold and Ti6ϕ by 4-fold), and bound $TiO_2$-A by ~1.5-fold more than the other $TiO_2$ NPs. B) Results from centrifugation and plate titer assays to examine Ti49ϕ cross-reactivity binding to similar and dissimilar materials. Results from the centrifugation titer assay (blue bars) indicates that Ti49ϕ binds $TiO_2$ and $TiO_2$ NPs from a secondary vendor ($TiO_2$-Mn) but minimal binding is observed to dissimilar materials including Au-powder particles, 20 nm Au (Au20), and CNTs. Using the plate titer assay (red bar), Ti49ϕ bound GSH-QDs at background levels. Colonies on the agar plates were counted manually and values plotted on the y-axis. Error bars are the (number of colonies)$^{½}$.

ders recognizing gelatin from round 1, thereby masking the enrichment of clones recognizing GSH-QDs since collagen and gelatin are similar proteins. Upon using a different protein in the second and third rounds, namely BSA, and using centrifugation to separate bound phage to NPs and unbound phages in the fourth round, we found that analyzing 16 random colonies picked from round 4 did not show evidence of enrichment in the form of pattern repeats as observed in the initial panning on GSH-QDs in solution. In contrast to literature reports[14], our attempts to enrich additional binders by panning on immobilized GSH-QDs on gelatin or BSA only yielded off-target clones (i.e. clones which did not specifically recognize GSH-QDs) (Appendix D, Table D3).

An attempt was made to eliminate generation of off-target clones during panning by using a different protein for QD immobilization in each round. The chosen proteins were LF for the round 1, followed by OVA for round 2 and HSA for round 3. A control well with only LF and no QDs was included in order to identify binding over background and no evidence of enrichment was observed in the case of wells containing GSH-QDs immobilized to LF. Additionally, a subtraction strategy[19,20] used to pre-clear non-specifically binding phages, such as phage binding to capture proteins or components in the panning system other than the target itself, was employed in order to eliminate phages binding the above-mentioned capture proteins used to immobilize GSH-QDs. In this attempt, the phage library was first panned on BSA coated plates, after which the unbound phages were transferred to wells immobilized with GSH-QDs (100 nM) coated on BSA. Three rounds of panning were performed using this method; however, no evidence of enrichment or binding above background levels (wells coated with BSA

alone) was observed. While two clones were identified in the form of pattern repeats out of 16 random colonies picked in a BstN1 fingerprinting, both the phage clones were found to bind BSA, and were therefore unable to recognize GSH-QDs specifically. Additionally, no evidence of enrichment was found upon performing panning on GSH-coated wells (Appendix D, Table D3).

### 5.3.6 Panning on GSH-QDs with a Chain Shuffled Phage Library

Since our efforts to discover a QD binder with improved enrichment over GSH43 using various immobilized QD panning protocols failed, we next tried panning on a chain shuffled library. A library was formed with the intact heavy chain of GSH43 clone paired with all the light chains and used for these experiments (swap-L phage library). While no obvious evidence of enrichment was observed in the case of GSH-QDs immobilized on a different protein (BSA, LF or OVA) in each round, a moderate enrichment was observed when a centrifugation technique similar to the one used to discover GSH43 initially, was used. Although a visible difference in binding over the existing GSH43 clone was not observed, two groups of clones (Figure 5.6, red and yellow boxes) with slight light chain differences in the amino acid sequence (Appendix D, TableD4) were identified using pattern repeats on a BstN1 fingerprinting as an evidence of clonal enrichment. While this proves that the best specific binder from the original library is indeed the $V_H$-$V_L$ pair in GSH43 clone, further studies would be necessary to analyze and characterize the newly identified clones using the swap-L library.

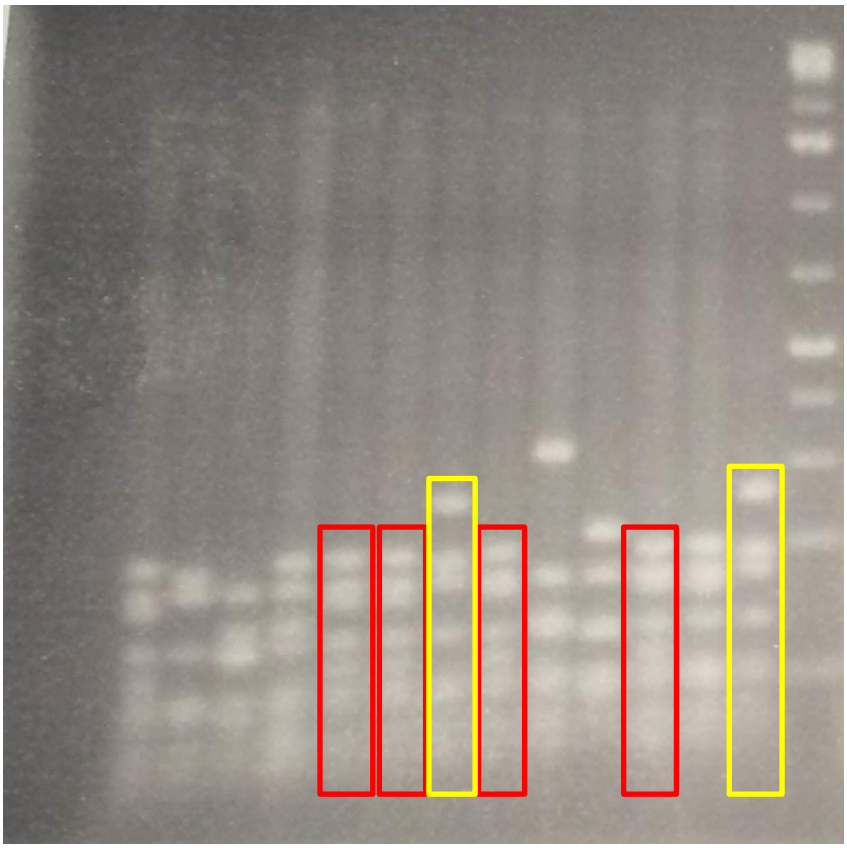

**Figure 5.6: BstN1 Fingerprinting After Round 4 of Swap-L Panning on GSH-QDs**

BstN1 fingerprinting analysis of 12 randomly picked colonies showing unique scFv patterns. Two groups of clones were observed (red and yellow boxes) enriched although slightly different in light chains.

# 5.4 Conclusions

Binders to GSH-QDs other than GSH43 clone were identified (HS2, 3, 4) using salt precipitation of NPs, thereby allowing for the use of lower speeds during ultracentrifugation in the panning process. The binders obtained were able to detect QDs *in vitro* and in a biological milieu, the high cross-reactivity to almost all NPs tested and the inability of these binders (phage format) to bind immobilized GSH-QDs and GSH led us to not pursue further studies with these clones. Although the GSH43 clone exhibited mild cross-reactivity to certain silica NPs and $TiO_2$ NPs, GSH43ϕ bound GSH-QDs whether immobilized or in solution, and GSH-coated plates. The clone binds 10-fold above background to GSH-QDs, and this was not further improved using the chain-shuffling experiments indicating that this clone potentially is the best binder to GSH-QDs from the phage library used in this thesis. Different protocols based on literature reports were used to perform panning by immobilizing the target, which is the widely accepted mode in phage display. However, none of the enrichments evidenced a potential binder with binding ability of more than 10-fold over background, demonstrating the success of the novel solution-phase panning method in the identification of a binder. Binders to $TiO_2$ NPs, namely Ti6 and Ti49, did not show any cross-reactivity to Au powder, similar in morphology to $TiO_2$, and bound universally all the $TiO_2$ NPs varying in composition tested in this thesis with low cross-reactivity to dissimilar materials.

# References

[1] Bradbury, A. R. & Marks, J. D. Antibodies from Phage Antibody Libraries. *Journal of immunological methods*, **2004**, 290(1-2), 29-49.

[2] Russell, S. J., Hawkins, R. E. & Winter, G. Retroviral Vectors Displaying Functional Antibody Fragments. *Nucleic Acids Res*, **1993**, 21(5), 1081-1085.

[3] Irving, R. A., Kortt, A. A. & Hudson, P. J. Affinity Maturation of Recombinant Antibodies Using E. Coli Mutator Cells. *Immunotechnology*, **1996**, 2(2), 127-143.

[4] Hawkins, R. E., Russell, S. J. & Winter, G. Selection of Phage Antibodies by Binding Affinity. Mimicking Affinity Maturation. *J Mol Biol*, **1992**, 226(3), 889-896.

[5] Clackson, T., Hoogenboom, H. R. *et al.* Making Antibody Fragments Using Phage Display Libraries. *Nature*, **1991**, 352(6336), 624-628.

[6] Marks, J. D., Griffiths, A. D. *et al.* By-Passing Immunization: Building High Affinity Human Antibodies by Chain Shuffling. *Biotechnology (N Y)*, **1992**, 10(7), 779-783.

[7] Crameri, A., Cwirla, S. & Stemmer, W. P. Construction and Evolution of Antibody-Phage Libraries by DNA Shuffling. *Nat Med*, **1996**, 2(1), 100-102.

[8] Glaser, S. M., Yelton, D. E. & Huse, W. D. Antibody Engineering by Codon-Based Mutagenesis in a Filamentous Phage Vector System. *J Immunol*, **1992**, 149(12), 3903-3913.

[9] Schier, R. & Marks, J. D. Efficient in Vitro Affinity Maturation of Phage Antibodies Using Biacore Guided Selections. *Hum Antibodies Hybridomas*, **1996**, 7(3), 97-105.

[10] Virnekas, B., Ge, L. *et al.* Trinucleotide Phosphoramidites: Ideal Reagents for the Synthesis of Mixed Oligonucleotides for Random Mutagenesis. *Nucleic Acids Res*, **1994**, 22(25), 5600-5607.

[11] Hoogenboom, H. R. Selecting and Screening Recombinant Antibody Libraries. *Nat Biotechnol*, **2005**, 23(9), 1105-1116.

[12] Bass, S., Greene, R. & Wells, J. A. Hormone Phage: An Enrichment Method for Variant Proteins with Altered Binding Properties. *Proteins*, **1990**, 8(4), 309-314.

[13] Smith, G. P. & Petrenko, V. A. Phage Display. *Chem Rev*, **1997**, 97(2), 391-410.

[14] Mardyani, S. & Chan, W. C. W. Quantification of Quantum Dots Using Phage Display Screening and Assay. *Journal of Materials Chemistry*, **2009**, 19(35), 6321-6323.

[15] Rothenstein, D., Claasen, B. *et al.* Isolation of Zno-Binding 12-Mer Peptides and Determination of Their Binding Epitopes by Nmr Spectroscopy. *J Am Chem Soc*, **2012**, 134(30), 12547-12556.

[16] Hattori, T., Umetsu, M. *et al.* A High-Affinity Gold-Binding Camel Antibody: Antibody Engineering for One-Pot Functionalization of Gold Nanoparticles as Biointerface Molecules. *Bioconjug Chem*, **2012**, 23(9), 1934-1944.

[17] Zheng, H., Mortensen, L. J. & DeLouise, L. A. Thiol Antioxidant-Functionalized Cdse/Zns Quantum Dots: Synthesis, Characterization, Cytotoxicity. *J Biomed Nanotechnol*, **2013**, 9(3), 382-392.

[18] Lamboy, J. A., Arter, J. A. *et al.* Phage Wrapping with Cationic Polymers Eliminates Nonspecific Binding between M13 Phage and High Pi Target Proteins. *J Am Chem Soc*, **2009**, 131(45), 16454-16460.

[19] Gnanasekar, M., Rao, K. V. *et al.* Novel Phage Display-Based Subtractive Screening to Identify Vaccine Candidates of Brugia Malayi. *Infect Immun*, **2004**, 72(8), 4707-4715.

[20] Hof, D., Cheung, K. *et al.* A Novel Subtractive Antibody Phage Display Method to Discover Disease Markers. *Mol Cell Proteomics*, **2006**, 5(2), 245-255.

# Chapter 6

*Isolation of Binders to Carbon-Based Nanomaterials*

# 6.1 Introduction

The use of carbon nanomaterials (CNMs), particularly carbon nanotubes (CNTs) and their potential application in biomedical applications[1,2] and electronics is increasing[3] owing to their fascinating mechanical, thermal and electrical properties[4]. CNMs include both fullerenes (spherical carbon NPs) and CNTs. While the worldwide CNT production capacity has increased at least 10-fold since 2006[5], fullerenes are also being increasingly used in a number of cosmetic products such as anti-aging creams[6,7]. CNTs are cylinders composed of one or more layers of graphene (single wall, SWCNTs or multi-wall, MWCNTs) with open or closed ends[8]. Their diameters typically range from 0.8-2 nm for SWCNTs, and 5-20 nm for MWCNTs. CNTs lengths range from less than 100 nm to several centimeters, spanning both molecular and macroscopic scales[5]. With the widespread use of CNTs in various applications including biotechnology-related use in ink-jet printed test strips for estrogen and progesterone detection, microarrays for DNA and protein detection[9] and *in vivo* cargo delivery to name a few[10,11] , the concern for human contact to CNMs and associated pulmonary toxicity[12] has grown including chronic occupational exposures[13]. Most studies used high doses of CNTs to examine dermal exposure; however, low dose exposure of both SWCNTs and MWCNTs in guinea pigs caused skin irritation[14]. Therefore, the breadth of CNT toxicity studies in the case of dermal exposures is minimal and is also further hampered by the use of varying doses, sizes and functional group modifications, which makes comparison of published data difficult. Additionally, the analytical techniques used in the detection of CNTs in biological samples and environment including SEM, TEM and Raman spectroscopy are

limited in their ability to detect trace quantities of CNTs in a sample[15]. While Raman spectroscopy is limited in its ability to detect trace quantities of CNTs in a macroscopic sample, SEM and TEM can be successful only if the CNTs are visible on the exterior surfaces or surfaces of cross-sections and suffer from low contrast[16]. These techniques, therefore, are prone to false negatives, i.e. lack of detection does not imply absence of CNTs[15]. Previously published studies have identified a monoclonal antibody against the fullerene $C_{60}$ that has been shown to bind CNTs with some selectivity[17]. Specifically, binding peptides for CNTs have also been discovered that may allow for new ways of manipulating, sorting, separating and dispersing CNTs[18], and acting as specific markers.

In this chapter, a strategy employing three different targets in order to identify a scFv to bind non-fluorescent carbon-based NPs using phage display technology will be discussed. Upon successful identification, CNTs can be detected using standard IHC and microscopic techniques in biological samples and in the environment, and used as a tool kit in conjuncture with existing analytical techniques. We employed three different CNMs namely MWCNTs, CNpaper (Bucky paper™) and SWCNTs, where the targets were exposed to a phage display library in order to attempt to find a binder with universal binding and cross-reactivity properties to different CNMs.

# 6.2 Materials and Methods

## Carbon-based Nanoparticles

Three different types of carbon-based materials were used for panning namely carboxylated MWCNTs (MWSusp-100, Nano-Labs, Inc.), CN bucky paper (CNpaper, Buckypaper™, diameter 40 mm, Nano-Labs Inc.) and carboxylated SWCNTs (Nano-Labs Inc., diameter=1.5 nm, length= 1-5 μm). MWCNTs and SWCNTs were tested for pellet formation in TBS using centrifugation and the speeds were optimized for panning with phage library. All other materials and procedures used were as outlined in Chapter 2.

# 6.3 Results

## Panning process

For MWCNTs, 100 μL of the stock solution (1 mg/mL) in water added to 300 μL TBS (0.2 mg/mL final concentration) and 100 μL of phage library ($10^{12}$ phages/mL in TBS containing 0.5% casein) were mixed together with gentle agitation for 2 h at room temperature. For the CNpaper, two small pieces (~1 mm by 1 mm each) were incubated with the phage library (100 μL) diluted in TBS (1:5 dilution) for 2 h at room temperature with gentle agitation. For SWCNTs, 2 mg/mL of the powder was added to the phage library (100 μL) diluted in TBS (1:5 dilution), and incubated for 2 h at room temperature with gentle agitation to allow for phage binding. Solutions of phages and MWCNTs, or SWCNTs were centrifuged at 29,000 rpm (30,000 g) or 10,000 g for 10 and 5 min, respectively, to separate the bound phage-NPs from the unbound phages (supernatant).

**A**

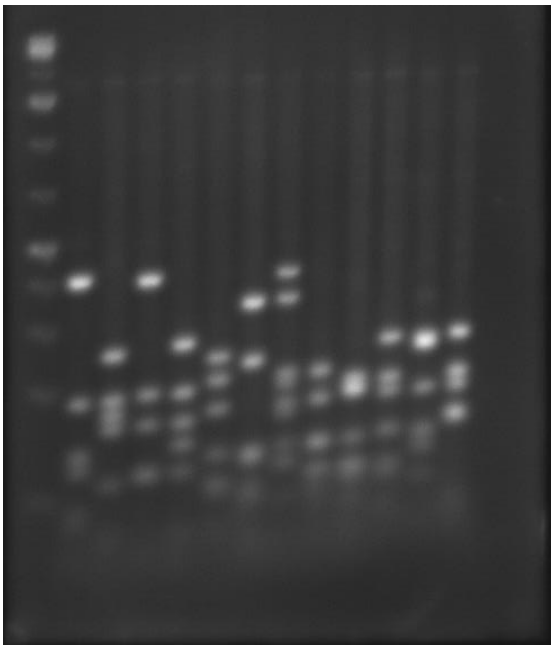

**B**

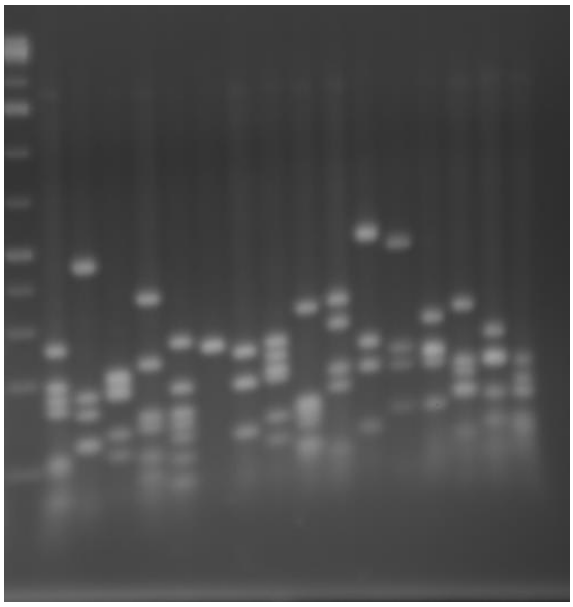

**Figure 6.1: BstN1 Fingerprinting Images for MWCNTs and SWCNTs**

BstN1 fingerprinting analysis showing unique scFv patterns for A) 12 random colonies picked for MWCNTs (after round 5) and B) 16 colonies picked for SWCNTs showing absence of pattern repeats and thereby lack of clonal enrichment (after round 4).

The bound phage-NP pellet was washed 5 times with TBST and once with deionized water. For CNpaper, the solution containing unbound phages was discarded and the papers were washed 7 times with TBST, and once with deionized water by rinsing the pieces of paper and discarding the solution each time. All bound phages from these materials were eluted using 200 µL of 0.1 M glycine (pH=2.2, containing 0.01% BSA) and neutralized using 12 µL of 2 M Tris base. As described in the previous chapters, the titer of the eluted phages was quantified by transduction of serial dilutions of the phage into TG1 cells to ampicillin resistance and the resulting colonies were counted. Input phage pools for the subsequent rounds were prepared, and 4 rounds of panning for each materials was performed before analyzing for clonal enrichment using a BstN1 fingerprinting method to detect pattern repeats indicative of relative clonal abundance. Although a slight increase in binding over background by 7-and 6-fold were observed post round 3 with SWCNTs and CNpaper respectively, this increase was not observed after round 4. A modest 2-2.5 fold increase above background was observed after round 5 in the case of panning on MWCNTs. However, the BstN1 analysis, particularly for MWCNTs and SWCNTs, did not show any evidence of enrichment via repeating patterns even though 12-16 colonies (Figure 6.1A, B) for each material were picked for the digest. Since no pattern repeats indicative of relative clonal abundance were found, alternative materials and panning methods must be investigated.

## 6.4 Conclusions

This chapter deals with an attempt to discover phage binders to commercially important and valuable materials such as MWCNTs, Buckypaper™ and SWCNTs using phage display technology. Although no binders were identified from the particular phage library used, the above-mentioned studies will serve as valuable preliminary knowledge and can pave the way for the use of different phage libraries displaying antibodies using the protocols described in this chapter and the thesis for carbon-based NPs. Further, more rounds of panning (rounds 5 and 6) could be performed to observe any slight enrichment of particular clones above the low background phage binding observed with these NPs similar to that observed after round 3 with CNpaper and SWCNTs.

# References

[1] Strasinger, C. L., Scheff, N. N. *et al.* Carbon Nanotube Membranes for Use in the Transdermal Treatment of Nicotine Addiction and Opioid Withdrawal Symptoms. *Subst Abuse,* **2009**, 3, 31-39.

[2] Welsher, K., Liu, Z. *et al.* A Route to Brightly Fluorescent Carbon Nanotubes for near-Infrared Imaging in Mice. *Nat Nanotechnol,* **2009**, 4(11), 773-780.

[3] Dang, X., Yi, H. *et al.* Virus-Templated Self-Assembled Single-Walled Carbon Nanotubes for Highly Efficient Electron Collection in Photovoltaic Devices. *Nat Nanotechnol,* **2011**, 6(6), 377-384.

[4] Green, M. J., Behabtu, N. *et al.* Nanotubes as Polymers. *Polymer,* **2009**, 50(21), 4979-4997.

[5] De Volder, M. F., Tawfick, S. H. *et al.* Carbon Nanotubes: Present and Future Commercial Applications. *Science,* **2013**, 339(6119), 535-539.

[6] Markovic, Z. & Trajkovic, V. Biomedical Potential of the Reactive Oxygen Species Generation and Quenching by Fullerenes (C60). *Biomaterials,* **2008**, 29(26), 3561-3573.

[7] Xiao, L., Takada, H. *et al.* The Water-Soluble Fullerene Derivative "Radical Sponge" Exerts Cytoprotective Action against Uva Irradiation but Not Visible-Light-Catalyzed Cytotoxicity in Human Skin Keratinocytes. *Bioorg Med Chem Lett,* **2006**, 16(6), 1590-1595.

[8] Iijima, S. Helical Microtubules of Graphitic Carbon. *Nature,* **1991**, 354(6348), 56-58.

[9] Star, A., Tu, E. *et al.* Label-Free Detection of DNA Hybridization Using Carbon Nanotube Network Field-Effect Transistors. *Proc Natl Acad Sci U S A,* **2006**, 103(4), 921-926.

[10] Hong, S. Y., Tobias, G. *et al.* Filled and Glycosylated Carbon Nanotubes for in Vivo Radioemitter Localization and Imaging. *Nat Mater,* **2010**, 9(6), 485-490.

[11] Liu, Z., Sun, X. *et al.* Supramolecular Chemistry on Water-Soluble Carbon Nanotubes for Drug Loading and Delivery. *ACS Nano,* **2007**, 1(1), 50-56.

[12] Lam, C. W., James, J. T. *et al.* Pulmonary Toxicity of Single-Wall Carbon Nanotubes in Mice 7 and 90 Days after Intratracheal Instillation. *Toxicol Sci,* **2004**, 77(1), 126-134.

[13] Manke, A., Luanpitpong, S. & Rojanasakul, Y. Potential Occupational Risks Associated with Pulmonary Toxicity of Carbon Nanotubes. *Occup Med Health Aff,* **2014**, 2,

[14] Ema, M., Matsuda, A. *et al.* Evaluation of Dermal and Eye Irritation and Skin Sensitization Due to Carbon Nanotubes. *Regul Toxicol Pharmacol,* **2011**, 61(3), 276-281.

[15] Irin, F., Shrestha, B. *et al.* Detection of Carbon Nanotubes in Biological Samples through Microwave-Induced Heating. *Carbon,* **2012**, 50(12), 4441-4449.

[16] Edgington, A. J., Petersen, E. J. *et al.* Microscopic Investigation of Single-Wall Carbon Nanotube Uptake by Daphnia Magna. *Nanotoxicology,* **2014**, 8 Suppl 1, 2-10.

[17] Braden, B. C., Goldbaum, F. A. *et al.* X-Ray Crystal Structure of an Anti-Buckminsterfullerene Antibody Fab Fragment: Biomolecular Recognition of C(60). *Proc Natl Acad Sci U S A,* **2000**, 97(22), 12193-12197.

[18] Wang, S., Humphreys, E. S. *et al.* Peptides with Selective Affinity for Carbon Nanotubes. *Nat Mater,* **2003**, 2(3), 196-200.

# Chapter 7

*Conclusions and Future Directions*

With the promise offered by nanotechnology-enabled consumer products and their increasing use, human contact with NPs is inevitable. Detection of NPs in the environment and those entering the body through skin, gastrointestinal tract and the respiratory tract is important in order to address potential toxicological and safety concerns. While currently available and widely used analytical tools for NP detection are certainly useful, limitations pertaining to each of these techniques hamper their ability to provide a clear idea of NP location, form and amount in the tissues. Various analytical methods used for NP detection and their associated limitations have been outlined in Chapter 1. In this thesis, I have developed scFv antibodies using phage display to commercially important NPs such as QDs and $TiO_2$ NPs to enable detection of NPs using conventional microscopic techniques and IHC. These novel reagents, when used in conjunction with other existing techniques, will comprise a powerful tool kit to provide information on both NP form and presence both *in vitro* and in a biological milieu.

In Chapter 2, the novel methods developed to isolate the scFvs recognizing QDs and $TiO_2$ NPs from a library of ~$2x10^9$ unique antibodies without the need for NP immunogenicity have been discussed. We have for the first time developed the method of panning on NPs dispersed in solution as opposed to the conventional method of immobilizing target antigens to isolate binding antibodies using phage display. GSH43 and Ti49 were the phage clones discovered from the library that bind GSH-QDs and $TiO_2$ NPs ~10- and 150-fold over background, respectively, and phage titer assays and TEM were used to demonstrate binding to these NPs.

Chapter 3 discusses the ability of GSH43 and Ti49-scFvs to recognize GSH-QDs and $TiO_2$ NPs respectively as shown using various custom-designed *in vitro* assays. First, dot blots were used to prove that GSH43-scFvs recognized GSH-QDs specifically and no binding to other dissimilar NPs including Au NPs and CNTs was observed. Moreover, Ti49-scFvs did not bind GSH-QDs, Au NPs or CNTs. Since the presence of $TiO_2$ NPs on the nitrocellulose membrane could not be verified by color, they were dried on to glass slides and Ti49-scFv binding was verified using confocal microscopy whereas an arbitrary clone from the library did not bind the NPs (Npep-scFv as negative control). While these experiments do show that the antibodies developed against NPs are capable of recognizing the respective NPs in an *in vitro* setting and thereby in the environment, binding to potentially 'transformed' NPs in a biological milieu has been investigated and discussed in Chapter 4.

The next chapter deals with testing the functionality of the isolated scFvs namely GSH43 and Ti49-scFvs in their binding to GSH-QDs and $TiO_2$ NPs in a biological milieu using an *ex vivo* human skin model. Both GSH-QDs and $TiO_2$ NPs could be detected using standard IHC procedures in skin and the presence of NPs in the bluish-purple stained areas (detection of AP-conjugated anti-FLAG antibody using BCIP/NBT substrate) were confirmed using secondary detection procedures including LCM/AAS and SEM/EDX. The detection of non-fluorescent NPs such as $TiO_2$ was shown using Ti49-scFvs using cost-effective conventional microscopes, and the data presented herein validates the preponderance of current literature, which reports $TiO_2$ NPs agglomerates to predominantly localize in the upper layers of the SC. However, mild instances of AP

staining were also observed below the SC in the case of application of $TiO_2$ NPs in water and $TiO_2$-containing sunscreen (Eucerin SPF 15). Upon using SEM to visualize presence of NPs in these stained areas, we found structures that morphologically resemble $TiO_2$ aggregates suggesting their possible presence in the viable skin layers. However, efforts to detect elemental Ti (EDX) proved inconclusive due to possible low limit of detection offered by the instrument, high sampling error and poor solubility of $TiO_2$ NPs (AAS could not be used for elemental detection). In the QD studies, we were able to confirm that the instances of AP staining with and without a co-localizing QD fluorescence signal did contain elemental Cd indicating presence of QDs using LCM/AAS. Hence, it is likely that the instances of mild AP staining in the epidermis on $TiO_2$ treated skin (albeit less frequent that in QD treated skin) do indeed contain NPs.

The cross-reactive binding properties of the binders to NPs other than the target NP against which they were isolated were investigated in Chapter 5. Moreover, the possibility of discovering binders with a greater binding ability to GSH-QDs was studied by performing panning on QDs immobilized on various proteins. Our efforts are unique in our approach to bio-pan on NPs dispersed in solution. Typically, phage display requires targets to be immobilized onto a solid support by non-covalent adsorption to a hydrophobic surface[1] or by means of chemical coupling[2]. Despite our attempts to perform enrichments using gelatin to immobilize QDs on polystyrene plates as described by Mardyani et al.,[3] only clones that bound gelatin were observed. This phenomenon has been previously reported, where often unrelated off-target clones binding other components used for immobilization other than the target itself are enriched[4]. For

example, phage binding to components other than the target itself such as the solid phase (plastic, plates, beads), blocking agents (BSA, casein, milk) and capturing agents (secondary antibodies, biotin) may predominate during the rounds of enrichment[4]. We also observed this in our efforts to immobilize QDs on BSA, where only clones binding BSA were generated. Moreover, a subtraction panning strategy where QDs immobilized on BSA were exposed to only those phages which did not bind wells coated with BSA in a previous step, also did not show any compelling evidence of enrichment. Hence, our novel solution-phase panning methodology helps to minimize occurrences of false positives and favors identification of clones binding NPs themselves dispersed in solution. While we do not fully understand the definitive mechanism of binding of the scFvs to the NPs, data presented in this thesis suggests that shape of the NPs in solution must be a key recognition element, as the CDRs of the antibody do not contain the expected metal binding amino acids. It has also increasingly become evident that the phages are exposed to transient aggregates of NPs in solution during the panning process. The ~150-fold more binding of Ti49ϕ and Ti6ϕ clones to $TiO_2$ NPs observed over background may be attributed to binding to Ti aggregates, which precipitate at a lower centrifugal force (g force), allowing more complete separation of unbound phage. The modest 10-fold binding of GSH43 clone to GSH-QDs observed over background may be due to the QDs being highly dispersed in solution compared to the inherently aggregate $TiO_2$ NPs. While we could not control the aggregation states of NPs in solution in these experiments, future experiments could be directed towards the use of size and shape controlled nanocrystals as targets for the panning process.

Although the light chain shuffling experiments did not yield binders with improved binding to QDs or significant differences in the amino acid sequence with respect to GSH43, future work can be directed towards *in vitro* mutagenesis of the whole scFv by mutagenic PCR. Further, once the critical residues for binding are identified using an alanine scanning of the CDRs, optimization of the CDR regions can then be done using site-directed mutagenesis. Future work could also be directed towards the use of biotinylated NPs as targets in order to efficiently capture them on streptavidin-coated substrates for the panning process. This will also help ensure that off-target clones do not predominate during panning. While our efforts to date to pan against economically important materials such as MWCNTs and SWCNTs have not yet yielded potential binders, future efforts could be directed towards use of other forms of CNTs from different sources as panning targets and additional libraries.

In summary, this thesis, for the first time, has described isolating scFv antibodies that bind NPs from a phage display library with over $10^9$ unique clones. Antibodies that bind and recognize GSH-QDs and $TiO_2$ NPs were discovered and their binding and cross-reactive properties towards other NPs were investigated. The scFvs were shown to successfully recognize and bind NPs even in a biological milieu (*ex vivo* human skin) as demonstrated through various proof-of-concept studies described in Chapter 4. This methodology of isolating antibodies to NPs can be further applied to various NPs, thereby providing an expansive tool kit that can complement other techniques to provide important information regarding NP presence and form, whether intact or soluble ions. The antibodies are especially useful to detect non-fluorescent NPs using common

microscopic techniques without the need for modifying the NPs themselves in order to render them fluorescent for ease of tracking. While, these reagents cannot quantitatively detect NPs, this technology, when advanced further, will form a tool kit to allow for the improvement of our NP detection abilities in the environment and various biological systems.

# References

[1] Smith, G. P. Filamentous Fusion Phage: Novel Expression Vectors That Display Cloned Antigens on the Virion Surface. *Science*, **1985**, 228(4705), 1315-1317.

[2] Bass, S., Greene, R. & Wells, J. A. Hormone Phage: An Enrichment Method for Variant Proteins with Altered Binding Properties. *Proteins*, **1990**, 8(4), 309-314.

[3] Mardyani, S. & Chan, W. C. W. Quantification of Quantum Dots Using Phage Display Screening and Assay. *Journal of Materials Chemistry*, **2009**, 19(35), 6321-6323.

[4] Vodnik, M., Zager, U. *et al.* Phage Display: Selecting Straws Instead of a Needle from a Haystack. *Molecules*, **2011**, 16(1), 790-817.

# Appendix A

*Chapter 2 Supplementary Data*

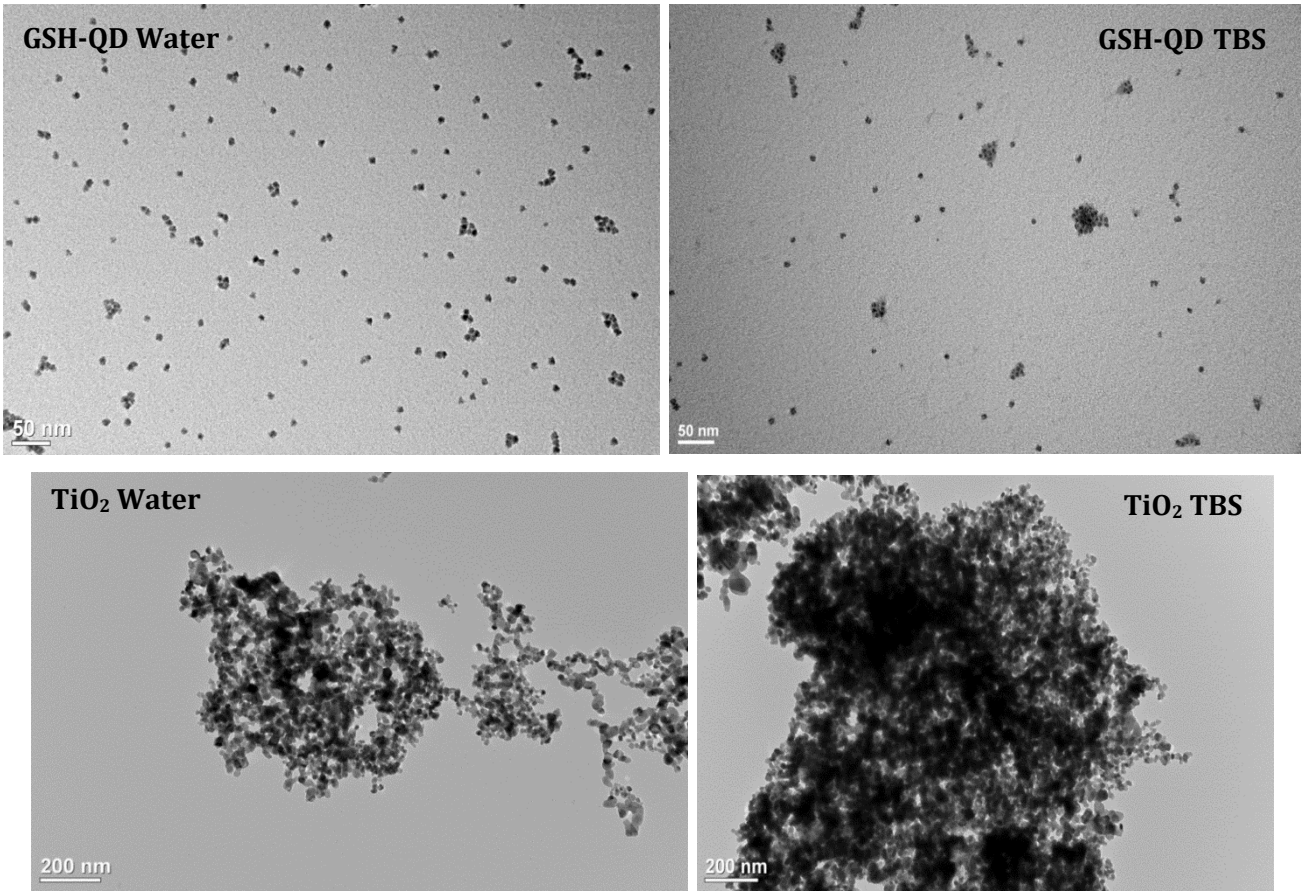


**Figure A1: TEM Images of GSH-QDs and $TiO_2$ NPs in Water and TBS**

Representative TEM images of GSH QDs in water and TBS showing stability of particles. $TiO_2$ NPs exist as aggregates in water and further forms larger aggregates in TBS whereas GSH-QDs do not. Scale bar=50 nm for GSH-QDs and 100 nm for $TiO_2$ NPs.

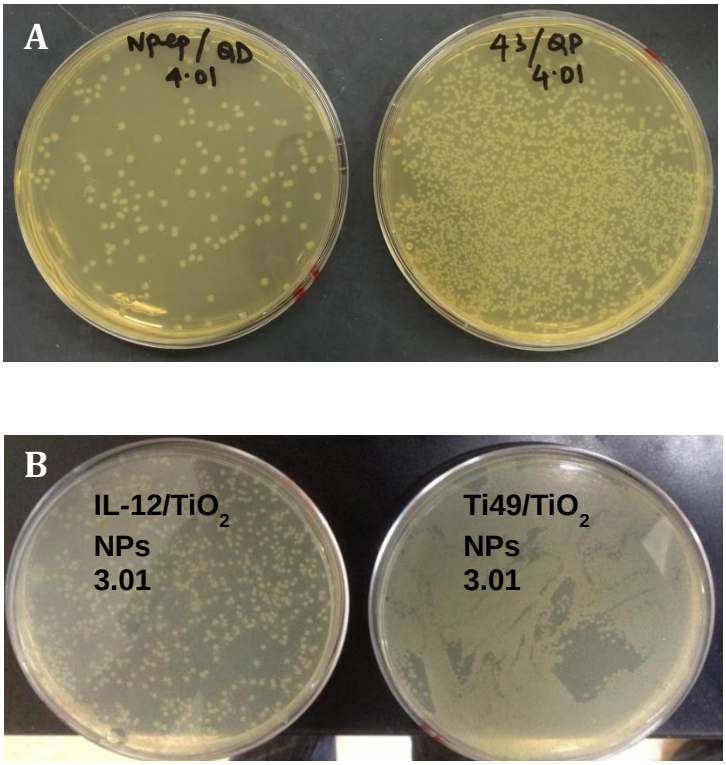


**Figure A2: Titer Plate Images of GSH43ϕ and Ti49ϕ Binding their Targets**

Centrifugation phage titer indicating high binding of phage clones to respective NP target relative to off-target negative control IL-12 phage clone. Plate label indicates Phage clone/NP type and the number indicates phage dilution factor. 4.01 dilution factor indicates 1:10,000 of phage diluted in TBS and 10 µL was used to TG1 cells. 3.01 dilution factor indicates 1:1000 of phage diluted in TBS and 10 µL was used to infect TG1 cells. A) Phage titer colonies showing ~10-fold more enrichment of GSH43ϕ on GSH-QDs compared to negative control IL-12ϕ on GSH-QDs. B) Phage titer colonies showing ~150-fold more enrichment of Ti49ϕ on $TiO_2$ NP compared to IL-12ϕ on $TiO_2$ NPs.

# Appendix B

*Chapter 3 Supplementary Data*

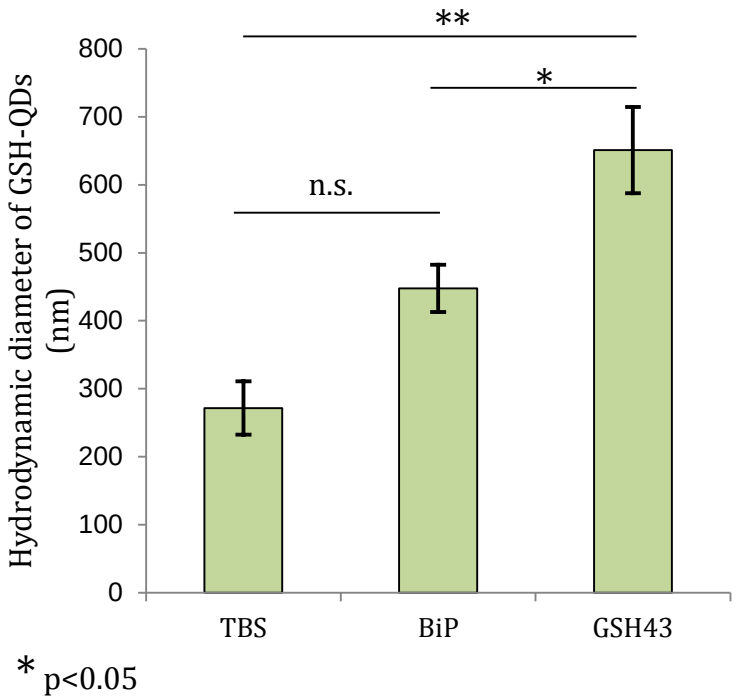


**Figure B1: DLS Assay to Verify GSH43-scFvs Binding GSH-QDs**

Hydrodynamic diameter measurements using the Malvern Zetasizer on GSH-QDs mixed 2 h with BiP or GSH43-scFvs, centrifuged, and re-suspended in TBS:water (3:7). GSH43-scfv-QD conjugate shows a significant increase in hydrodynamic diameter compared to BiP-associated QDs ($p<0.05$) and QDs processed in TBS alone ($p<0.01$) using a one-way ANOVA test, whereas BiP-associated complexes do not show any significance (n.s.) compared to QDs in TBS. Error bars indicate SEM of 4 independent experiments.

**Beads+BiP-scFv**

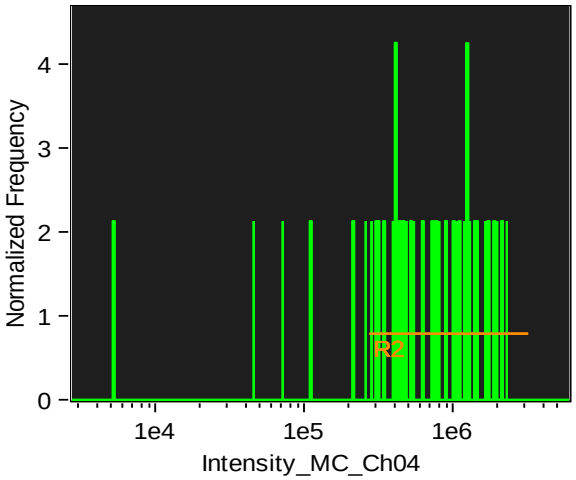


Intensity_MC_Ch04

| Population | Count | %Gated | Median |
|---|---|---|---|
| beads & Focus | 47 | 100 | 772117.11 |
| R2 & beads & Focus | 41 | 87.2 | 891699 |

**Beads+GSH43-scFv**

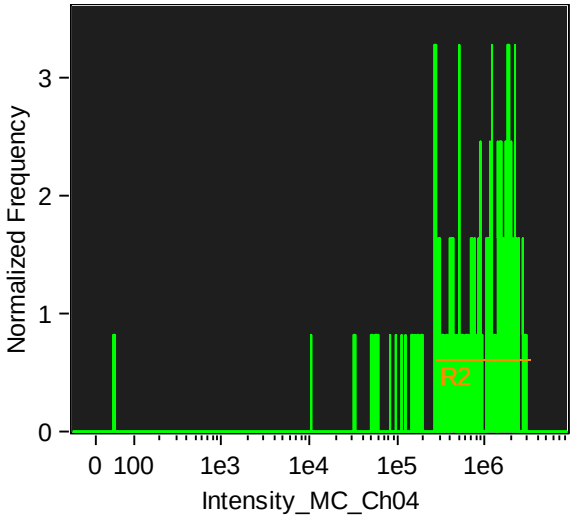


Intensity_MC_Ch04

| Population | Count | %Gated | Median |
|---|---|---|---|
| beads & Focus | 122 | 100 | 1100419.15 |
| R2 & beads & Focus | 104 | 85.2 | 1208120.55 |

**Figure B2: Binding of GSH43-scFv to Anti-FLAG-conjugated Beads**

Table showing values of median intensities (red boxes) of GSH-QDs binding scFv-coated anti-FLAG-conjugated beads analyzed using Image Stream. The median intensity of GSH-QDs binding GSH43-scFv coated beads is ~1.5-fold more than those binding to negative control (BiP)-scFv coated beads.

**A**

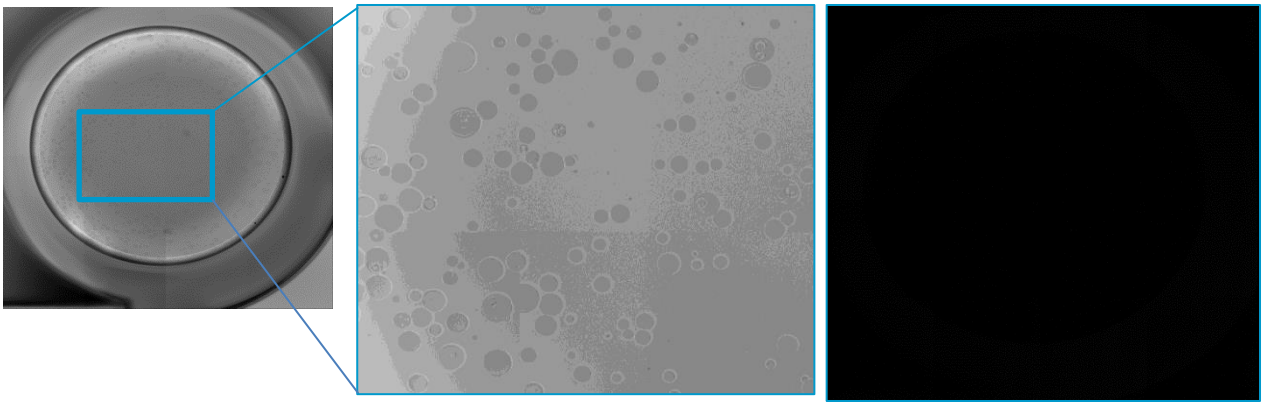

**B**

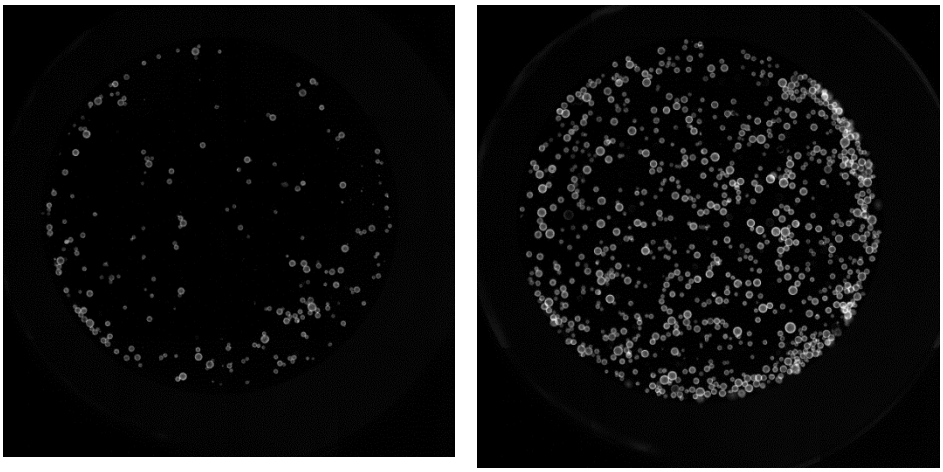

**C**

| Sample | Average Integrated Intensity |
|---|---|
| NT3-scFv on beads-QD | 349678.96 |
| GSH43-scFv on beads-QD | 652255.01 |

**Figure B3: Imaging of GSH-QDs Bound to Beads Using Celigo Instrument**

A) 'Beads only' sample showing brightfield with heterogeneously sized beads (blue box) and corresponding fluorescence field showing no presence of QDs. B) Fluorescence images showing GSH-QD fluorescence of a single well of NT3-scFv coated beads (left) and GSH43-scFv coated beads (right). C) Table showing average integrated intensity of images in B). GSH43-scFv coated beads show ~2-fold more intensity than NT3-scFv coated beads.

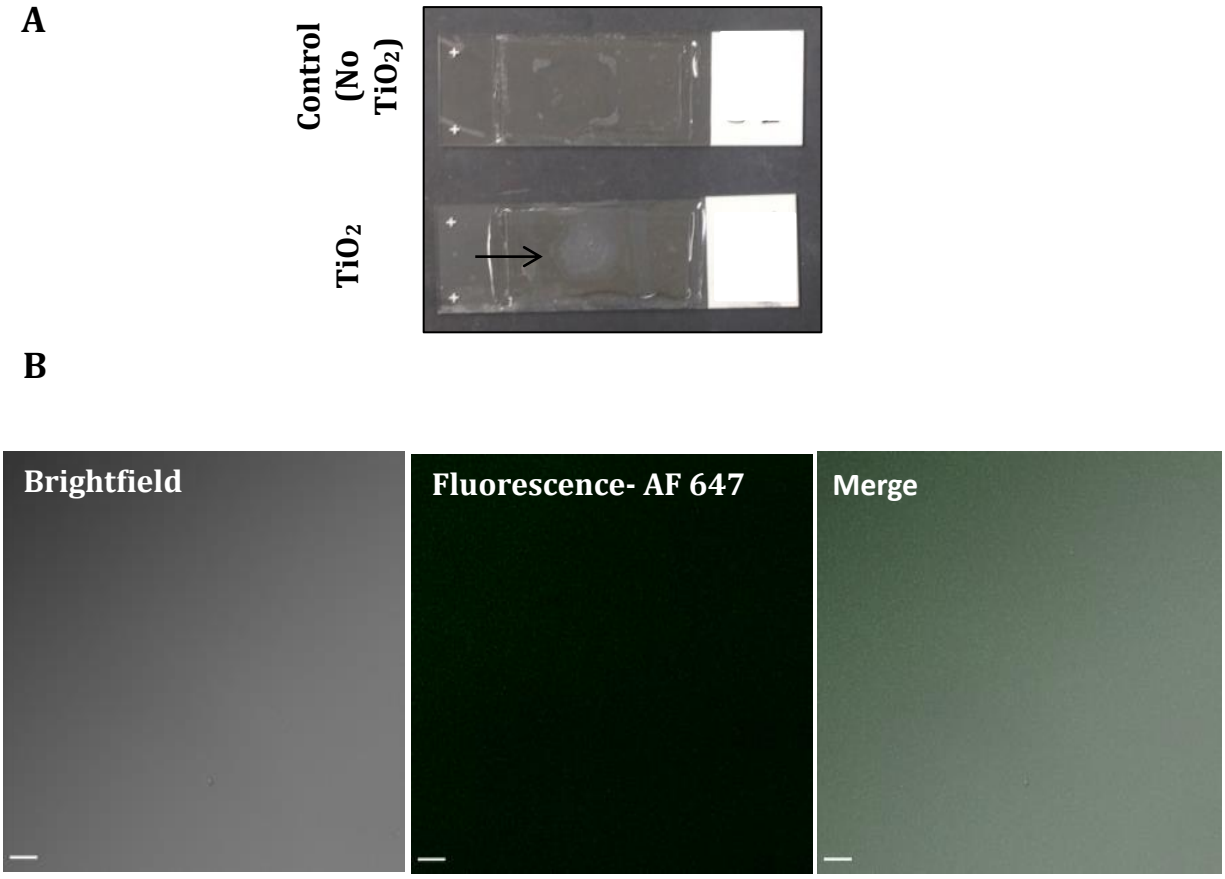


**Figure B4: $TiO_2$ NPs immobilized on glass slide**

Slides showing TiO2 NPs in water dried indicated by the black arrow (bottom) whereas control shows no white spot (top). B) Confocal images of slide without TiO2 NPs incubated with Ti49-scFvs followed by detection with Alexa Fluor 647-(pseudo-color green) conjugated anti-FLAG antibody. No non-specific staining was observed. Scale bar=20 μm.

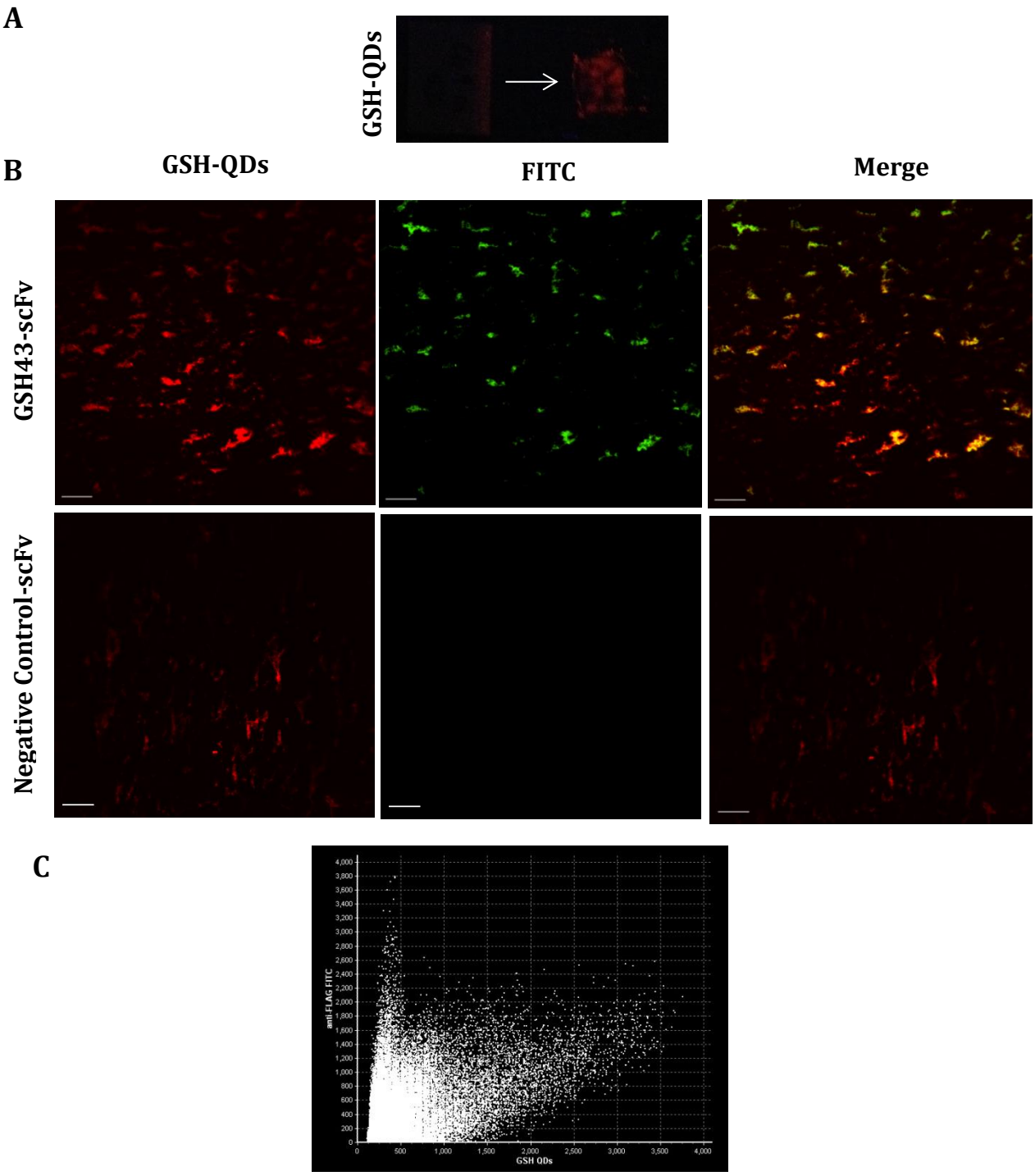


**Figure B5: Confocal Imaging Showing GSH43-scFvs Binding GSH-QDs**

Representative confocal single slice images to show GSH43-scFvs binding to QDs. A) GSH-QDs coated on a slide as seen under a UV lamp (white arrow). B) GSH43-scFvs binds GSH-QDs as detected by FITC-conjugated anti-FLAG antibody. Merge image shows co-localization proving binding of scFvs to QDs, whereas negative control (Npep) shows absence of FITC-conjugated anti-FLAG fluorescence and hence no binding. Scale bar=20 µm. C) Co-localization plot obtained for 'Merge' image of GSH43-scFv. Pearson's co-localization coefficient was found to be 0.65.

# Appendix C

*Chapter 4 Supplementary Data*

**[$TiO_2$]=0.01 mg/mL**

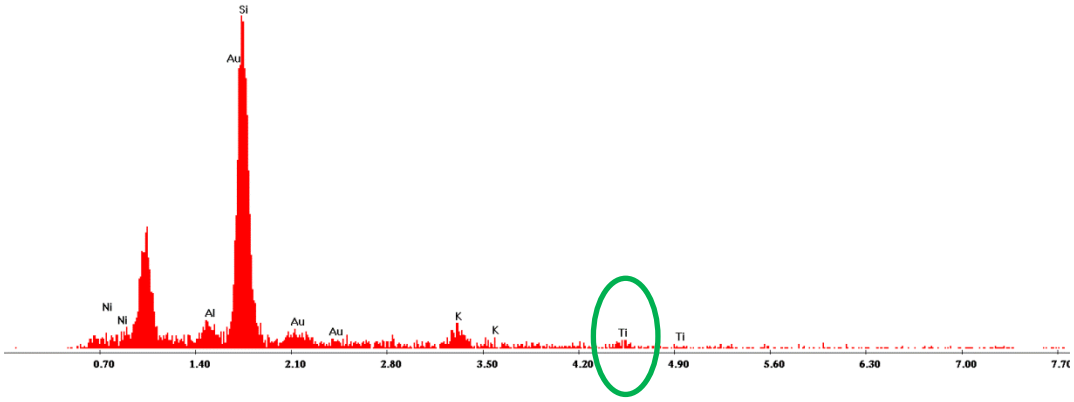


**[$TiO_2$]=0. 1 mg/mL**

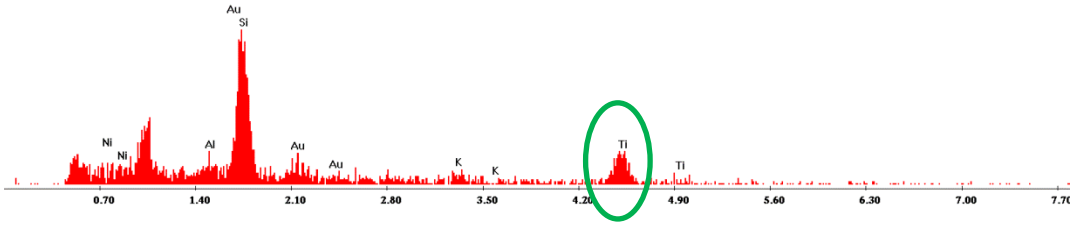


**[$TiO_2$]=1 mg/mL**

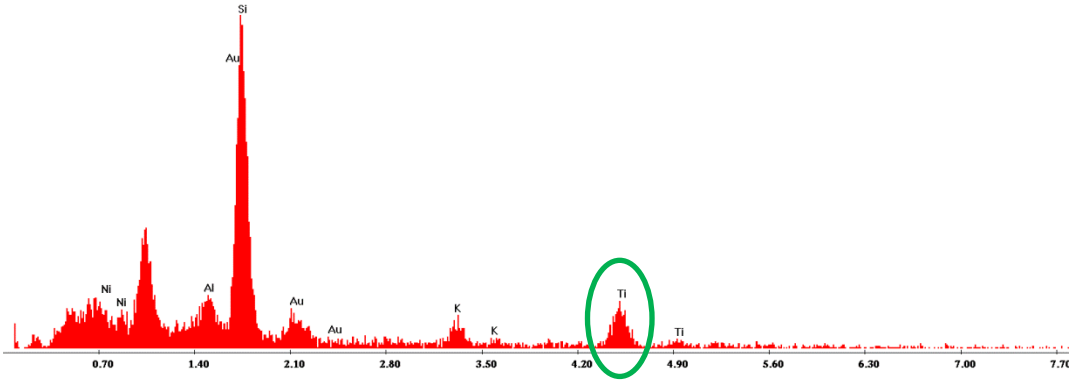


**Figure C1: SEM/EDX Spectra of $TiO_2$ NPs Adhered onto Coverslips**

$TiO_2$ NPs at various concentrations (0.01, 0.1 and 1 mg/mL) were dried onto coverslips and imaged using SEM/EDX. Discernable peaks (green ellipse) indicative of Ti presence in the EDX spectra were observed for 0.1 and 1 mg mL $TiO_2$ NP concentration but not for the 0.01 mg/mL sample.

# Appendix D

*Chapter 5 Supplementary Data*

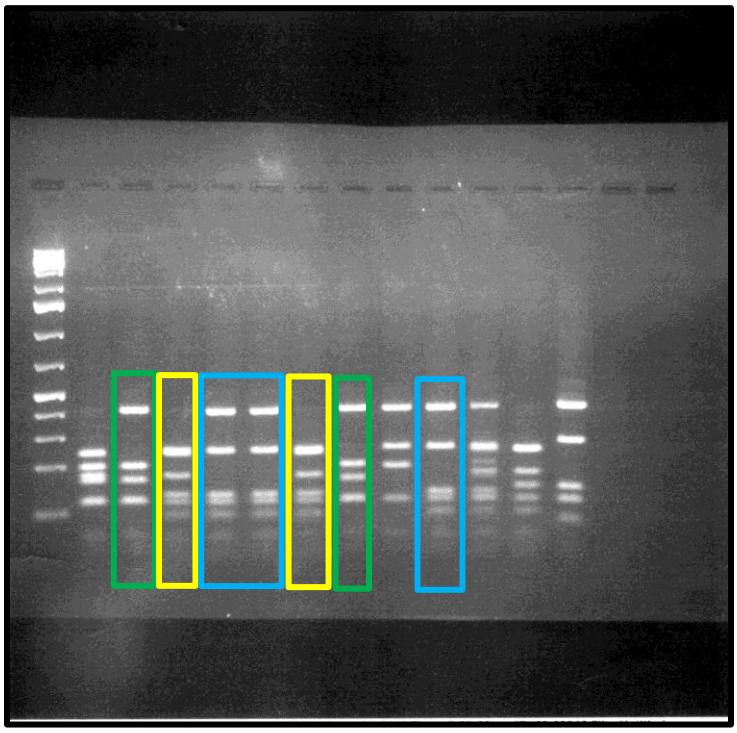

**Figure D1: BstN1 Fingerprinting Image for GSH-QDs (salt panning)**

BstN1 fingerprinting analysis showing unique scFv patterns for GSH-QD panning with the addition of salt to precipitate QDs at a lower speed. Green, yellow and blue boxes represent pattern repeats for clone designated HS2, HS3 and HS4 respectively.

## HS2

QSVLTQPPSASGTPGQRVTISCSGSSSNIGSNTVNWYQQLPGTAPKLLIYSNNQRPSGVPDRFSGSKS
GTSASLAISGLQSEDEADYYCAAWDDTLNGWQFGGGTKLTVLGEGKSSGSGSESKASQVQLQQSGP
GLVKPSETLSLTCTFSGGSVRNYYWSWIRQSPGKGLEWIGYIYPRGSTNYSESTNYNPSLKSRVTISV
DTSKNQFSLKLNSVTAADTAVYYCARLVHPTRNRGMDVWGQGTTVTVSS

## HS3

QSVLTQPPSVSVAPGQTARIPCGGDNIGSKSMHWYQQKPGQAPVLVVYADSDRPSGIPERFSGSNS
GNTATLTISRVEAGDEADYYCQVWDSSSDHWVFGGGTKLTVLGEGKSSGSGSESKASQVQLQQSGP
GLVKPSETLSLTCTFSGGSVRNYYWSWIRQSPGKGLEWIGYIYPRGSTNYSESTNYNPSLKSRVTISV
DTSKNQFSLKLNSVTAADTAVYYCARLVHPTRNRGMDVWGQGTLVTVSS

## HS4

QSVLTQPPSMSVAPGQTARITCEGHNIGIKSVHWYQQKPGQAPVLVVYDDSDRPSGIPERFSGSNSG
NTATLTISRVEAGDEADYYCQVWDSSSDHVVFGGGTKLTVLGEGKSSGSGSESKASQVQLQQSGPG
LVKPSETLSLTCTFSGGSVRNYYWSWIRQSPGKGLEWIGYIYPRGSTNYSESTNYNPSLKSRATISV
DTSKNQFSLKLNSVTAADTAVYYCARLVHPTRNRGMDVWGQGTTVTVSS

**Table D1: Amino Acid Sequences of Clones HS2,3,4 Isolated Against GSH-QDs**

**IL-12ϕ on GSH-QDs**

**HS2ϕ on GSH-QDs**

**HS3ϕ on GSH-QDs**

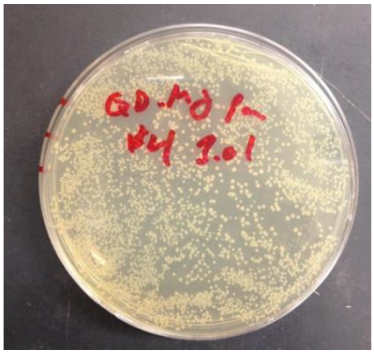

**HS4ϕ on GSH-QDs**

**Figure D2: Titer Images Showing Binding of HS2, 3, 4ϕ to GSH-QDs**

Plate titer images showing HS2, 3, 4ϕ isolated using salt precipitation during panning, binding 100-fold more than background (IL-12ϕ) to GSH-QDs. Labels are of the format phage/target NP and the number indicates dilution. 3.01 represents 1:1000 dilution of phage and 10 µL of phage was used to infect TG1 cells.

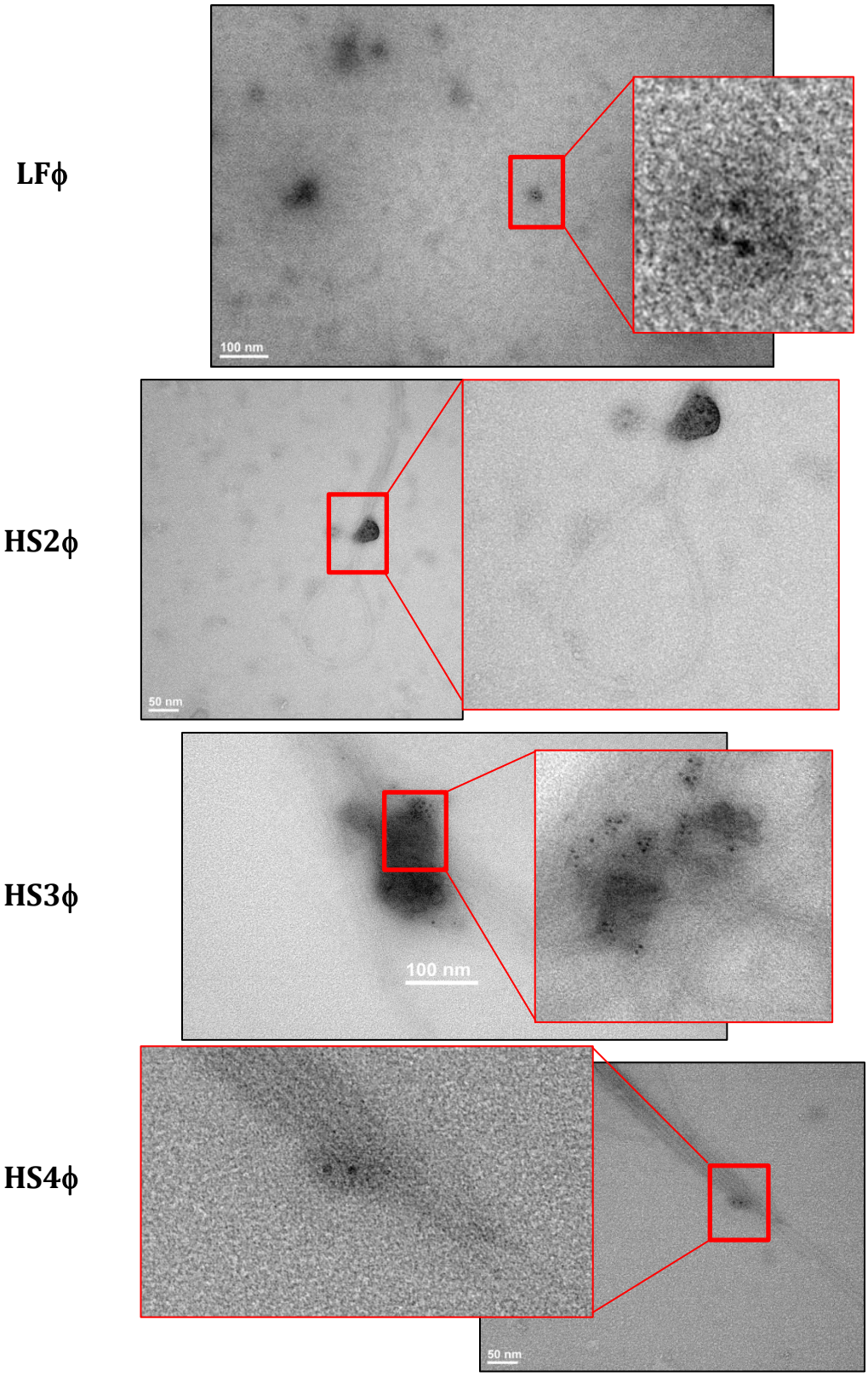


**Figure D3: TEM Images Showing HS2,3,4ϕ Binding to GSH-QDs**

TEM images showing binding of HS2, 3, 4ϕ to GSH-QDs whereas negative control LFϕ does not (top). Inset in each image shows a magnified image of the area surrounded by the red boxes.

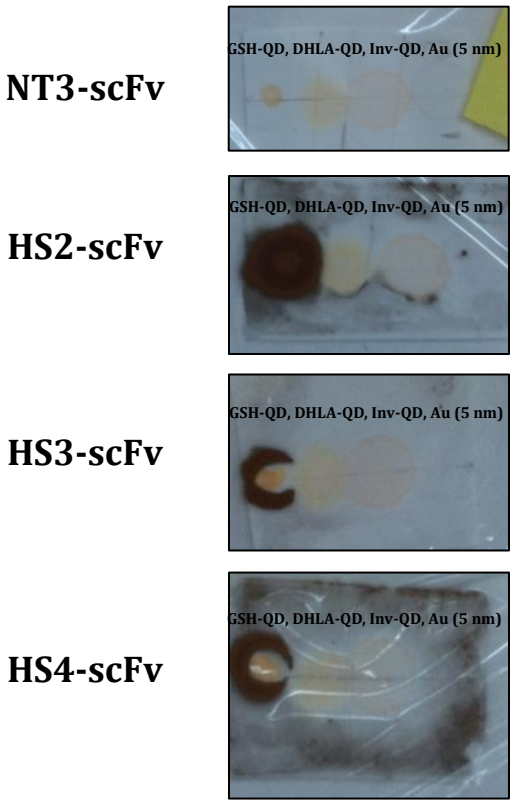


**Figure D4: Dot Blot Images Showing Binding Behavior of HS2, 3, 4-scFvs to NPs**

Dot blot images with film superimposed over membrane showing negative control NT3-scFv not binding GSH-QDs, DHLA-QDs, Inv-QDs or Au 5 nm (tannic acid coated) NPs spotted on a nitrocellulose membrane. HS2, 3, 4-scFvs exhibit binding to GSH-QDs as indicated by the dark chemiluminescent spot formed on the area where the NPs were spotted, but no other NPs.

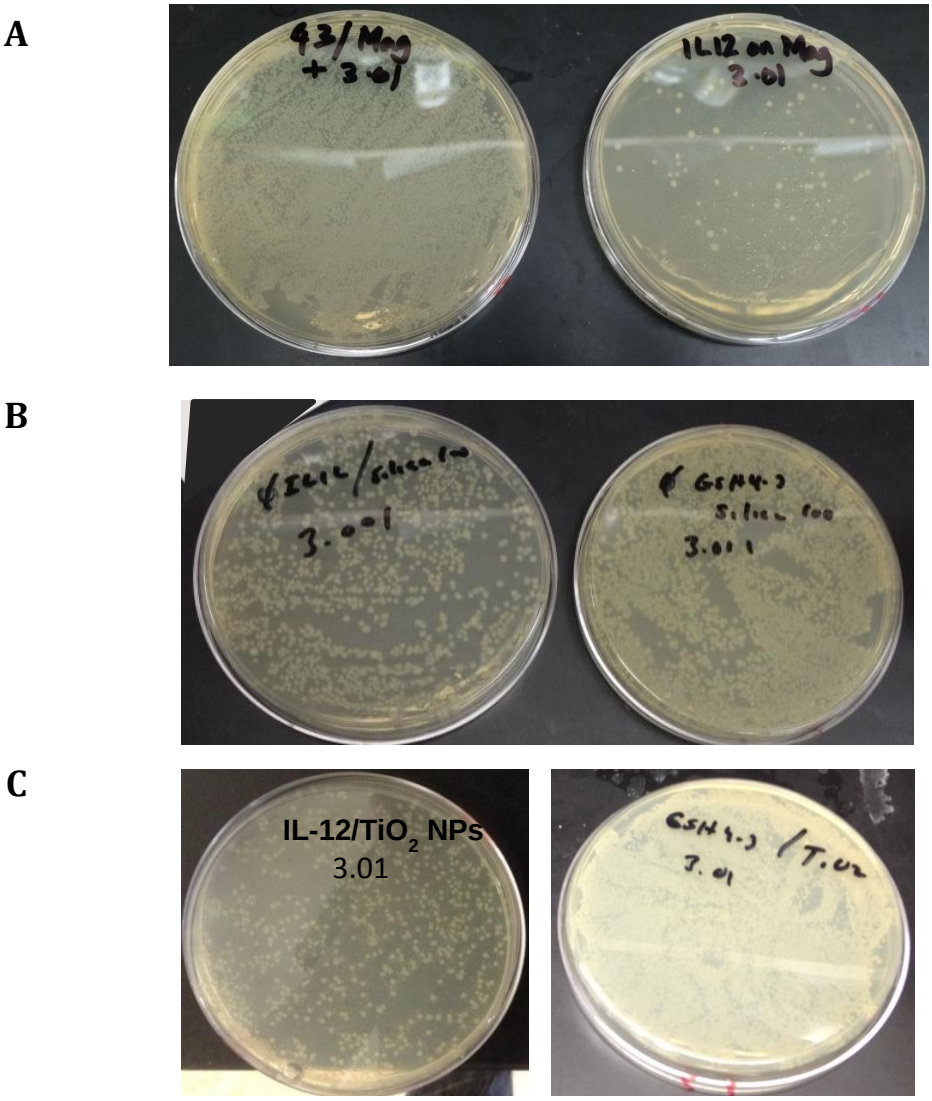


**Figure D5: Titer Images Showing Cross-reactivity of GSH43ϕ to Other NPs**

Plate titer images showing A) GSH43ϕ (left) exhibiting cross-reactivity binding to magnetic NPs whereas (IL-12ϕ, right) does not. B) GSH43ϕ binds silica NPs (100 nm, right) compared IL-12ϕ (left). C) GSH43ϕ also binds $TiO_2$ NPs (right) compared to IL-12ϕ (left). Labels are of the format phage/target NP and the number indicates dilution. 3.01 represents 1:1000 dilution of phage and 10 µL of phage was used to infect TG1 cells. 3.001 represents 1:1000 dilution of phage and 1 µL of phage was used to infect TG1 cells.

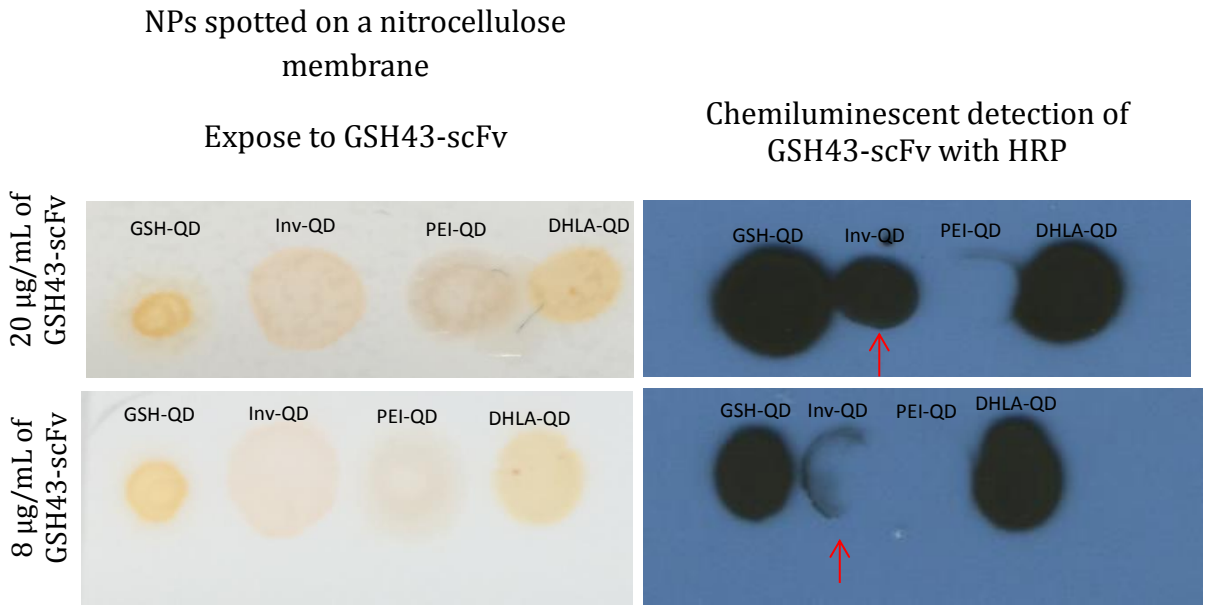


**Figure D6: Dot Blot to Test Cross-reactivity of GSH43-scFvs to Other QDs**

Dot blot to verify binding of GSH43-scFvs at different concentrations to Invitrogen ITK™ 565-QDs (Inv-QDs, 1 µL) spotted on a nitrocellulose membrane. GSH43-scFv binds Inv-QDs at 20 µg/mL and 8 µg/mL but not 5 µg/mL as discussed in Chapter 5. Red arrows detect spot formed upon chemiluminescent detection using HRP indicative of binding to Inv-QDs.

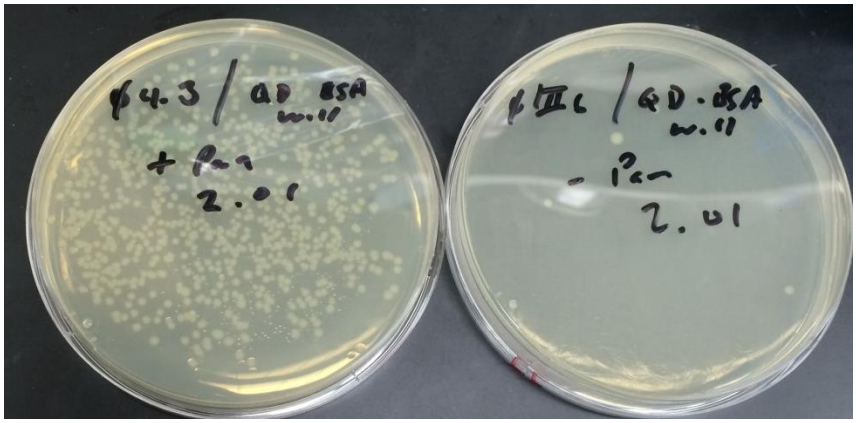

**Figure D7: Titer Images Comparing Empty Vector Phage and GSH43ϕ Binding GSH-QDs**

Plate titer images showing GSH43ϕ (left) exhibiting binding to GSH-QDs (~200-fold) immobilized on BSA, whereas negative control empty phage (not displaying an antibody, right) does not. Labels are of the format phage/target NP and the number indicates dilution. 2.01 represents 1:100 dilution of phage and 10 µL of phage was used to infect TG1 cells.

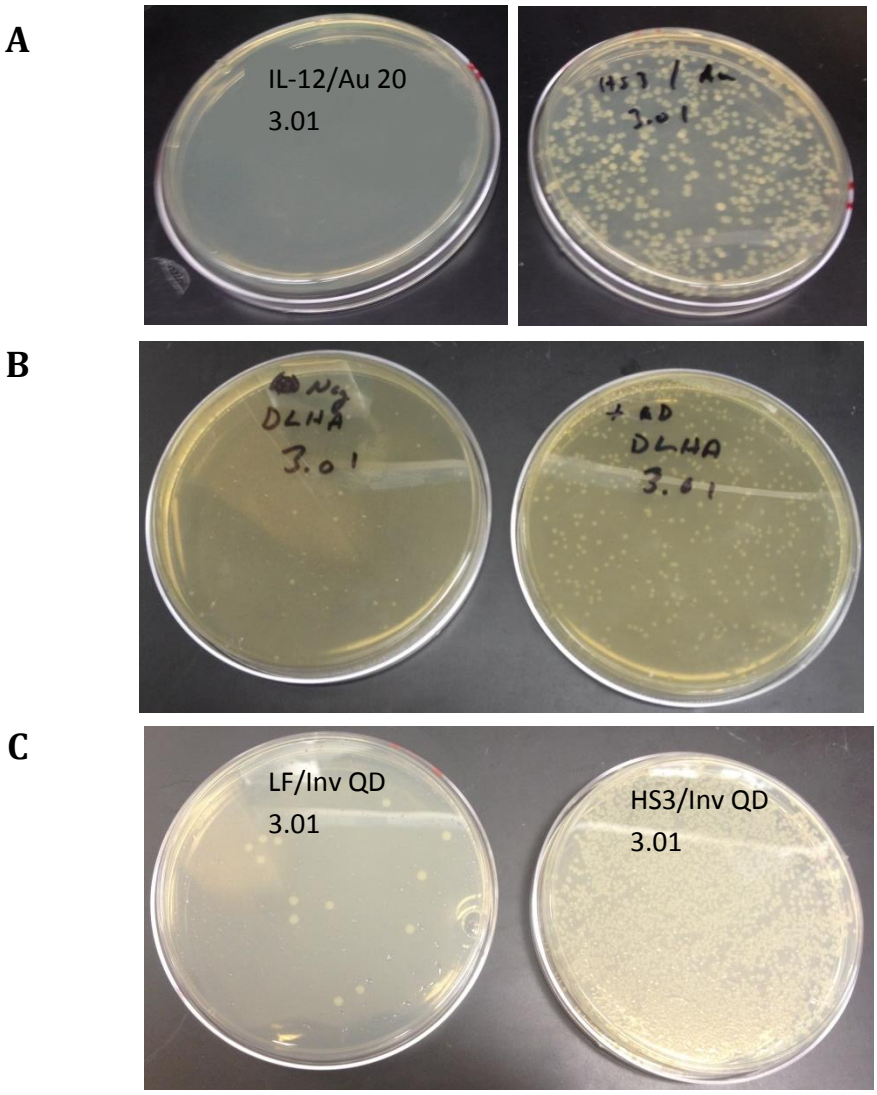


**Figure D8: Titer Images Showing Cross-reactivity of HS3ϕ to QDs**

Plate titer images showing A) HS3ϕ (right) exhibiting binding to Au 20 nm NPs (citrated) whereas (IL-12ϕ, left) does not. B) HS3ϕ binds DHLA-QDs (right) compared to negative control (left) phage. C) HS3ϕ binds Inv-QDs (right) compared to negative control LFϕ (left). Labels are of the format phage/target NP and the number indicates dilution. 3.01 represents 1:1000 dilution of phage and 10 µL of phage was used to infect TG1 cells.

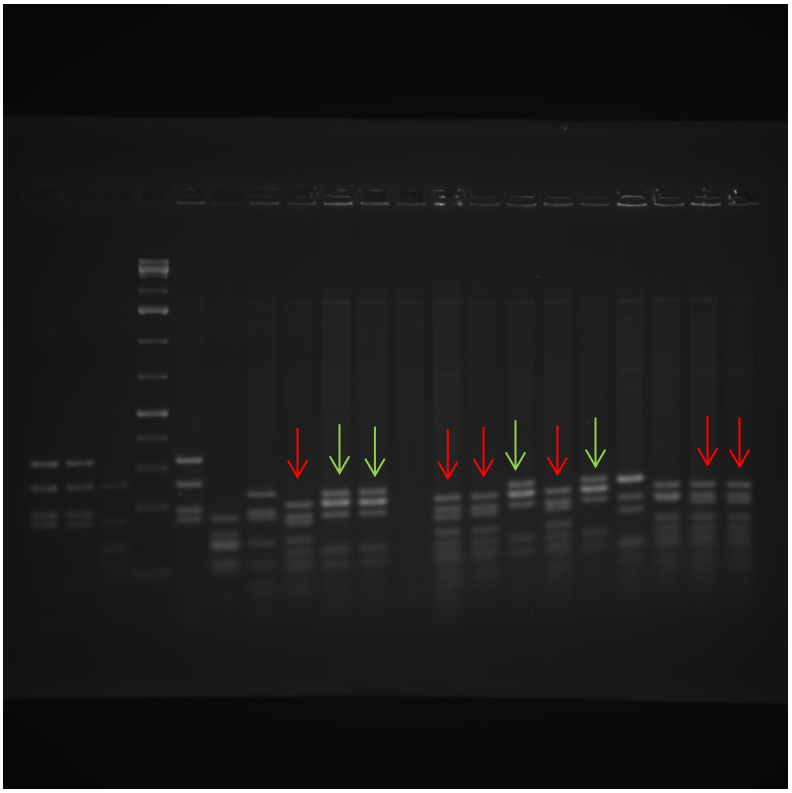

**Figure D9: BstN1 Fingerprinting Image for $TiO_2$ NPs**

BstN1 fingerprinting analysis showing unique scFv patterns for $TiO_2$ panning with green arrows representing Ti6 clone and red arrows representing Ti15 clone.

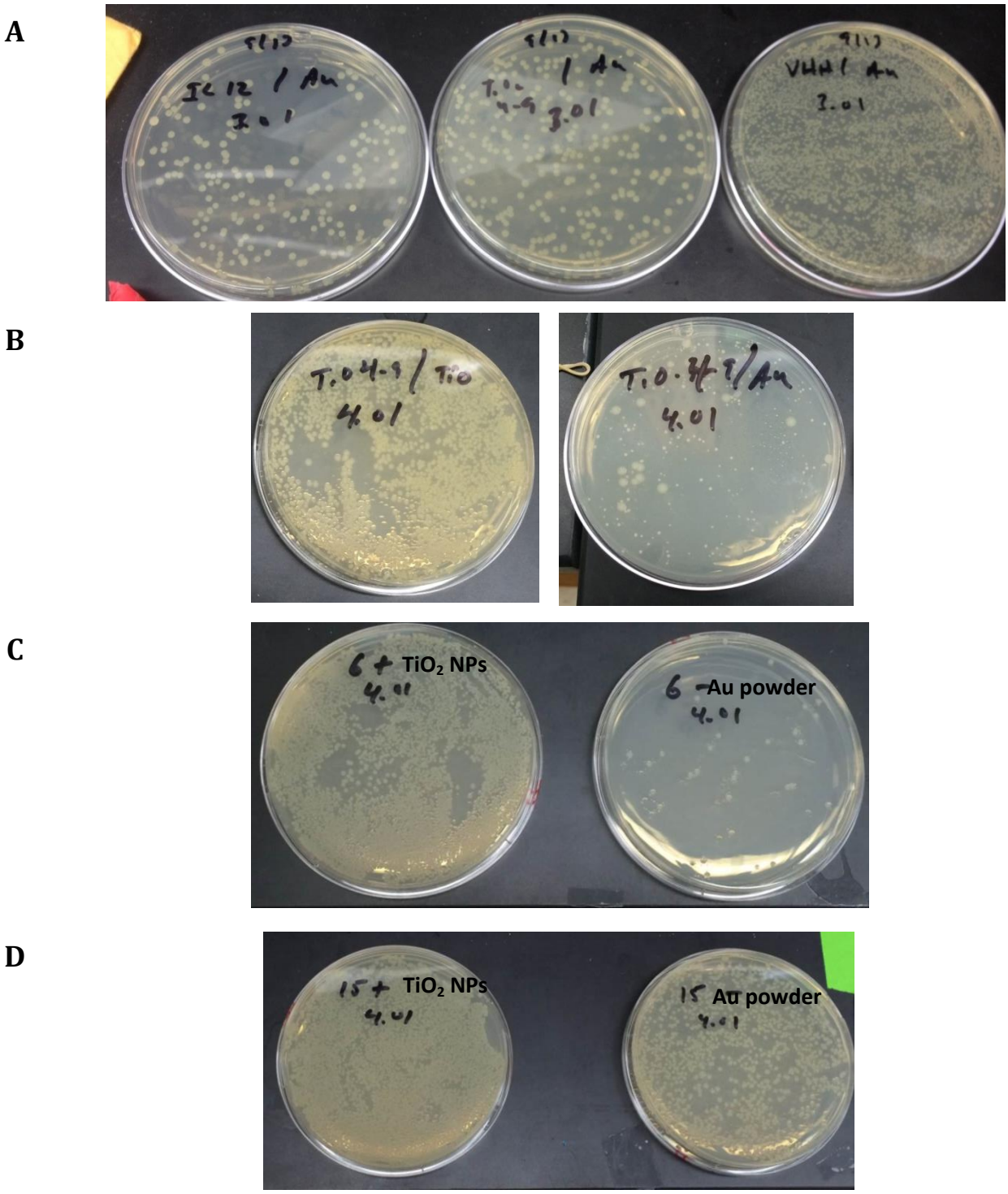


**Figure D10: Titer Images Showing Cross-reactivity of Ti Phage Clones to Au Powder**

Plate titer images showing A) Ti49ϕ (center) exhibiting background (IL-12ϕ, left) levels of binding to Au powder compared to VHH clone (right). B) Ti49ϕ does not bind Au powder (right) compared to $TiO_2$ NPs (left). Similarly C) Ti6ϕ does not bind Au powder (right) compared to $TiO_2$ NPs. However, D) Ti15ϕ binds Au powder albeit to a lesser extent than binding to $TiO_2$ NPs. Labels are of the format phage/target NP and the number indicates dilution. 4.01 represents 1:10,000 dilution of phage and 10 µL of phage was used to infect TG1 cells.

## Ti-6

SYELTQPPSASGTPGQRVTISCSGSSSNIGSNYVYWYQQLPGTAPKLLIYRNNQRPSGVPDRFSGSKS
GTSASLAISGLRSEDEADYYCAAWDDSLSGRVFGGGTKLTVLGEGKSSGSGSESKASEVQLVESGGG
VVQPGRSLRLSCAASGFTFSSYGMHWVRQAPGKGLEWVAVISYDGSNKYYADSVKGRFTISRDNSK
NTLYLQMNSLRAEDTAVYYCAKAHPPLLWFGEFDYWGQGTLVTVSS

**Table D2: Amino Acid Sequence of Clone Ti6 Isolated Against $TiO_2$ NPs**

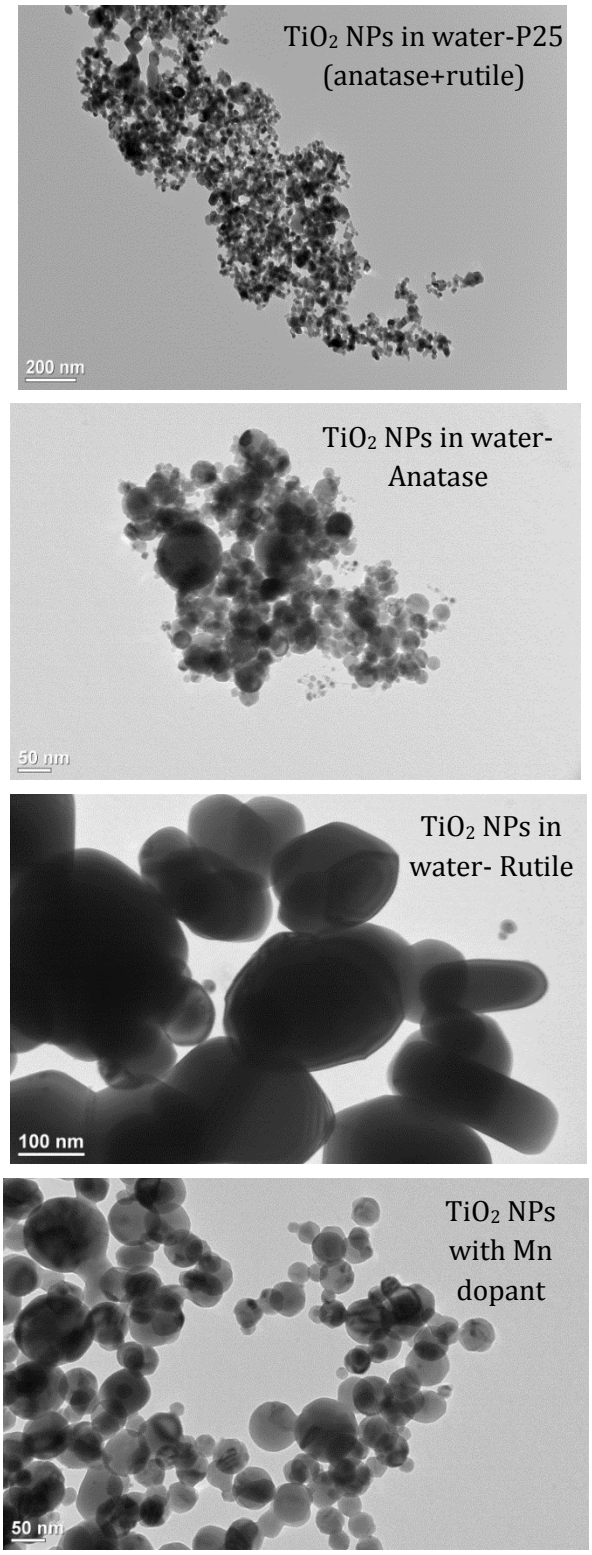


**Figure D11: TEM Images of $TiO_2$ NPs**

TEM images showing morphology of various $TiO_2$ NPs including anatase+rutile (P25), anatase only, rutile only and $TiO_2$ NPs with 1% Mn as dopant in water. Scale bar= 200, 50, 100, 50 nm respectively.

**A**

**B**

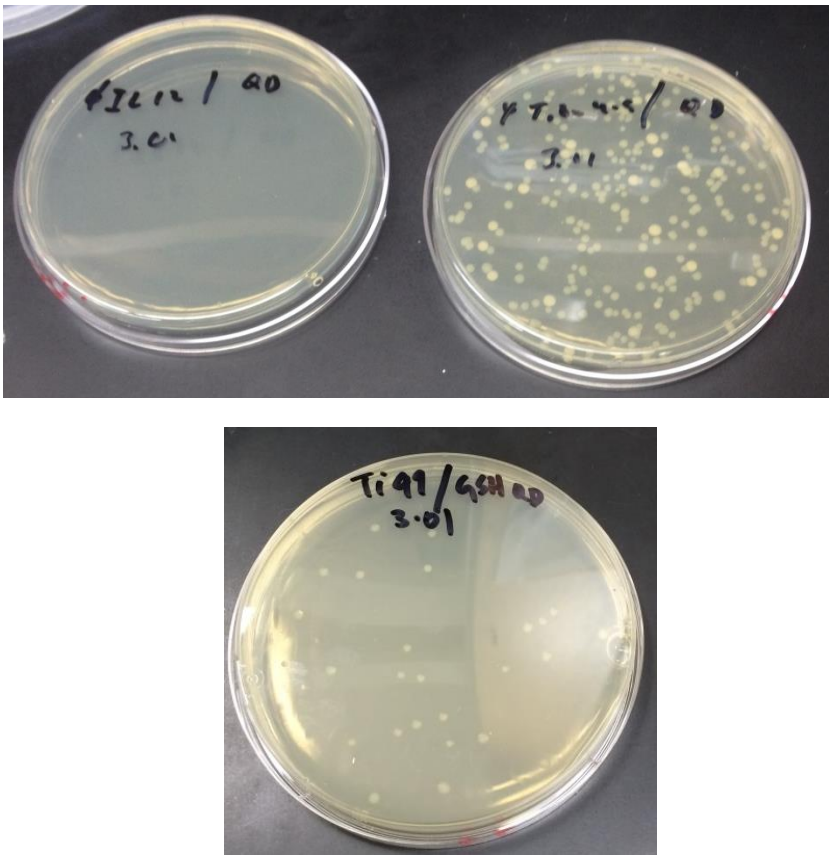


## Figure D12: Titer Images Showing Cross-reactivity of Ti49ϕ to GSH-QDs

Plate titer images showing A) Ti49ϕ (right) exhibiting cross-reactivity to GSH-QDs compared to IL-12ϕ exhibiting no cross-reactivity (left) when using centrifugation to pellet NPs. B) Ti49ϕ does not bind show binding to GSH-QDs upon panning on GSH-QDs immobilized on wells coated with BSA. Labels are of the format phage/target NP and the number indicates dilution. 3.01 represents 1:1000 dilution of phage and 10 μL of phage was used to infect TG1 cells.

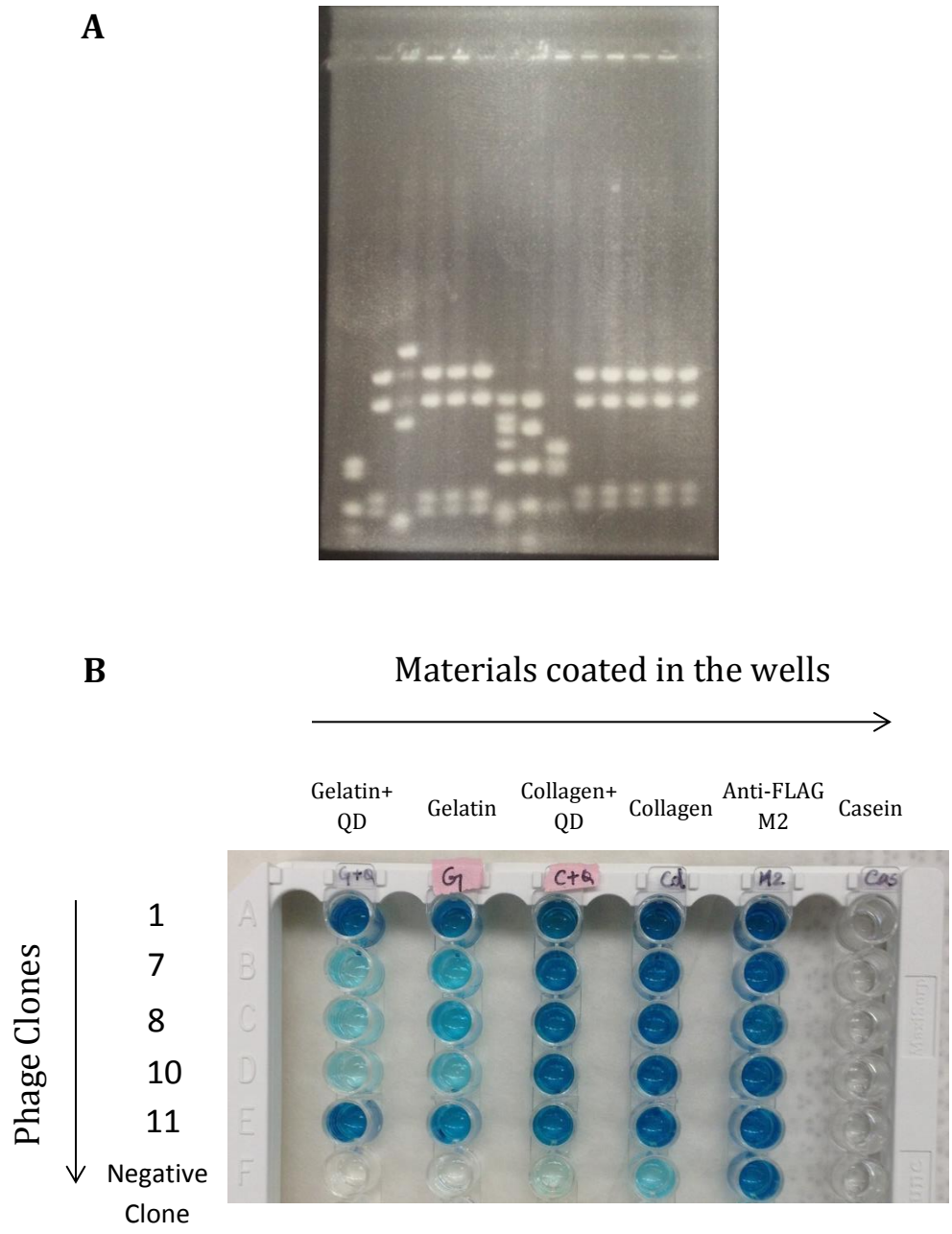


**Figure D13: Enrichment on GSH-QDs Immobilized in Wells**

A) BstN1 fingerprinting analysis showing pattern repeats of scFvs randomly picked after round 4. Clones 1, 7, 8, 10 and 11 (dominant clone) were picked for further analysis for binding using phage ELISA. B) Clones 1, 7, 8, 10, 11 were tested for binding to QDs immobilized on gelatin and collagen along with 'no-QD' controls. The clones did not selectively bind QDs alone but also bound gelatin and collagen (columns 2 and 4). Anti-Flag M2 coated wells were used as a positive control. Phages did not bind casein.

**A**

| QD Enrichment 1 Round 1 | QD Enrichment 1 Round 2 | QD Enrichment 1 Round 3 | QD Enrichment 1 Round 4 |
|---|---|---|---|
| QDs on gelatin coated wells | QDs on gelatin coated wells | QDs on collagen coated wells | QDs on collagen coated wells |

**B**

| QD Enrichment 2 Round 1A | QD Enrichment 2 Round 2A | QD Enrichment 2 Round 3A | QD Enrichment 2 Round 4A |
|---|---|---|---|
| QDs on gelatin coated wells | QDs on BSA coated wells | QDs in BSA coated wells | Centrifugation (QDs dispersed in solution) |

**C**

| QD Enrichment 3 Round 1 | QD Enrichment 3 Round 2 | QD Enrichment 3 Round 3 |
|---|---|---|
| QDs on lactoferrin coated wells | QDs ovalbumin coated wells | QDs on human serum albumin coated wells |

**D**

| QD Enrichment 4 Round 1 | QD Enrichment 4 Round 2 | QD Enrichment 4 Round 3 |
|---|---|---|
| ▪ BSA coated wells<br>▪ QDs on BSA | ▪ BSA coated wells<br>▪ QDs on BSA | ▪ BSA coated wells<br>▪ QDs on BSA |

**E**

| QD Enrichment 5 Round 1 | QD Enrichment 5 Round 2 |
|---|---|
| GSH coated wells | QDs on BSA coated wells |

**Table D3: Alternative Enrichment Strategies on GSH-QDs**

A) Table showing 4 rounds of panning on QDs immobilized on gelatin and collagen. B) A mixed strategy including different proteins and panning on dispersed QDs in solution. C) Three rounds of panning using different proteins at each round for QD immobilization. D) Subtraction panning strategy where unbound phages from BSA-coated wells were transferred to wells containing QDs immobilized on BSA. E) A mixed strategy where the first round was panning on GSH-coated wells (no QDs) and the second round on QDs immobilized using BSA.

## SWAP4-5

QSVLTQPPSASGTPGQRVTISCSGDTSNIGSNSVNWYQQFPGTAPKLLIYSNNQRPSGVPDRFSGSK
SGTSASLAISGLQSEDEADYYCATWDDRLNGWVFGGGTKLTVLG
EGKSSGSGSESKASQVQLQSGAEVKKPGASVKVSCKASGYTFNTHGFSWVRQAPGQGLEWMGWIS
ASNGNTKYPQNLQGRVTMTVDTFTTTAYLELRSLRSDDTAVYYCVRDRTDYYVPGTFDPLYGPFD
YWGQGTLVTVSS

## SWAP4-6

QPVLTQPPSASGTPGQRVTISCSGSDSNIGSNTVNWYQQVPGTAPKLLIYSNTQRPSGVPDRFSGSK
SGTSASLAIRGLQSEDEADYYCAAWDDRLNGWVFGGGTKLTVLG
EGKSSGSGSESKASQVQLQSGAEVKKPGASVKVSCKASGYTFNTHGFSWVRQAPGQGLEWMGWIS
ASNGNTKYPQNLQGRVTMTVDTFTTTAYLELRSLRSDDTAVYYCVRDRTDYYVPGTFDPLYGPFD
YWGQGTLVTVSS

## SWAP4-8

QAVLTQPPSASGTPGQRVTISCSGSSSNIGSNTVSWYQQLPGTAPKLLIYSNNQRPSGVPDRFSGSKS
GTSASLAISGLQSEDEADYYCAAWDDSLNGHWVFGGGTKLTVLG
EGKSSGSGSESKASQVQLQSGAEVKKPGASVKVSCKASGYTFNTHGFSWVRQAPGQGLEWMGWIS
ASNGNTKYPQNLQGRVTMTVDTFTTTAYLELRSLRSDDTAVYYCVRDRTDYYVPGTFDPLYGPFD
YWGQGTLVTVSS

## SWAP4-11

QPVLTQPPSASGTPGQRVTISCSGSSSNIGSNTVNWYQQLPGTAPKLLIYSNNQRPSGVPDRFSGSK
SGTSASLAISGLQSEDEADYYCAAWDDSLNGHWVFGGGTKLTVLG
EGKSSGSGSESKASQVQLQSGAEVKKPGASVKVSCKASGYTFNTHGFSWVRQAPGQGLEWMGWIS
ASNGNTKYPQNLQGRVTMTVDTFTTTAYLELRSLRSDDTAVYYCVRDRTDYYVPGTFDPLYGPFD
YWGQGTLVTVSS

## GSH4-3

LPVLTQPPSASGSPGQRVTISCSGSSSNIGSNTVNWYQQLPGTAPKLLIYSNNQRPSGVPDRFSGSKS
GTSASLAISGLRSEDEADYYCAAWDDSLNGWVFGGGTKLTVLG
EGKSSGSGSESKASQVQLQSGAEVKKPGASVKVSCKASGYTFNTHGFSWVRQAPGQGLEWMGWIS
ASNGNTKYPQNLQGRVTMTVDTFTTTAYLELRSLRSDDTAVYYCVRDRTDYYVPGTFDPLYGPFD
YWGQGTLVTVSS

### Table D4: Amino Acid Sequences of Swap-L clones Isolated Against GSH-QDs

Light chain and heavy chain amino acid sequences of the various swap-L clones identified based on the pattern repeats from BstN1 fingerprinting showing slight variations from the light chain of original clone GSH43.